**Geological Survey of Finland, Bulletin 346**

# EMPLACEMENT AND STRUCTURAL SETTING OF GRANITOIDS IN THE EARLY PROTEROZOIC TAMPERE AND SAVO SCHIST BELTS, FINLAND — IMPLICATIONS FOR CONTRASTING CRUSTAL EVOLUTION

by

MIKKO NIRONEN

with 49 figures and 3 appendices

GEOLOGIAN TUTKIMUSKESKUS
ESPOO 1989

Vammala 1989. Vammalan Kirjapaino Oy

**Nironen, M. 1989.** Emplacement and structural setting of granitoids in the early Proterozoic Tampere and Savo Schist Belts, Finland — implications for contrasting crustal evolution. *Geological Survey of Finland, Bulletin 346.* 83 pages, 49 figures and 3 appendices.

Five Svecofennian granitoid plutons, belonging to the synkinematic age group (1.90—1.87 Ga), were studied with emphasis on the structures in and around the plutons. The Hämeenkyrö batholith and the Värmälä stock lie within the Tampere Schist Belt, and the Silvola, Kaartila and Varparanta stocks are within the Savo Schist Belt.

The Hämeenkyrö batholith and the Värmälä stock are predominantly granodioritic in composition. The Hämeenkyrö batholith shows normal zoning, with increasingly felsic phases in the center. In contrast, the Värmälä stock is reversely and asymmetrically zoned. The Varparanta and Silvola stocks are tonalitic/trondhjemitic in composition. In the Varparanta stock, the most felsic rocks are in the center of two domal structures. In the Silvola stock, the compositional variation is obscured by deformation of the pluton. The compositionally heterogeneous Kaartila stock is differentiated mainly with respect to minor and trace elements.

There is no field evidence for major wall rock contamination, or magma mixing, but the typical microgranitoid enclaves indicate that magma mingling occurred. In addition, magma mingling during emplacement produced compositional banding in the Varparanta stock. Possibly initial mixing and mingling between crustal and more mafic subcrustal magma generated the tonalitic plutons, and subsequent mixing in the crust resulted in the granodioritic plutons. The Kaartila stock is an exception: it is devoid of microgranitoid enclaves, and it probably was generated by partial melting of supracrustal rocks. Fractional crystallization occurred during final emplacement of the plutons.

The Hämeenkyrö and Värmälä plutons were emplaced first rather passively, at the culmination of fairly low grade metamorphism, and subsequently more forcefully with continued injection of magma. The emplacement of the Silvola and Kaartila stocks was diapiric, before the culmination of high grade metamorphism. Strike-slip faulting controlled the emplacement of the Varparanta stock.

The Tampere Schist Belt is part of an early Proterozoic volcanic arc system. The tectonothermal evolution culminated 1.90—1.88 Ga ago when the volcanics extruded and the granitoid plutons were emplaced. The Hämeenkyrö batholith and the Värmälä stock are syntectonic with respect to $D_1$ deformation which dominates the structure of the central Tampere Schist Belt. The clasts of igneous rocks in the metaconglomerate interlayers, with similar 1.89—1.88 Ga ages, show that evolution was rapid. The 1.86 Ga age of $D_2$ deformation records the waning stage of evolution.

The plutons in the Savo Schist Belt were emplaced 1.89—1.88 Ga ago. The Silvola and Kaartila stocks were emplaced during $D_2$ deformation. Progressive metamorphism in the southeastern part of the belt culminated about 1.83 Ga ago, roughly coevally with large scale $D_3$ faulting. The slow cooling of the Silvola stock, expressed as ductile deformation during $D_4$ about 1.80 Ga ago, was due to the late peak of metamorphism. The $D_{2-3}$ faulting which controlled the emplacement of the Varparanta stock preceded the $D_3$ faulting around the Silvola and Kaartila stocks.

The two belts represent areas of different crustal evolution and level. Thus structural correlation between the two belts or even between isolated areas within a single belt may not be warrated, although plutonism was coeval.

Key words: granites, intrusions, structural analysis, geochemistry, emplacement, crust, evolution, Proterozoic, Finland

*Mikko Nironen*
*Department of Geology, University of Helsinki, P.O. Box 115*
*SF-00171 Helsinki*
*FINLAND*

## CONTENTS

## INTRODUCTION

Development in theory, laboratory techniques and experiment is reflected in studies of granitoids (granites, granodiorites and tonalites). The extensive field studies concerning the internal structures of granitoids in the 1930's (e.g. Balk 1937) and the experimental studies of Ramberg (1967, 1970) with centrifuge models directed interest toward the emplacement mechanisms and associated structures of igneous bodies. From the late 1970's onward, interest shifted to petrochemistry due to the development of laboratory techniques. During this period, modern structural analysis methods were applied to study the strain state in plutons and their host rocks. As a result of the dualism in granitoid studies, petrochemistry and emplacement have been considered together in few cases (Bateman and Chappell 1979, Phillips et al. 1981, Bateman 1985a, Bateman 1985b, Bayer et al. 1987).

The Proterozoic plutonic rocks in Finland have traditionally been classified as syn-, late- and post-kinematic, or syn-, late- and post-orogenic, with respect to orogenic movements. The distinction between synkinematic and late-kinematic plutonic rocks was made on the degree of foliation within the plutons, and the grouping was correlated with compositional differences (Eskola 1932). Later studies have shown, however, that the structural criterion is ambiguous (Simonen 1960, Nurmi et al. 1984, Nironen 1985). Recently, a growing amount of U-Pb zircon isotopic evidence has shown that the Proterozoic plutonic rocks in Finland fall into rather restricted age groups. These age groups have been associated with the magmatectonic classification (e.g. Nurmi and Haapala 1986).

The terms syntectonic, late-tectonic and post-tectonic are currently used as synonyms for synkinematic etc. However, in modern structural and metamorphic geology these terms are used to define the emplacement of a pluton, or growth of a metamorphic mineral *with respect to a specific deformational event.* The former defines the *structural setting* of a pluton. Thus a pluton may be syntectonic with respect to a certain deformational event but post-tectonic with respect to a preceding one. To prevent misinterpretations in this study, the terms syn-, late- and post-tectonic have a structural/metamorphic connotation, whereas synkinematic (synorogenic) etc. are considered as age groups loosely related to orogenic processes.

A single progressive deformational event and orogenic processes as a whole vary in space, time and intensity (Park 1969; Hobbs et al. 1976, p. 354—355, Williams 1985). Hence, igneous rocks emplaced coevally in a schist belt may have different structural settings and, vice versa, rocks of the same structural setting may have been emplaced at different times. Subsequent faulting of the crust into gigantic blocks may further complicate the subject. These ambiguities set constraints on the structural correlation of restricted, separate areas. However, the petrochemistry and structural setting of plutonic bodies with existing isotope data are among the few clues in delineation of the crustal evolution in old areas such as the Finnish Precambrian.

Detailed structural studies of schists have been made in various parts of Finland, but their areal extent is still rather small. Less is known about the structural settings of the plutons, the published examples being from the archipelago of southern Finland (Hopgood et al. 1976, Ehlers 1978, Hopgood 1984, Hubbard and Branigan 1987) and eastern Finland (Gaál and Rauhamäki 1971, Halden 1982, Park and Bowes 1983). The petrological characteristics, including major element geochemistry, of the synkinematic granitoids in southern Finland have been discussed recently (Front and Nurmi 1987). However, geochemical

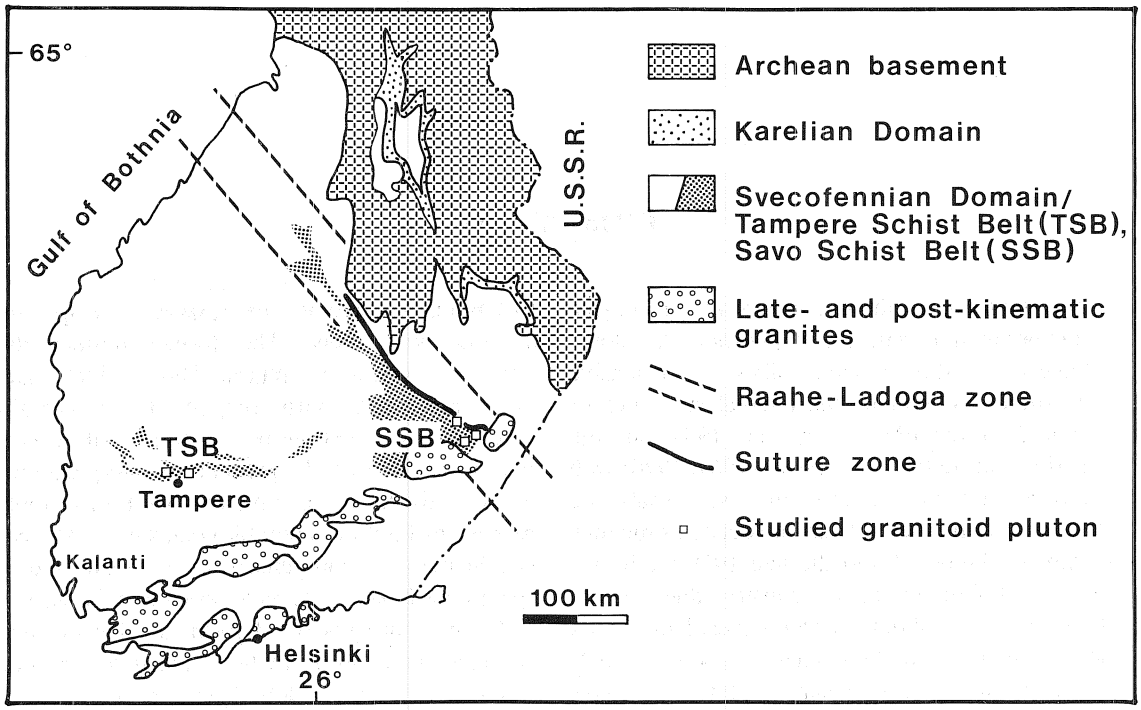


Fig. 1. Generalized geological map of southern Finland, showing the location of the Tampere and Savo Schist Belts and the studied plutons (modified from Simonen 1980, and Gaál and Gorbatschev 1987).

characteristics of few individual plutons belonging to this group have been published (Parras 1958, Gaál and Isohanni 1979, Gaál et al. 1981, Nurmi 1983).

The author worked as a researcher in the Porphyry Project, in the University of Helsinki, from 1980 to 1983 (see Nurmi et al. 1984). Of the 21 granitoids studied in southern Finland during the Project, five synkinematic granitoids lying within the early Proterozoic Tampere and Savo Schist Belts (Fig. 1) were chosen for this work for detailed analysis. The evolution of the two belts are compared on the basis of structural setting, emplacement mechanism and (predominantly) major element geochemistry of the granitoids. Moreover, the implications of the results for the evolution of the Svecofennian crust are discussed.

## METHODS

Before field mapping, available remote sensing material (topographic maps, stereo-pair air photos, aeromagnetic maps) was used to detect structures of the granitoids, their contacts and regional structures that might control the emplacement of the granitoids. In addition to existing field data, the author mapped the granitoids and their surroundings with an average spacing between observation sites of 0.5—1 km. Oriented samples were collected for laboratory studies, and the author studied, in about 300 thin sections, the mineralogy and microstructures in the granitoids and their country rocks. The available modal composition data was supplemented so that at least one modal composition was determined for each rock type (see Appendix 1).

The available geochemical data was used to consider the possible origin and differentiation processes of the plutons. Major element geochemistry was mostly used, with minor and trace elements from three plutons. The heterogeneity of the analytical methods restricted more profound use of geochemistry*.

The structural fabric elements were named according to the notation of Bell and Duncan (1978). For example, an intersection lineation between lithological layering and $S_1$ is $L_1^0$, whereas a stretching lineation formed during $D_1$ is $L_1^1$. The terminology of metamorphic mineral growth also follows the common usage: a mineral which has grown during $D_1$ is called $MS_1$, and one which has grown after $D_1$ (but before $D_2$) is $MP_1$.

## Strain analysis methods

Passive strain markers are objects within a deformed rock which, during deformation, retained their identity but did not differ from their surrounding material in their mechanical behavior. In strain analysis, the information on shape changes due to geological strain is converted into the form of strain ellipsoids. The strain in granitoids is usually seen as elongate quartz aggregates, biotite flakes, hornblende grains or biotite-hornblende aggregates. All of these have been used to determine finite strain (Schwerdtner et al. 1977, Brun et al. 1981, Schwerdtner et al. 1983). Polycrystalline quartz aggregates can be used as strain markers if they show only crystal-plastic deformation, i.e. if there is no evidence of widespread diffusive deformation, grain growth, cataclastic deformation etc. In quartz aggregates, the total strain may be the result of several crystal-plastic deformation events, and the strain may involve volume change. Moreover, the aggregates do not record the strain that was attained before the crystallization of quartz, or strain accommodated by intergranular slip while melt was present. Hence, the strain is a minimum estimate.

Since quartz aggregates were abundant in one of the studied granitoids (the Värmälä stock), they were used for local estimates of finite strain. Oriented rock samples were cut so that, of the three perpendicular surfaces, one contained foliation and lineation (the XY plane of the strain ellispoid with axes $X \geq Y \geq Z$), one was perpendicular to both foliation and lineation (the YZ plane), and one was perpendicular to foliation but parallel to lineation (the XZ plane). For each principal section of the strain ellipsoid, the long and short axes through the centers of 40 deformed quartz aggregates were measured and the axial ratios were calculated. According to the method of Robin (1977), the axial-strain ratio of each surface was considered as the logarithmic average of all the axial ratios measured on that surface. Two-dimensional strain ratios on the principal planes were combined to give the three-dimensional strain ellipsoid. The values for the finite state were recorded in terms of the Flinn parameter $k=(X/Y-1)/(Y/Z-1)$ (Flinn 1962), and the strain intensity parameter $r=X/Y+Y/Z-1$ (Watterson 1968).

The finite strain at each outcrop was determined qualitatively from sheet silicates, quartz aggregates, and K-feldspar megacrysts, if present, by evaluation of the LS tectonite fabric, i.e. the relative strength of lineation (L) with respect to that of foliation (S). For field identification, Flinn (1965) divided the continuous LS fabric system into five subdivisions: L, L>S, L=S, L<S, and S fabric. The relationship between the LS fabric system, and the k and r parameters is shown in Fig. 2. The line $k=1$ divides the graph into the fields of (apparent) flattening ($k<1$) and constriction ($k>1$; see Ramsay and Huber 1983, p. 172).

Enclaves in granitoid rocks can also be used as strain markers, provided they have behaved as passive markers, i.e. they do not show effects of competence contrast. For this reason, country rock xenoliths are not recommended, although they have been used for strain analysis (see Holder 1979). In contrast, mafic microgranitoid enclaves (microdiorite enclaves, cognate xenoliths; Vernon 1983,

* Geochemical data is available on request to the author.

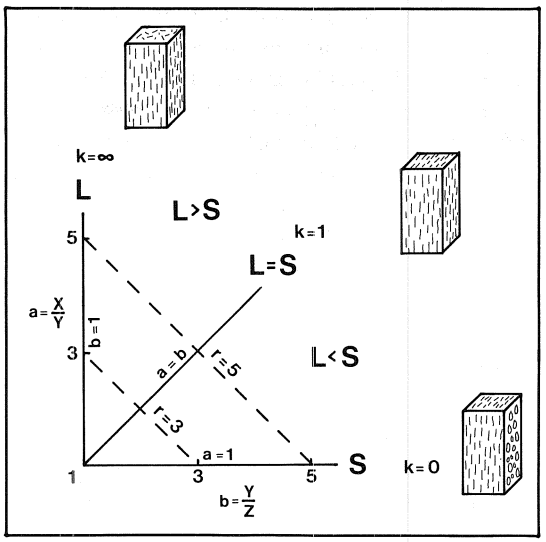


Fig. 2. Diagram showing the relationship between the shape of strain ellipsoid (k), strain intensity (r) and LS tectonite fabric. The axial ratios of the strain ellipsoid with axes X≥Y≥Z can be expressed in two dimensions by the ratios a=X/Y and b=Y/Z. The ratios a and b give the deformation plot (Flinn 1962). All ellipsoids can be characterized by the Flinn parameter k=(a—1) /(b—1). The line k=∞ connects all prolate ellipsoids (pure linear, L fabric), k=0 all oblate ellipsoids (pure planar, S fabric). All the other ellipsoids comprise both L and S. Ellipsoids in which no change has taken place in the length of the intermediate axis are arranged along the line a=b (Flinn 1965). The intensity of strain is recorded as the parameter r=a+b-1 (Watterson 1968).

Didier 1987), have been used as strain markers (Barriere 1977, Holder 1979, Ramsay 1981, Courrioux 1987). Inaccuracies due to initial non-spherical shape of the strain markers of up to 10—15 % are to be expected (Holder 1979). Because of difficulties in finding suitable surfaces on mostly subhorizontal outcrops, deformed enclaves could be used in this study only to qualitatively support other measurements or estimations.

The anisotropy of magnetic susceptibility has been applied from the 1960's in structural analysis of igneous rocks (e.g. Balsley and Buddington 1960, Guillet et al. 1983, Rathore and Kafafy 1986), and a comprehensive review of magnetic anisotropy was presented by Hrouda (1982). The studies have demonstrated the general coaxiality of magnetic fabric and petrofabric ellipsoids. The magnetic fabric in an igneous rock may be due to magma flow (mainly in volcanic rocks), solid state deformation during emplacement, or regional post-emplacement deformation. One of the plutons (the Silvola stock) contained ferrimagnetic minerals enough for the study of the magnetic fabric. Core samples were drilled from hand specimens vertically with respect to the original orientations of the specimens, or perpendicular to foliation plane. The anisotropy of magnetic susceptibility of oriented samples, 3.2 cm in diameter and 2.8 cm in length, was measured in the Petrophysical Laboratory of the Geological Survey of Finland. The measurements were made by the author with a low-field AC-bridge (Puranen and Puranen 1977), and the measuring design A of Hext (1963) was applied.

## AN OUTLINE OF GRANITOID GENERATION AND EMPLACEMENT

### Segregation and intrusion of granitoid magma

In orogenic environments, granitoid magma is generally thought to be formed as a result of partial melting either in lower crust or upper mantle. Large volumes of magma, especially tonalitic, are probably initiated by partial melting of the mantle (Green 1980, Barker 1981, Barker et al. 1981, Hyndman 1981, Brown 1982). Andesitic or basaltic magma, the product of partial melting, differentiates and when transported to lower crust, assimilates and/or melts crustal material. Mixing between mantle-derived and crustal magma results in calc-alkaline granitoid magma with features intermediate between the source magmas (Fourcade and Allègre 1981). The transfer of heat and volatiles from mantle to lower crust may also cause partial melting of crustal material (Bailey 1970).

Experimental studies indicate that partial melting can take place locally in the crust during regional metamorphic conditions, producing $H_2O$-undersaturated granitic melts (Wyllie 1977). Deeply buried, mica-rich sedimentary rocks may release sufficient amounts of water through metamorphic reactions to induce melting (e.g. Harris et al. 1970).

On the basis of the above it may be concluded that granitoid magma is generated predominantly in deep levels of the continental crust. However, magma that derives all of its water by breakdown of muscovite is probably formed at relatively shallow crustal levels and only a few kilometres deeper than its final emplacement level (Hyndman 1981).

Buoyancy can be considered the most important of the physical factors affecting the rise of granitoid magma. The density of magma with granitic or granodioritic composition is lower than that of surrounding metasediments both in deep and shallow crustal levels (Ramberg 1980, Soula 1982). Pressure gradients may control magma ascent toward areas of lower pressure. Leake (1978) inferred that block movements in the Irish Caledonides penetrated the crust, lowered pressure and caused rapid re-melting in the lower crust. The granitic magma thus formed rose along the deep faults. A lineament control is observed for numerous granitoid batholiths of different ages (e.g. Pitcher 1979, p. 645). Many intrusive bodies may ascend along the same zone of weakness and form large batholiths. The viscosity of wall rock at the contact controls the ascent velocity of magmas. The ascent of relatively viscous granitoid magmas is facilitated by passageways which were pre-heated by hot, volatile-rich basic magmas (Marsh 1982).

An ascending granitoid magma contains various amounts of crystals. Especially at the final stage of emplacement (intrusion), the amount of solid material is considered to be significant, probably more than 70 % (Soula 1982, Bateman 1984). As the viscosity of the magma increases, it no longer behaves as a Newtonian liquid. Experimental studies with centrifuge models suggest that viscosity contrast between magma and wall rock is the main factor that controls the emplacement mechanism (Ramberg 1970, 1980). If the contrast is great (i.e. magma has a low viscosity), magma will ascent along vertical zones as dike swarms. If the viscosity contrast is low, emplacement is forceful. Natural examples suggest that external (regional) stress is also a major factor controlling the intrusion of magma (Castro 1987).

Buddington (1959) classified granitoids into catazonal, mesozonal and epizonal types according to their emplacement levels and mechanisms. The Caledonian granitoids of Donegal were emplaced at the same crustal level but with different mechanisms (Pitcher and Berger 1972, Holder 1979, Hutton 1982), showing that the classification expresses only broad characteristics of emplacement and should not be taken too strictly.

## Emplacement mechanisms of granitoid plutons

A granitoid pluton can be emplaced in such a way that the thermal and mechanical effect of the magma and volatile-rich fluids causes the country rock to break into blocks. The blocks which sink gravitatively into the magma, may range substantially in size. If they are relatively small (up to tens of cubic meters), the mechanism is stoping. If huge, cylindrical or conical blocks separate from the roof along ring fractures, the mechanism is called cauldron subsidence. Stoping and cauldron subsidence are essentially passive emplacement mechanisms with brittle deformation of the country rock, and they do not create a tectonite fabric in the plutonic rock. These mechanisms are typical of high level plutons, e.g. the subvolcanic plutons of the Andes (Pitcher 1978).

Another emplacement mechanism is forceful intrusion, or diapirism as it is more commonly called. Bates and Jackson (1980) defined diapirism as "the process of piercing and rupturing of domed or uplifted rocks by mobile core material, by

tectonic stresses as in anticlinal folds,...or by igneous intrusion, forming diapiric structures" (diapirs). However, as Van den Eeckhout et al. (1986) pointed out, the use of piercement as a criterion for diapiric processes is not very successful, because it excludes structures where a pluton has deformed its aureole without piercement, such as ballooning plutons (see below). Here, only buoyant, gravity-driven structures with ductile deformation are considered diapiric.

Based on centrifuge model experiments, diapirs are named immature when they have domal or antiformal shapes, and mature when they are mushroom-shaped (e.g. Ramberg 1970). Several factors, such as thickness, rigidity and density of the overburden and spacing between adjacent diapirs contribute to the final shape of the diapir; not all diapirs reach the mature stage.

Experimental models with centrifuges, concerning the distribution of finite strain in and around diapirs (Dixon 1975), indicate that immature diapirs are characterized by subvertical extension except in the crestal area where subhorizontal extension dominates. Subhorizontal extension is even more intense in the passive overburden directly above the diapir. There is a surface of zero finite strain between the crestal area and the trunk region. Complex structures may be generated during a single non-coaxial deformation within the diapir.

When a mature diapir reaches its final emplacement level due to growing crystal content, it starts to spread out laterally (balloon). Continued or pulsatory injection of magma leads to a ballooning pluton. Ballooning produces bulk flattening in the pluton and the country rock, with increasing strain toward the contact (Holder 1979, Brun and Pons 1981, Brun et al. 1981, Ramsay 1981, Sanderson and Meneilly 1981, Soula 1982, Bateman 1985b).

The characteristics of a diapir are controversial (e.g. Bateman 1984, Van den Eeckhout et al. 1986), especially because immature diapiric structures may be confused with structures due to simultaneous or successive cross folding (doubly plunging folds or fold interference structures). The difficulty of interpretation in the latter case is expressed in the fact that some granitoid complexes have been interpreted by means of structural analysis both as diapiric and as due to cross folding (the Chindamora batholith, see Ramsay 1981 and Snowden 1984; and the Thor Odin gneiss dome, see Duncan 1984 and Van den Driessche 1986).

The structure of a pluton is the consequence of the mechanism whereby it has attained its final position, or a combination of final emplacement and regional deformation. Therefore, the structure may not tell much about the way the magma ascended in the crust. Marsh (1982) considered diapirism as the leading process of magmatic transfer both in the mantle and the crust. In contrast, Bateman (1984) stated that granitoid magmas are largely molten when ascending through the crust, and therefore they rise via dikes and fracture systems; diapirism typically occurs only during the final emplacement.

## GEOLOGICAL SETTING OF THE SVECOFENNIAN SCHIST BELTS

The two major geological units of the Precambrian bedrock of southern Finland are the Archean basement (2.9—2.6 Ga) and the early Proterozoic Svecokarelian terrain (Fig. 1). The latter is divided into the intracratonic Karelian Domain and the orogenic Svecofennian Domain (Gaál and Gorbatschev 1987). The epicontinental sediments of the Karelian Domain, deposited on the Archean crust, were intruded by diabase dikes of 2.1 Ga age (Sakko 1971).

The Svecofennian Domain constitutes most of southern Finland and extends to central Sweden. It consists of several fairly well-preserved volcanic-sedimentary belts (including the Tampere and Savo Schist Belts), separated by migmatitic gneisses and plutonic rocks. The volcanics and marine sediments

were deposited 2.0—1.9 Ga ago (Gaál and Gorbatschev 1987). Most of the U-Pb zircon ages determined from the Svecofennian igneous rocks yield 1.90—1.87 Ga ages (Huhma 1986, Patchett and Kouvo 1986, Welin 1987). The plutonic rocks of this synkinematic group range in composition from peridotite to granite, with rocks of granitoid composition prevailing. Migmatite-forming late-kinematic granites of southern Finland have zircon ages of 1.84—1.81 Ga (Hopgood et al. 1983, Korsman et al. 1984, Huhma 1986), post-kinematic granitoids around 1.80 Ga (Vaasjoki 1977, Welin et al. 1983, Korsman et al. 1984, Huhma 1986), and the rapakivi granites 1.70—1.54 Ga (Vaasjoki 1977).

Metamorphism during the Svecofennian orogeny was of the high-temperature low-pressure type (Korsman 1977, Campbell 1980, Korsman et al. 1984, Schreurs 1984, Hölttä 1986). Metamorphic studies of still rather restricted areas indicate two episodes of metamorphic culmination in the Svecofennian Domain: 1.90—1.87 Ga ago (Hopgood et al. 1983, Korsman et al. 1984, Vaasjoki and Sakko 1988), and 1.84—1.81 Ga ago in the belt characterized by late-kinematic granites, in southern Finland (Fig. 1; Korsman et al. 1984, Hölttä 1986, Vaasjoki and Sakko 1988).

The NW-SE trending Raahe-Ladoga zone (Fig.1) is a major strike-slip fault system (Gaál 1972, Talvitie 1975). The faults also had a vertical component, leading to a block structure (Korsman et al. 1984, Luosto et al. 1984)). The zone is characterized by a negative gravity anomaly, Ni-Cu deposits (Gaál 1972), and a distinctive Pb isotopic composition of galenas (Kouvo and Kulp 1961, Vaasjoki 1981). Along the boundary of the Savo Schist Belt, parallel to the Raahe-Ladoga zone, a major suture zone has been delineated (Koistinen 1981). Paleomagnetic data (Neuvonen et al. 1981) and Sm-Nd isotopic studies of plutonic rocks from both sides of the suture zone (Huhma 1986) suggest the existence of an Archean basement northeast of the suture zone, below the Proterozoic cover rocks.

## THE TAMPERE SCHIST BELT

The narrow, discontinuous, approximately E-W trending Tampere Schist Belt lies between a large area of granitoids to the north, and migmatitic gneisses to the south (Fig. 1). Its length is about 200 km and maximum width is about 20 km. The Hämeenkyrö batholith and the Värmälä stock are in the central part of the belt, near Tampere (Fig. 3).

The metavolcanic rocks of the belt were originally mafic to felsic pyroclastics, and minor mafic sills, lavas and felsic tuffites. The metasedimentary rocks were turbiditic greywackes and mudstones, and conglomerates with predominantly volcanic clasts (Sederholm 1897, Seitsaari 1951, Simonen 1952, Matisto 1977, Ojakangas 1986). Intermediate rocks with calc-alkaline affinities are the most common metavolcanic rocks (Kähkönen 1987).

The rocks were metamorphosed near the greenschist facies — amphibolite facies transition (Simonen and Neuvonen 1947, Seitsaari 1951, Campbell 1978). Based on existing mineral assemblages, Campbell (1978) estimated conditions between 500°C, 1.5 kb and 600°C, 3 kb for the peak of metamorphism in Ylöjärvi (Fig. 3). Likewise, Mäkelä (1980) suggested conditions of ca. 550°C, 2.5 kb in Viljakkala. Törnroos (1982) estimated a considerably higher pressure of 6—7 kb by sphalerite geobarometry for the culmination of metamorphism in the Tampere Schist Belt. The estimation of peak metamorphism is complicated by the fact that retrograde alteration phenomena are common in the rocks.

According to Simonen (1952), near Tampere the metaturbidites are lowermost in the stratigraphic sequence. They are overlain by felsic metatuffites, and uppermost in the sequence are intermediate and mafic metavolcanic rocks separated into two units by a metaconglomerate interlayer. Kähkönen (1987) called the metavolcanic rocks in the

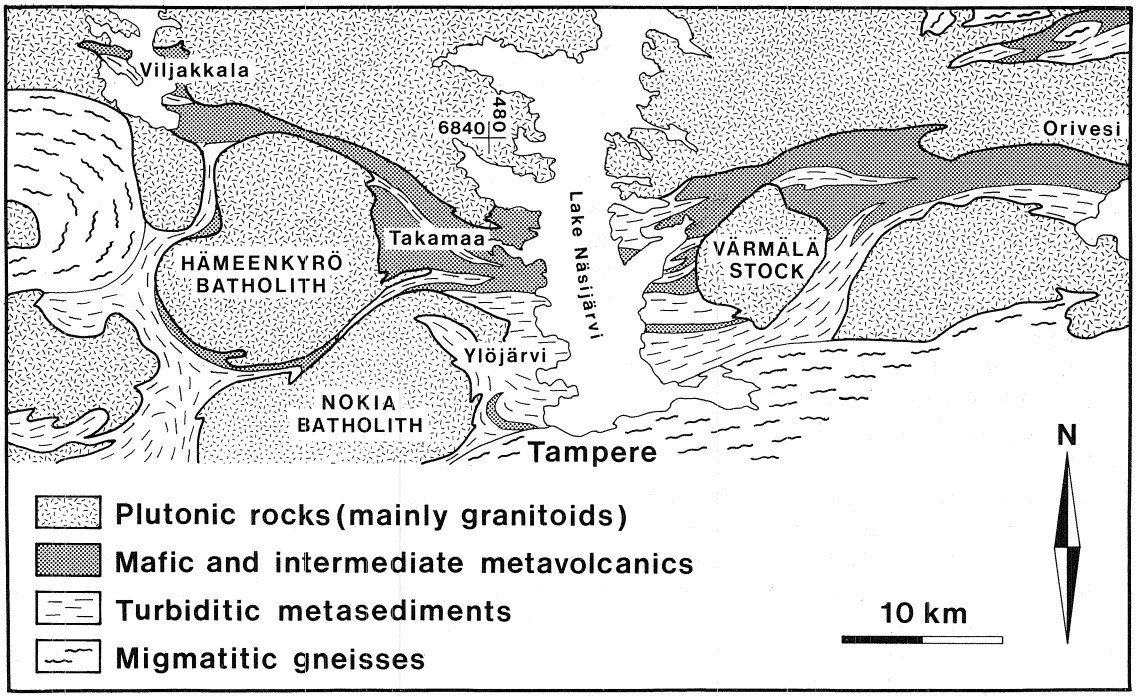


Fig. 3. Geological map of central Tampere Schist Belt (modified from Seitsaari 1951, Huhma et al. 1952, Simonen 1953a, Matisto 1961, Matisto 1964, Matisto 1967 and Laitakari 1986)

Ylöjärvi-Takamaa area (Fig. 3) below and above the metaconglomerate the Lower Volcanic Unit and the Upper Volcanic Unit, respectively. The mainly volcanic sources of the lowermost metaturbidites indicates an earlier volcanic episode, or volcanism contemporaneously with deposition (Ojakangas 1986). Campbell (1978) tentatively suggested contemporaneous formation for the volcanics and the turbidites in laterally different areas, and juxtaposition of the two by "pre-tectonic" thrusting. So far, there is no evidence for such early thrusting.

## Structures

Primary structures (graded bedding, cross bedding, convolute bedding, channelling, load structures) are well preserved, especially at the shore-line of Lake Näsijärvi (Sederholm 1897, Simonen and Kouvo 1951, Ojakangas 1986). Top of strata directions of metaturbidites and the orientation of the earliest tectonite fabric indicate that there is a major E-W trending $F_1$ syncline in the northern part of the belt, with minor upright synclines and anticlines in the limb areas (Fig. 4; Nironen, in press). Hence, the wavelength of $F_1$ folds varies from less than a meter to over a kilometer. Open to isoclinal mesoscopic $F_1$ folds vary in style from similar in mica-rich lithologies (Fig. 5) to parallel in greywacke units. Fold axes are subhorizontal to steep, the latter occurring in the marginal areas of the belt. The penetrative, subvertical $S_1$ schistosity, striking approximately E-W, is expressed as a preferred orientation of micas in metaturbidites, and as an elongation of hornblende and biotite in pyroclastic rocks. In the limb areas of isoclinal $F_1$ folds, the lithologic

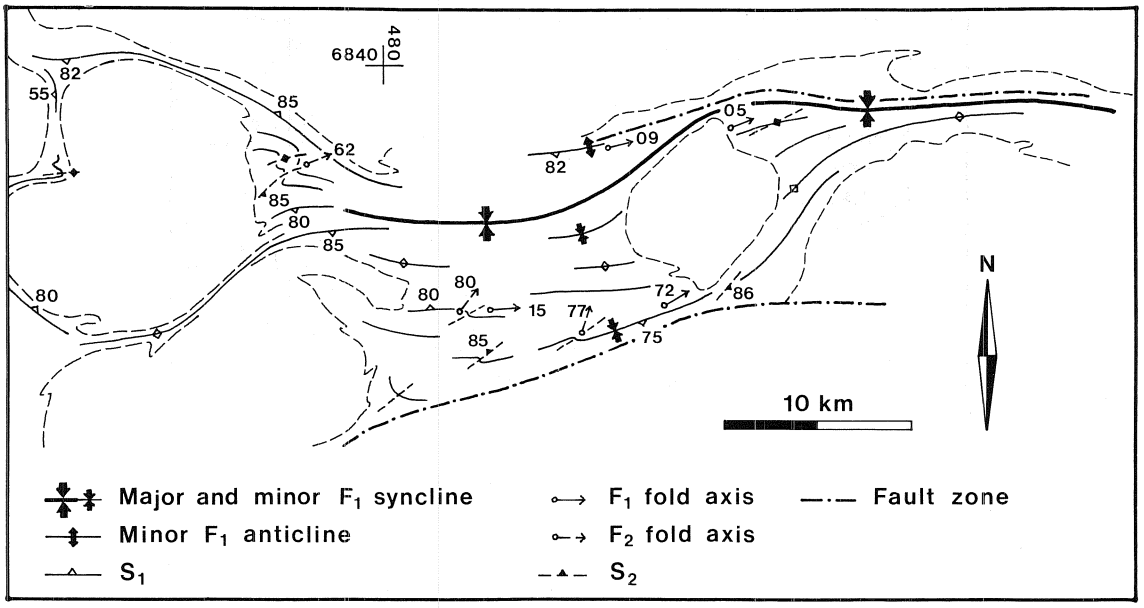


Fig. 4. Structural map of central Tampere Schist Belt.

layering is transposed into subparallelism with $S_1$. In places $S_1$ grades into mylonite zones from a few centimeters up to several meters wide.

The steeply to vertically plunging $L_1^1$ mineral stretching lineation is seen as an elongation of mica and quartz. In metaconglomerates and fragmented metavolcanics, $L_1^1$ is expressed as an elongation of pebbles and fragments, respectively.

The boundary between the Tampere Schist Belt and the migmatitic gneisses to the south is sharp. Near the boundary, $S_1$ dips steeply to the south in the schists. The intensity of $S_1$ increases toward the boundary, and the granodiorite pluton emplaced in the boundary zone is mylonitic. The increase of strain, the abrupt change of metamorphic grade together with an aeromagnetic and topographic lineament indicate that the boundary is a major shear zone. Asymmetric porphyroclasts (Passchier and Simpson 1986) and S-C textures (Berthé et al. 1979) observed in samples from several sites within the mylonitic granodiorite (Nironen, in press) indicate uplift of the southern part with respect to the northern part.

Another shear zone trends E-W in the northern part of the belt (Fig. 4). Vertical mylonitic foliation and associated steeply plunging stretching lineation within the shear zone are in places deformed by later ($D_2$) crenulation. A cataclastic overprint largely obscures the mylonitic foliation.

Open to tight $F_2$ folds, with wavelength varying from a few centimeters to several meters, are found especially in micaceous rocks. The folds are similar in style, asymmetric and have dextral vergence with respect to $S_1$. Subvertical axial surfaces range from E-W to NE-SW in strike, and fold axes plunge steeply to the east. Although $F_2$ folds occur all over the central Tampere Schist Belt, they dominate the structure only in localized zones. $S_2$ crenulation cleavage is widespread albeit weak, except in zones dominated by $F_2$ folding. $S_2$ is subvertical and has dextral vergence with respect to $S_1$. The development of $F_2$ microfolds was associated with retrogressive growth of $MS_2$—$MP_2$ biotite, muscovite and chlorite.

The effects of $D_3$ deformation were minor. Monoclinal $F_3$ kink folds with kink band widths from some millimeters to some tens of centimeters occur together with en echelon extensional fractures. The moderately to steeply dipping kink planes usually strike NW-SE to NNW-SSE, having

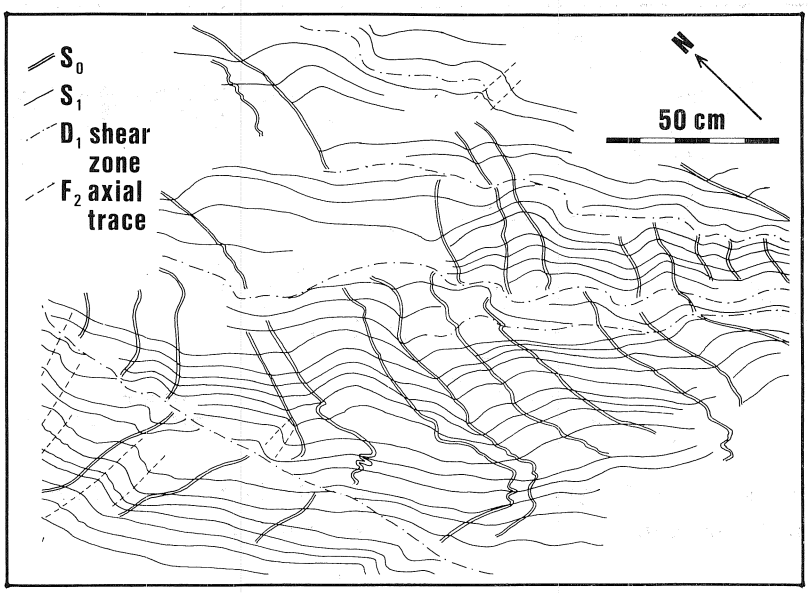


Fig. 5. $F_1$ fold closure with refracted $S_1$ and $D_1$ shear zones, overprinted by weak $F_2$ folding. Takamaa, Ylöjärvi. Sketch drawn from a photo mosaic.

sinistral sense of movement with respect to $S_1$. Also very open kink folding with N-S striking kink planes and varying movement sense, NE-SW striking planes with dextral sense of movement, and extensional, NW-SE striking dextral kink folds were observed. Biotite is altered into chlorite in the zones, and the fractures are filled with K-feldspar, carbonate or quartz.

Campbell (1978) distinguished a deformational sequence with five folding phases in the Ylöjärvi-Takamaa area (Fig. 3). He observed rare opposite younging directions on the single limbs of folds (named as $F_1$ by the author) in graded metagreywacke at the western shore-line of Lake Näsijärvi. He inferred the opposite sedimentary facing directions due to either penecontemporaneous slumping in unconsolidated sediments, or to an early phase of recumbent folding. Partly based on evidence of Simonen and Kouvo (1951), Campbell (1978, Fig. 4—3) constructed a profile of tight main folding, assuming that the fold axis plunges 30° to the east. However, his measurements of fold axes (Campbell 1978, Fig. 4—2) imply that the fold axis is almost horizontal on an average, and that the folding is isoclinal. In such a case, the attitude of structural facing to sedimentary facing can be determined only at hinge areas, because primary layering and axial plane schistosity are subparallel on the limbs. Moreover, inverted grading may occur at the base of turbiditic beds (Stow 1986, p. 416). Although the possibility of local early folding exists, the ambiguity of the rather poorly documented evidence, and the lack of supporting evidence such as identification of fold hinges and tectonite fabric, led the author to dismiss an early, pre-$F_1$ recumbent folding in the structural sequence.

In addition, Campbell (1978) identified folds which overprint $F_1$ folding ($F_2$ of Campbell) but are themselves refolded by the dextral $F_2$ folding ($F_4$ of Campbell). The folds, denoted as $F_3$ by Campbell, occur only in mica-rich lithologies in a small area in the Takamaa area (Fig. 3). They are open to tight, with wavelengths of a few centimeters. The gently dipping crenulation cleavage, associated with weak mica growth, and the older composite foliation produce a moderately to gently SE plunging intersection lineation

(Campbell 1978, Fig. 4—5). Because of refolding, the original orientation of the crenulation surfaces is uncertain. It is improbable that the structures are due to local strain heterogeneity during early $D_2$, because the orientation of the crenulation surfaces and intersection lineations differ considerably from the axial planes and axes of the $F_2$ folds ($F_4$ folds of Campbell). Because of limited data and local occurrence, the author did not consider these structures as due to a separate deformation phase, although their origin remains obscure.

## Structural and kinematic analysis

The E-W strike of $F_1$ fold axial surfaces indicate large scale horizontal shortening along the present N-S direction during $D_1$. In the marginal areas of the belt, the originally subhorizontal $F_1$ fold axes were reoriented toward the direction of maximum finite extension, i.e. the steeply plunging $L'_1$ stretching lineation (e.g. Escher and Watterson 1974). The strain analysis of Campbell (1978) on deformed clasts in metaconglomerates and agglomerates indicates that strain was of the apparent flattening type in the Takamaa area. Deformation may have started as bulk shortening, with a simple shear component leading to the development of shear zones.

The south dipping $S_1$ at the southern boundary of the Tampere Schist Belt and the kinematic indicators in the mylonitic granodiorite imply that the southern shear zone is a thrust or reverse fault zone with vergence to the north. The increase of $D_1$ strain toward the boundary, and the $D_2$ structures overprinting the mylonitic foliation in the northern zone suggest that both shear zones were formed at a late stage of progressive $D_1$ deformation.

The peak of metamorphism and anatexis in the migmatites was associated with $D_2$ deformation (Campbell 1980). The E-W striking, steeply dipping $S_2$ schistosity and small shear zones, crosscutting $S_2$ at small angles near the southern fault, indicate that $D_2$ in the migmatites can possibly be correlated with $D_1$ in the schists. Studies at the eastern termination of the Tampere Schist Belt (Nironen and Bateman, in press) suggest that the main, penetrative foliation in that area overprints a weak tectonite fabric. Hence, the central part of the belt may represent a relatively high crustal level where sedimentation was still in progess during the earliest deformation, with the possible development of synsedimentary faults.

Campbell (1978) correlated his rare $F_3$ structures, described above, with large scale folds which govern the macroscopic structure of the migmatites immediately south of the schists. He admitted the difficulty in correlation, because the large scale folds have subvertical axial surfaces (Campbell 1980), whereas he inferred the small folds in the Takamaa area to have gently dipping axial surfaces. He assumed that initial subhorizontal compression resulted in upright folding, and continued compression led to lateral translation of rock masses to the present N-NE and the formation of $F_3$ folds. Another possibility is that the two folding events are unrelated; the large scale folding may have been formed during the juxtaposition of the migmatites along the thrust against the schists.

Campbell (1978, p. 68) considered, in terms of kink fold theory and experiments in multilayers (Reches and Johnson 1976), that the dextral $F_2$ folds ($F_4$ folds of Campbell) were formed by sinistral transpression (simultaneous horizontal shortening and horizontal sinistral shear), which initially produced dextral layer-parallel shear and monoclinal, dextral kink-folding (Fig. 6a). Although the experiments show that dextral kink folds may be generated during sinistral transpression, they do not support the development of tight folds with well developed axial plane cleavage. Moreover, the vergence of $S_2$ crenulation in areas where $F_2$ folds have not developed is incompatible with sinistral transpression, applying the model of Gray and Durney (1979) for the development of crenulation cleavage. An alternative interpretation with an E-W oriented, horizontal dextral shear is presented (Fig. 6b). The dextral shear caused buckling of the layering and intense development of $F_2$ folds in appropriate lithologies where $S_1$ trended NW-SE, i.e. was at high angles to to the maximum

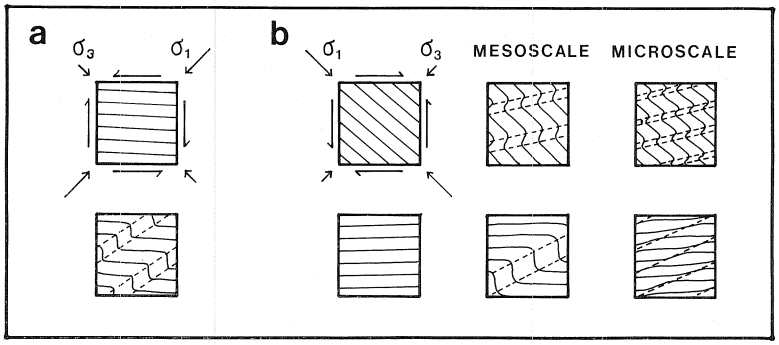


Fig. 6. Kinematic models for the development of $D_2$ structures in central Tampere Schist Belt. a) Campbell's (1978) model: sinistral shear, leading to layer-parallel shear and monoclinal kink folding. b) The author's model: dextral shear. Orientation of pre-existing foliation determines the deformation style and orientation of $F_2$ axial surfaces.

compression direction. In areas with E-W to WSW-ENE strike of $S_1$, local $F_2$ folds and dextral crenulation developed. The reorientation of $S_1$ from the original E-W strike was due to the emplacement of the plutonic bodies (see p. 26).

The prevalence of NW-SE to NNW-SSE striking monoclinal $F_3$ kink folds suggests that the principal compressional stress during $D_3$ was inclined from the orientation of $S_1$ toward NW-SE direction, producing dextral layer-parallel shear (cf. Cobbold et al. 1971, Reches and Johnson 1976). However, the existence of extensional kink folds implies that all the observed structures cannot be explained by such a mechanism. The data of $D_3$ structures is too limited for a detailed kinematic analysis.

## THE HÄMEENKYRÖ BATHOLITH

The Hämeenkyrö batholith is 14 km x 15 km in size and covers a 147 km$^2$ area (Fig. 7). Between the batholith and adjacent plutonic bodies there are rocks of mainly volcanic origin (pyroclastics, conglomerates), with intercalations of meta-turbidites.

The batholith consists of multiply intruded rocks ranging in modal composition from tonalite to monzogranite (Front 1981). The prevailing rock type is granodiorite. The distribution of the main rock types shows normal zoning, the most felsic and silicic ones being in the center. Grainsize increases from 1—4 mm in the marginal tonalites to 3—6 mm in the granite. The rocks are equigranular or slightly porphyritic with subhedral microcline megacrysts and zoned, subhedral to euhedral plagioclase megacrysts 5—15 mm in length. The megacrysts may be considered as phenocrysts, i.e. megacrysts grown in magma, applying the criteria of Vernon (1986). The anorthite content of plagioclase diminishes from $An_{44—40}$ to $An_{16—12}$ toward the center of the pluton (Front 1981). Microcline also occurs as strongly poikilitic megacrysts, suggesting late stage crystallization. All rock types contain hornblende and biotite in approximately equal proportions. Hydrothermal alteration (propylitic alteration, scapolitization, tourmalinization) is widespread at the eastern margin (Gaál et al. 1981).

Contacts between the granitoid types have not been observed, except at the southeastern margin where granodiorite brecciates tonalite. The

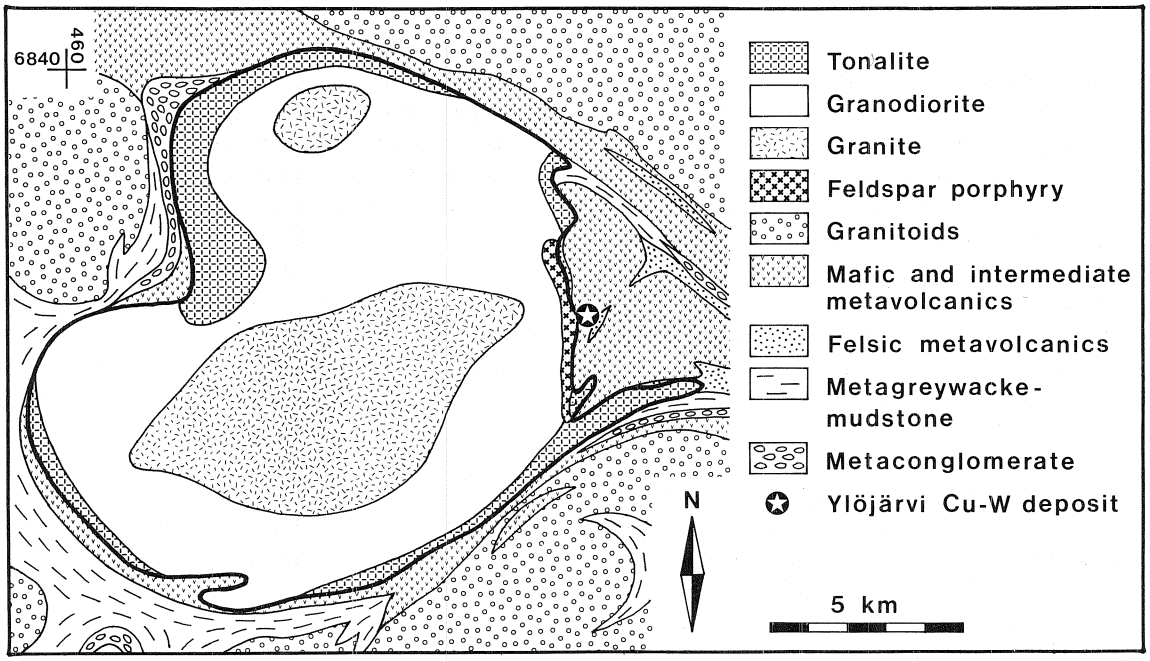


Fig. 7. Geological map of the Hämeenkyrö batholith and surrounding schists (based on Gaál et al. 1981 and the author's observations).

granodiorite and the granite can be distinguished as separate phases by major element ratios (see below), although the modal compositions between the phases slightly overlap. Hence, the main phases of the pluton are the marginal tonalite, the prevailing granodiorite, and the granite (Fig. 7).

Two types of porphyritic rock, a feldspar porphyry and a plagioclase porphyry, occur at the eastern margin (see also Simonen 1952, Gaál et al. 1981). They crosscut country rocks, older plutonic rocks and each other. The pink feldspar porphyry of granitic to granodioritic composition is areally more significant (Fig. 7). It is characterized by euhedral, zoned plagioclase with albitic rims, microcline phenocrysts, and micrographic intergrowth of microcline and quartz. There are aplitic portions in the feldspar porphyry. The plagioclase porphyry occurs sporadically in the center of the eastern margin, and extends into country rocks around the Ylöjärvi Cu-W deposit (Himmi et al. 1979). It is a dark, biotite-rich rock containing euhedral, zoned andesine phenocrysts. Gaál et al. (1981) considered the plagioclase porphyry as the youngest phase of the batholith. The equivocal emplacement chronology between the porphyries is possibly due to different viscosities of contemporaneously intruded magmas (cf. Marre 1986, p. 59).

The only dikes that were observed in the batholith are few aplite dikes and even fewer dark, dioritic dikes. The dikes are usually less than 20 cm wide, and they generally rectilinearly crosscut their host plutonic rocks. However, near the southeastern contact where the plutonic rock is strongly foliated, the aplite dikes are also deformed, although less than the host granodiorite. They dip steeply but do not show any distinct systematics in strike.

Tourmaline and tourmaline-quartz veins and breccias crosscut all the above-mentioned rock types. They occur at several localities along the eastern margin. The Ylöjärvi Cu-W deposit is within a tourmaline breccia (Himmi et al. 1979).

## Structure

The main foliation (Fig. 8) in the schists surrounding the Hämeenkyrö batholith is commonly a $S_0$-$S_1$ transposition structure associated with metamorphic layering. It is locally overprinted by $F_2$ mesoscopic folding and associated $S_2$ crenulation cleavage, especially in sericite schists (altered tuffites). The contact between the batholith and the schists is best exposed at the eastern margin, where feldspar porphyry is at the contact. Here, the weakly developed $S_1$, striking at high angles to the contact, can be distinguished from $S_0$. The contact is angular in mesoscale, and no foliation parallel to it could be observed. Similarly, at the western contact where the trend of the schists changes from E-W to N-S (Fig. 7), $S_0$ is parallel to the contact whereas $S_1$ strikes E-W. Elsewhere, $S_1$ is subparallel to the contact of the batholith. The few observed granitoid apophyses in the schists show asymmetric pinch and swell structures along $S_1$.

In the batholith, the northwestern, southeastern and central parts are isotropic or weakly foliated. Foliation intensity increases toward the northern and southern margins, and the southern contact is mylonitic. The steeply dipping to vertical foliation is subparallel to contacts at the northern and southern margins, but at high angles to contact at the eastern margin (Figs. 8 and 9). The fabric is of the S type except at the southern margin where it is L<S to L=S in the mylonitic rock. Here, the feldspar phenocrysts are aligned subparallel to the foliation, with c-axes parallel to the mineral lineation. The foliation occurs as fractures and seams of preferentially aligned dark minerals. In microscale, deformation is seen as recrystallization of quartz into fine-grained seams, fracturing of feldspars, and kinking of biotite. In intensely deformed rocks, hornblende is altered into biotite which occurs as anastomosing fine-grained seams. In addition to penetrative deformation, discontinuous deformation occurs as mylonite zones (some tens of centimeters wide) and as thin (less than 1 cm wide), anastomosing shear zones between domains of moderately strained rock. Discontinuous deformation occurs typically along the northern and southern margins. The shear zones continue across the contact into the schists (Fig. 10a).

The foliation in the pluton is mostly related to $S_1$ in the schists. At one outcrop at the western contact, the contact-parallel foliation in the plutonic rock is clearly crenulated by $D_2$. The crenulation is expressed as bent and fractured plagioclase, recrystallized quartz and kinked biotite.

In the central part of the batholith, zones of high strain occur between nearly isotropic domains. These zones occur on all scales, i.e. they are from a few millimeters to several meters wide. Typically they are ductile shear zones with subhorizontal shear direction, but also cataclastic fractures with no visible movement sense occur. The cataclastic fractures occur as seams with crushed rock material and carbonate filling. Some fractures are parallel to $S_2$ in the schists, indicating that at least some zones were formed during $D_2$.

The tourmaline breccia, the host rock of the Ylöjärvi deposit, occurs as two subvertical zones which trend roughly parallel to the lithological layering. Himmi et al. (1979) suggested that the breccia was formed by explosion of mineralizing fluids, derived from the Hämeenkyrö batholith. An explosive origin for brecciation and mineralization is supported by the exceptionally high pressure of about 7.5 kb, obtained by sphalerite geobarometry (Törnroos 1982). Although the southeastern margin of the breccia is a shear zone, Himmi et al. (1979) concluded that the brecciation was not controlled by tectonic movements. A NE-SW trending zone of high strain continues from the Ylöjärvi Cu-W deposit into the batholith (Fig. 9). In the feldspar porphyry, plagioclase grains are disrupted, and biotite is strained, showing microkinking. In the country rock, the mafic tuffite has been retrogressed into a tourmaline-bearing chlorite schist. $MS_2$ chlorite, still showing the earlier, crenulated fabric, wraps around tourmaline grains, but in places tourmaline prisms clearly crosscut the chlorite (Fig. 10b). This evidence suggests, although not conclusively (e.g. Ferguson and Harte 1975), close temporal association between $D_2$, tourmalinization and mineralization (see also Gaál et al. 1981).

The zone of high strain in the area of the deposit and other minor zones differ in strike from $F_2$ axial trend where $D_2$ was less intense. The zones probably

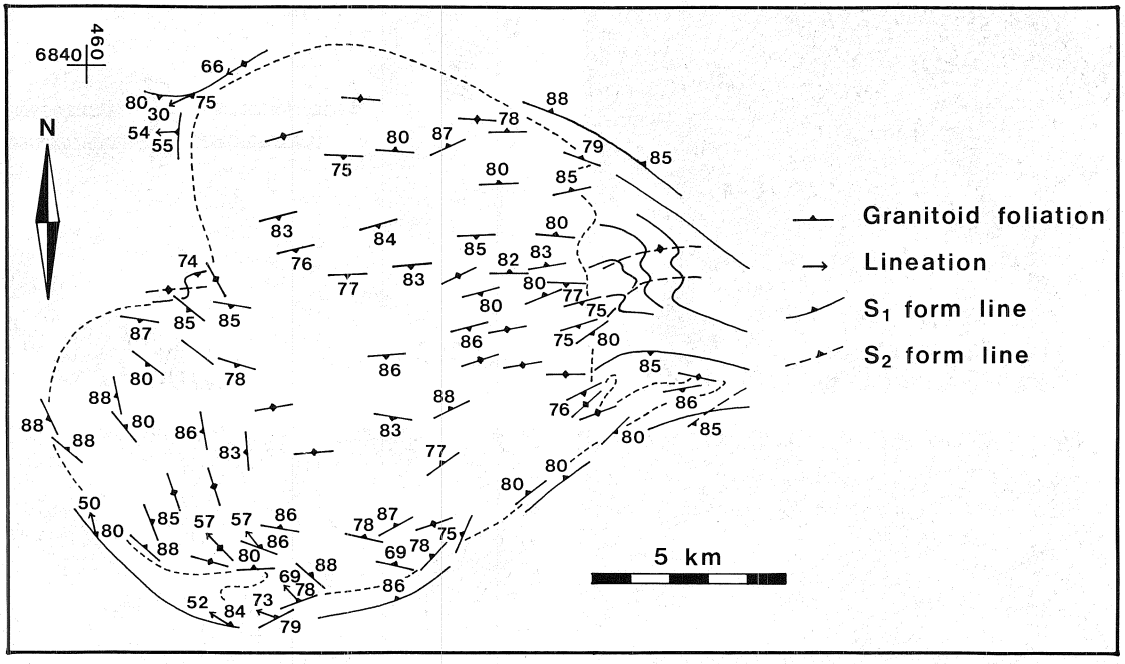


Fig. 8. Structural map of the Hämeenkyrö batholith and surrounding schists.

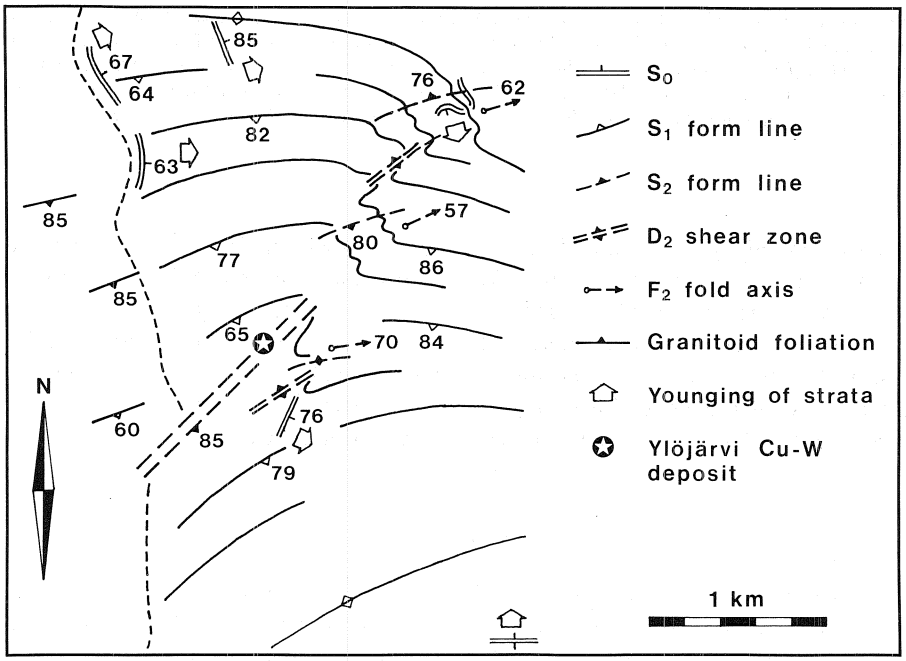


Fig. 9. Map of structures near the eastern contact of the Hämeenkyrö batholith.

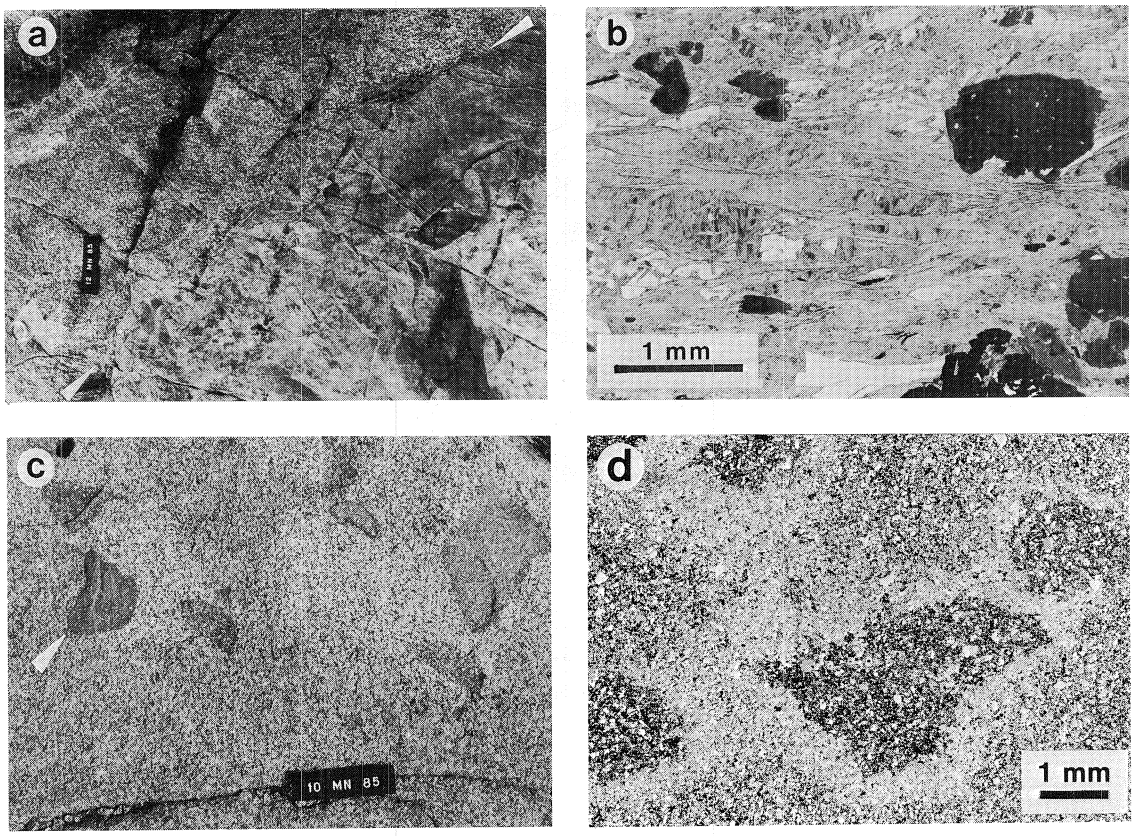


Fig. 10. a) Southeastern contact of the Hämeenkyrö batholith. Shear zones crosscut the contact (shown by arrows) between tonalite and metatuffite. Length of scale bar 20 cm. b) Photomicrograph, showing $MS_2$ chlorite flakes wrapping around tourmaline and ore minerals, and in places crosscut by tourmaline. Chlorite schist near the Ylöjärvi deposit. c) Microgranitoid enclaves in granodiorite near the southeastern contact of the Hämeenkyrö batholith. The enclave at the left (shown by arrow) consists of two rock types. d) Photomicrograph of biotite (?) pseudomorphs in felsic schist at the eastern contact of the Hämeenkyrö batholith. Nicols partly crossed.

developed by shearing along the limb of $F_2$ folds. Such shear zones, deviating in strike from the axial plane foliation, are not uncommon in heterogeneous lithologies (e.g. Ramsay 1967, p. 388—389). The shear zone probably controlled the explosion of the mineralizing fluids that generated the Ylöjärvi deposit. Another zone of intense $S_2$ development (not shown in Fig. 9) is characterized by tourmalinization, mineralization and alteration of the intermediate volcanics into sericite schists. At other localities along the eastern contact, tourmaline and tourmaline-quartz veins mimetically take up the orientation of older structures ($S_0$ or $S_0$-$S_1$), or they rectilinearly crosscut the latter.

## Enclaves

Two main types of enclaves were encountered in the Hämeenkyrö batholith. Along the eastern, southeastern and western contacts, especially in the feldspar porphyry, there are rounded or subangular enclaves within a few meters or tens of meters from the contact. Most of the enclaves are xenoliths of metavolcanic or metasedimentary wall rock schists. They range in diameter from a few

centimeters up to 3 meters. Feldspar megacrysts are common in the felsic xenoliths. Hornfelsing has overprinted structures, and the hazy, rounded contacts suggest rather strong assimilation and a low viscosity for the magma (cf. Marre 1986, p. 76). The subangular mafic metavolcanic xenoliths are better preserved. According to Didier (1987), the subangular character of xenoliths indicate small transport distance. Normally the xenoliths do not have a preferred elongation, but at the southeastern contact they tend to be aligned parallel to the foliation of the host plutonic rock.

The other main type consists of dark, fine-grained enclaves which occur all over the batholith (maximum enclave density 3/m$^2$). They are usually roundish or ovoidal in plan but in places subangular, ranging from a few centimeters to some tens of centimeters in length. Where the host rock is foliated, the enclaves are elongated subparallel to the foliation. The composition of the enclaves ranges from tonalite to diorite. Few enclaves consisting of two rock types were encountered (Fig. 10c). They may be parts of double enclaves (see Didier 1973, p. 147). The subhedral, zoned ($An_{32-20}$) plagioclase phenocrysts, uralite aggregates with rare relics of pyroxene, and apatite needles suggest igneous origin, although the texture is granoblastic rather than igneous in some enclaves. Hence, they can be regarded as microgranitoid enclaves (Vernon 1983). K-feldspar occurs as euhedral megacrysts several millimeters in diameter. According to Vernon (1986) and Didier (1987), feldspar megacrysts in the enclaves of granitoid bodies are phenocrysts due to introduction of material from granitoid magma into mafic magma. Similarly, small felsic blobs in some enclaves may be relics of granitoid magma trapped in mafic magma.

## Contact metamorphism

Because of poor outcrop, contact metamorphic effects were observed only along the eastern margin where dark grey spots can be seen in fine-grained felsic schists (tuffites and sedimentary rocks) within a few tens of meters from the contact. The spots are slightly elongated in plan with longitudinal orientation parallel to $S_1$. They range in length from a few millimeters up to one centimeter. The spots are mica-rich (mainly biotite) and have light-colored K-feldspar-quartz rims (Fig. 10d). The groundmass has a hornfels texture and consists mainly of quartz, plagioclase and biotite. The potassium-rich composition of the spots suggests that they are pseudomorphs after biotite, rather than staurolite or cordierite, which grew due to the thermal effect of the intruding pluton. The felsic rims were formed during the growth of the porphyroblasts, or the porphyroblasts were recrystallized and segregated into a biotite-rich inner part and K-feldspar-rich outer part during lower temperature. It is noteworthy that the small biotite flakes in the spots are oriented parallel to the schistosity.

## Geochemistry

The rock types in Fig. 7 were distinguished by petrographic criteria as well as chemical and modal compositions. The rock nomenclature differs from that of Gaál et al. (1981), because they used the normative (Barth's mesonorms) compositions instead of modal ones.

The variation diagrams of $TiO_2$, MgO, FeO* and CaO against $SiO_2$ (Fig. 11) define fairly straight linear trends with a negative slope from 52 % to 70 % $SiO_2$, i.e. from the marginal tonalite through granodiorite and granite to feldspar porphyry. The tonalite and granodiorite form a continuous trend, but in the MgO versus $SiO_2$ diagram, the granite and feldspar porphyry form separate groups. The plagioclase porphyry analyses plot close to the tonalite and granodiorite. In the $Al_2O_3$ versus $SiO_2$ diagram, there is a negative slope from 52 % to 66 % $SiO_2$, followed by an abrupt change into a

* Total Fe is expressed as FeO throughout the text.

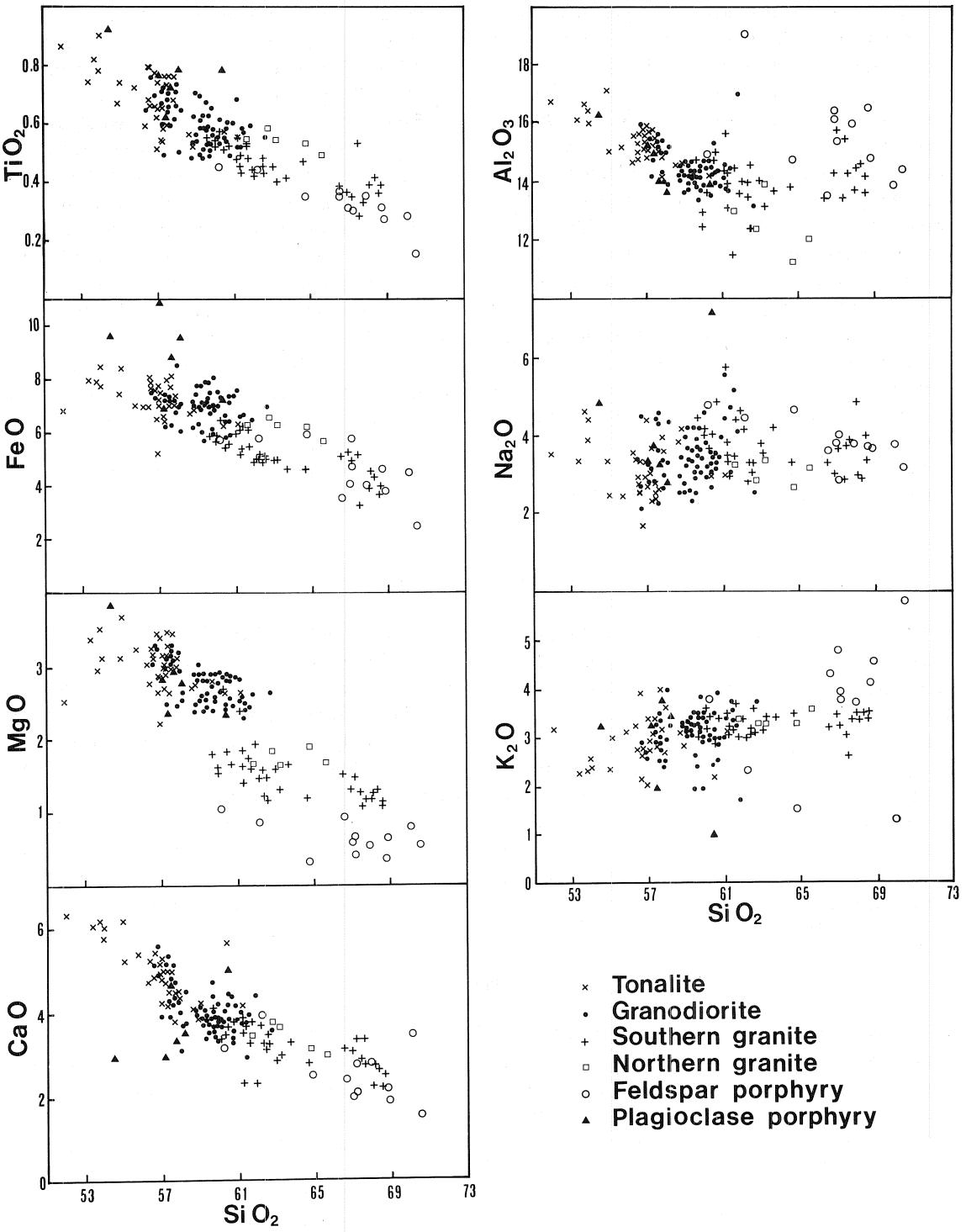
TiO2
FeO
MgO
CaO
Al2O3
Na2O
K2O
SiO2
Tonalite
Granodiorite
Southern granite
Northern granite
Feldspar porphyry
Plagioclase porphyry

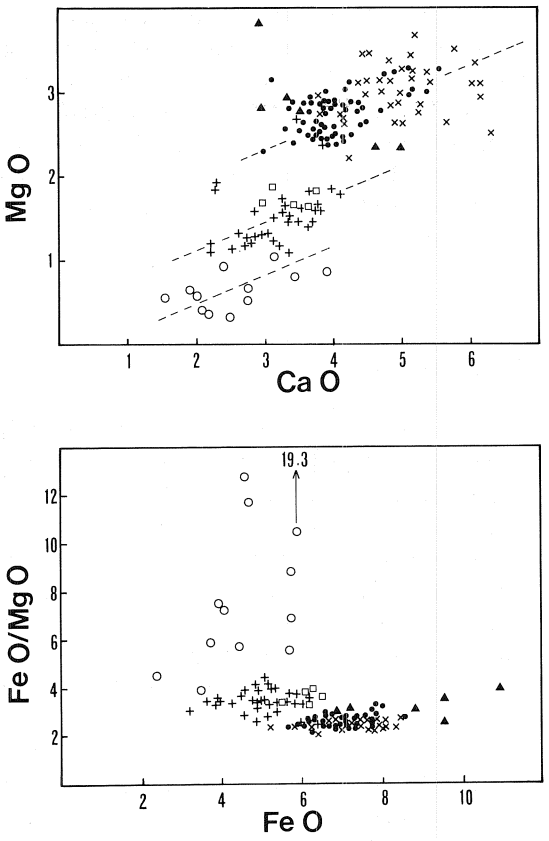


Fig. 11. Variation diagrams for rocks of the Hämeenkyrö batholith (165 analyses). Total Fe expressed as FeO (in all figures).

positive slope. $Na_2O$ and $K_2O$ contents are rather constant within the silica range, although the $K_2O$ content of the feldspar porphyry varies considerably.

In MgO versus CaO, there is a positive correlation with the two elements from feldspar porphyry to tonalite. All the rock types form separate groups. Within each group, the MgO/CaO ratio has a regular trend. In the FeO/MgO versus FeO diagram, each granitoid phase has a rather constant FeO/MgO ratio regardless of change in FeO content, a characteristic already noted by Front (1981). The feldspar porphyry is distinct for its high and highly variable ratios. The constant-ratio trend in the FeO/MgO versus FeO diagram is possibly due to (simultaneous?) crystallization of hornblende and biotite in equal proportions.

The tonalite is chemically fairly similar to the granodiorite, but the slightly different FeO/MgO ratios and the brecciating contact observed between the two rock types show that they are separate phases. The slightly higher $TiO_2$, MgO and FeO arithmetic mean compositions of the northern granite (see Fig. 7) led Front (1981) to consider it as a separate, somewhat older phase. The most $SiO_2$-enriched (over 66 % $SiO_2$) granites occur in the center of the southern granite. The compositional gap in the southern granite, best visible in the MgO-$SiO_2$ diagram, is hardly due to simple fractional crystallization is situ. Hence, the granite may have injected as two or three phases to the final emplacement level.

The feldspar porphyry is evidently the most evolved phase of the magma. It is distinct from the other phases by high and variable FeO/MgO ratios and Ba contents (diagram not shown). Although the plagioclase porphyry plots close to the tonalite-granodiorite range in major element variation diagrams, the age difference and the high FeO content of the plagioclase porphyry do not support a direct comagmatic relationship with the granitoids.

Partial melting of igneous material involving melt-restite unmixing (White and Chappell 1977), or mingling between a felsic (granitoid) and a mafic magma (e.g. Vernon 1983) are possible mechanisms to account for the microgranitoid enclaves in the Hämeenkyrö batholith. In the former case, they would represent the unmelted restite and in the latter case blobs of mafic magma. The igneous texture of most enclaves and the felsic blobs in some enclaves favor magma mingling. According to Didier (1987), several types of enclaves indicate several mingling processes, but as Pitcher (1987) pointed out, even comagmatic enclaves may have various origins, e.g. as restites, wall rock accumulations or wall-rocks of comagmatic volcanics. However, neither magma mixing and mingling nor partial melting can fully explain the chemical characteristics of the Hämeenkyrö batholith.

The separation of the phases in the FeO/MgO versus FeO and MgO versus CaO diagrams preclude any simple process to account for the zonation in the batholith. The high viscosity of

granitoid magmas makes fractionation by convection and crystal settling improbable (Rice 1981). Neither can the gaps be explained by interaction (assimilation, contamination) between the magma and country rock during continuous magma ascent. Injection of already differentiated magma as separate phases with decreasing age from the margins to the center is a more viable mechanism to explain the chemical characteristics. Differentiation in a deeper level, subsequent ascent of the magma as separated batches, and mixing and mingling between the batches with a basic magma may have brought about the compositional gaps. Fractional crystallization within each phase may have occurred at the final emplacement level. Thus the emplacement involved differentiation in two or more environments.

## Structural setting and emplacement

The continuation of $S_1$ into the plutonic rocks at the eastern contact of the Hämeenkyrö batholith (Fig. 9), the contact metamorphic pseudomorphs along the eastern contact that are foliated parallel to $S_1$, and the granitoid apophyses with pinch and swell structures along $S_1$ are indicative of the emplacement of the batholith before the end of $D_1$.

The relatively high strain in the schists along the southern and northern margins may be due to forceful emplacement, strain partitioning around the rigid pluton after emplacement, or a combination of these. A pre-$D_1$ diapiric emplacement would have caused a circular foliation within the batholith, overprinted by regional foliation. If the pluton was emplaced passively before $D_1$ and acted as a rigid body during $D_1$, at most the northern and southern marginal areas would be expected to be foliated. However, the general foliation pattern within the entire batholith is lenticular (Fig. 8). The lenticular pattern probably formed during the emplacement of the pluton at an early stage of $D_1$. During progressive $D_1$, the pluton acted as a rigid body, and the areas near the eastern and western contacts were strain shadows, leading to a weak development of $S_1$ in the schists.

Campbell (1978, p. 34) stated that the emplacement of the plutons around the schists in the Takamaa area (including the Hämeenkyrö batholith) took place after $D_2$ ($D_4$ of Campbell) because the plutons "grossly truncate the strike of $S_2$ and $S_4$ fabrics in the schists". He concluded that the major swing in strike of $S_1$ around the Hämeenkyrö batholith and the dextral vergence of $D_2$ structures throughout the central Tampere Schist Belt (Campbell's $S_2$ and $D_4$, respectively) are due to sinistral shear during $D_3$ (Campbell's $D_5$). The conclusion was based partly on the structural setting of the plutons. According to the interpretation of the author, the swing in strike of $S_1$ is due to the emplacement of the batholith during $D_1$. The shear zones in the central part of the pluton may be due to $D_2$ deformation, but no signs of major $D_3$ deformation (kinking, fracturing) was observed in the schists in the vicinity of the Hämeenkyrö batholith.

Because of the combination of continuous deformation (penetrative foliation) and discontinuous deformation (anastomosing zones of high strain), the bulk strain could not be deduced by mineral fabric. The scarcity of vertical outcrop surfaces prohibited the use of microganitoid enclaves as strain markers. The undeformed aplite dikes in the central part of the batholith indicate that deformation was minimal after the intrusion of the dikes in the central part except in zones of high strain. The general lack of mineral lineations implies that the major component of bulk progressive deformation during the emplacement of the batholith was subhorizontal flattening perpendicular to the contacts. Choukroune and Gapais (1983) pointed out that both continuous and discontinous deformation can develop within a single bulk inhomogeneous flattening event. The total strain within the pluton probably is a combination of regional ($D_1$) and emplacement strain.

When the emplacement mechanism of the batholith is considered, the concentric distribution of the main phases of the pluton with normal zoning must be taken into account. Major stoping is an

improbable mechanism, because large xenolith blocks within the pluton are lacking. Minor stoping took place during the intrusion of the feldspar porphyry.

The younging of strata in the triangular area east of the Hämeenkyrö batholith, including the east facing strata near the eastern contact of the batholith (Fig. 9) indicate that the triangular schist area is either a sedimentary basin, or a structural basin that developed during the diapiric emplacement of the batholith. In the latter case, the basin would be part of a rim syncline. A rim syncline is a structure that has rarely been described around plutons inferred as diapirs (see Burg 1987), although it characteristically forms around mature diapiric structures in centrifuge experiments (cf. Ramberg 1970). The lenticular foliation pattern within the pluton, the general S-type fabric, the growing intensity of granitoid foliation toward the southern and northern contacts and the warping of $S_0$ and $S_1$ into concordance with these contacts suggest a rather passive emplacement at first, and expansion as a ballooning pluton at a later stage. The geochemical trends indicate at least three pulses of magma, consistent with progressive ballooning.

The position of the most differentiated feldspar porphyry at the eastern margin is curious. Since it brecciates the granodiorite, it must have intruded after the margin of the batholith had already been solidified, as noted by Front (1981). Simonen (1952) suggested that the pluton is tilted, the highest structural level being at the eastern margin. However, the rock type distribution and geochemistry show rather concentric zonation, and structural evidence does not support tilting after emplacement.

## THE VÄRMÄLÄ STOCK

The roundish Värmälä stock (Fig. 12) is about 7,5 km in diameter and covers a 47 $km^2$ area. The geological setting of the pluton is analogous to the Hämeenkyrö batholith. Granodiorite, the most widespread rock type, is leucocratic, medium- to coarse-grained, and equigranular or slightly porphyritic. In the latter case there are subhedral feldspar phenocrysts (both plagioclase and microcline) from 0.5 cm up to 2 cm in size. The plagioclase phenocrysts are zoned with cores of oligoclase and rims of oligoclase-albite. Quartz occurs commonly as polycrystalline aggregates. Microcline and quartz occupy interstitial positions. Biotite, the main mafic mineral, occurs as a green (Z axis) and a brown type. Hornblende occurs only as a minor constituent. Metamict allanite is a characteristic accessory mineral in the granodiorite as well as in the other granitoids of the pluton. Zircon is abundant as inclusions in biotite. Chlorite, epidote and carbonate occur as alteration products.

Along the southern, western and northern margins, the rock is monzogranitic in composition (labelled as granite in Fig. 12) and slightly coarser in grainsize than the granodiorite. Sharp boundaries were observed between the two rock types, but the boundary may in places be gradational. The intrusion sequence between the granodiorite and the granite could not be determined in the field. Fluorite is a sporadic accessory mineral in the granite.

In the center of the pluton, there is a lenticular area occupied by a small- to medium-grained porphyritic rock ranging in modal composition from prevailing quartz monzodiorite to monzogranite (labelled as quartz monzodiorite in Fig. 12). The southwestern contact with the granodiorite is gradational over a few meters, but the rectilinear southeastern contact is a shear zone. Plagioclase occurs as small (1—2 mm), euhedral, distinctly zoned grains, with cores of oligoclase ($An_{22-15}$) and rims of albite. Subhedral microcline phenocrysts 4—15 mm in size contain inclusions of small, euhedral plagioclase laths with albitic rims. Quartz characteristically forms roundish aggregates 3—5 mm in diameter. The aggregates are slightly reddish due to hematite pigment. Quartz, microcline and biotite are the intestitial minerals. The euhedral plagioclase grains, with

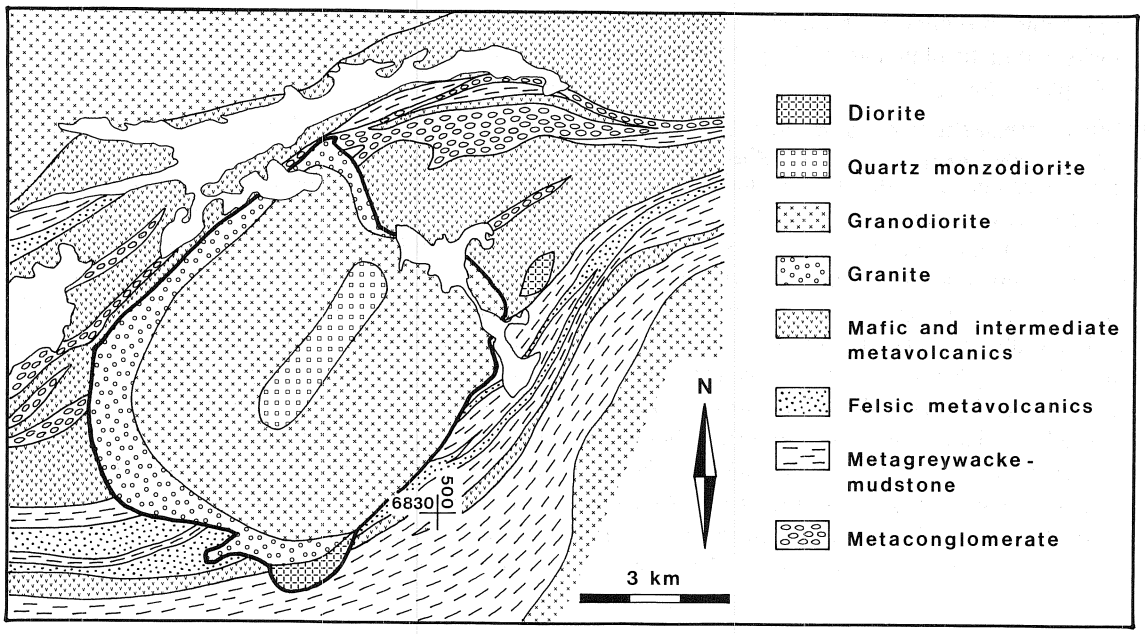


Fig. 12. Geological map of the Värmälä stock and surrounding schists (partly after Seitsaari 1951).

quartz in the interstices, suggest a cumulus texture (Fig. 13). In places subhedral biotite grains have a rim against microcline, consisting of small biotite clots. The texture is due to either reaction between biotite and melt, or intergrowth between interstitial microcline and biotite.

At the northern edge of the stock, another distinctly porphyritic rock with a granodioritic to monzogranitic composition is encountered in a small area (not shown in Fig. 12). Subhedral to euhedral microcline and zoned plagioclase ($An_{15-10}$) phenocrysts 2—5 mm in size are abundant in a fine-grained groundmass. Quartz aggregates 2—4 mm in size and with sharp, angular boudaries are characteristic of the rock type. The groundmass consists of quartz, K-feldspar and biotite. The texture and small areal extent suggest a dike rock, possibly even a subvolcanic one. Small molybdenite flakes were observed in this rock type.

At the southern margin of the Värmälä stock, there is a separate pluton with quartz dioritic to dioritic composition (labelled as diorite in Fig. 12). It is brecciated by the granodiorite at the contact. The rock is rather heterogeneous, fine- to medium-grained, and the texture is ophitic (see also Seitsaari 1951, p. 80). Plagioclase ($An_{50}$) occurs as elongate laths, and mafic minerals have altered into cummingtonite, biotite and chlorite.

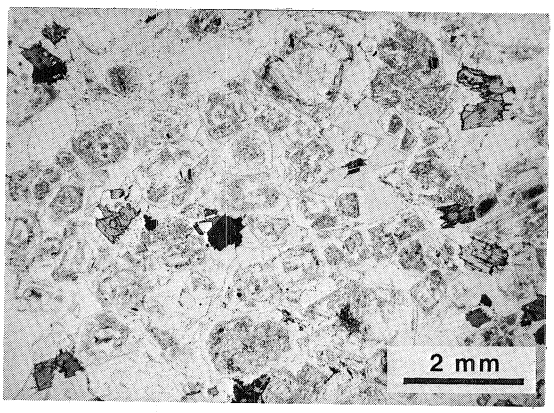


Fig. 13. Photomicrograph of the quartz monzodiorite in the Värmälä stock. Note the cumulate-type texture with euhedral plagioclase grains and interstitial quartz. Nicols parallel.

## Structure

The schists around the pluton exhibit well preserved primary layering. $S_0$ curves slightly toward parallelism with the contacts near the southern and northwestern margins, whereas at the western and northeastern parts the plutonic body truncates $S_0$ at high angles (Fig. 12). At outcrops, the plutonic rocks usually crosscut $S_0$ without causing deflection of strata.

The $S_1$ schistosity, subparallel to $S_0$, is generally well developed in the wall rocks. Foliation intensity is pronounced near the northern and southern contacts but almost negligible near the western and northeastern contacts where it strikes at high angles to the contact (Fig. 14). $L_1^1$ stretching lineation is well developed near the eastern contact. At the northern contact, $L_1^1$ can be discerned as an elongation of conglomerate pebbles, but the fabric is of the L<S type.

At outcrops, the plutonic rock seems to crosscut $S_1$ abruptly (Fig. 15a), but in places $S_1$ can be seen to continue across the contact into the marginal part of the igneous body (Figs. 15b and 15c). Granodiorite dikes injected into wall rock are parallel to $S_1$, but the dikes are also slightly boudinaged, with quartz crystallized in the boudin necks (Fig. 16). Granodiorite apophyses a few centimeters to some tens of centimeters thick occur in several places in the schists near the contacts.

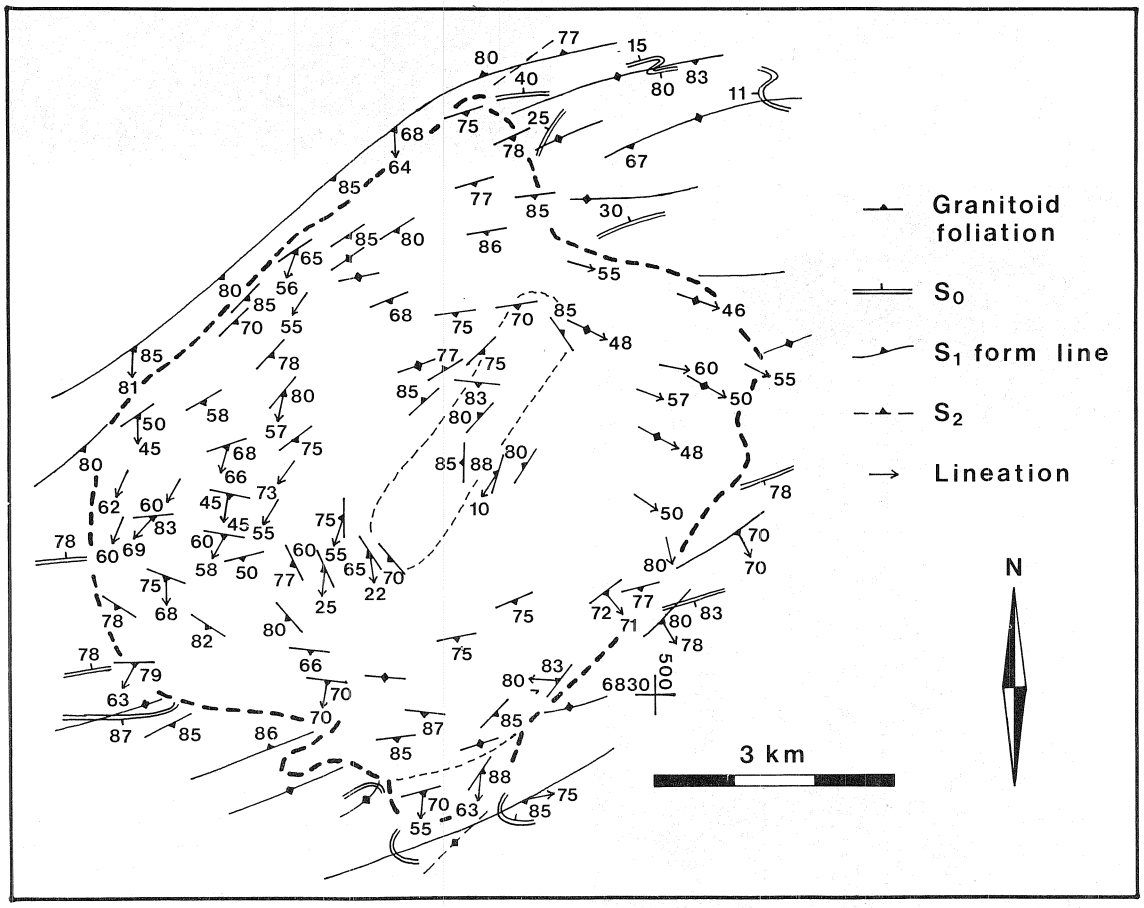


Fig. 14. Structural map of the Värmälä stock and surrounding schists.

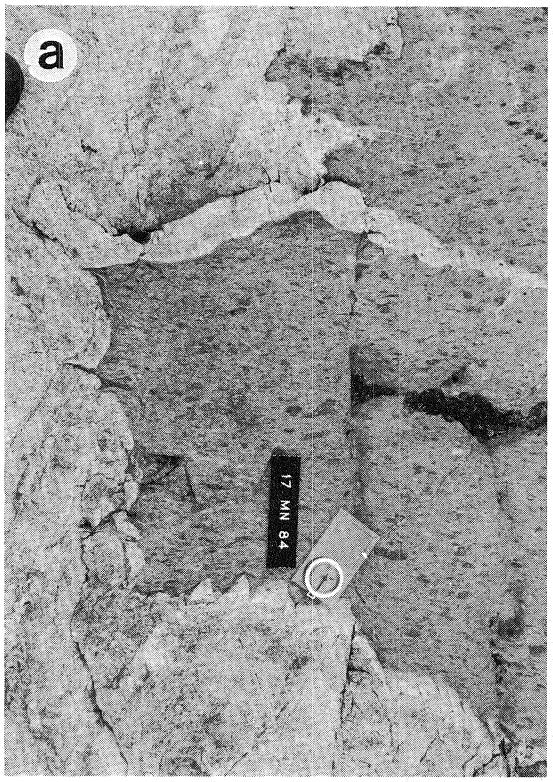


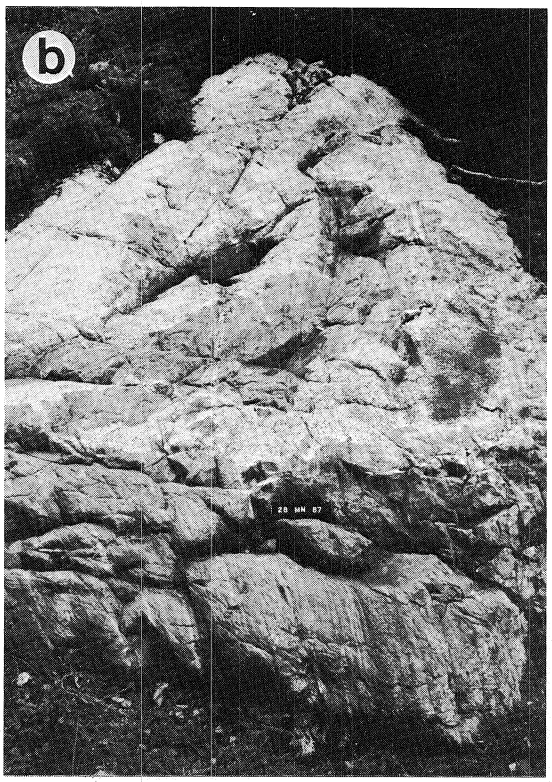


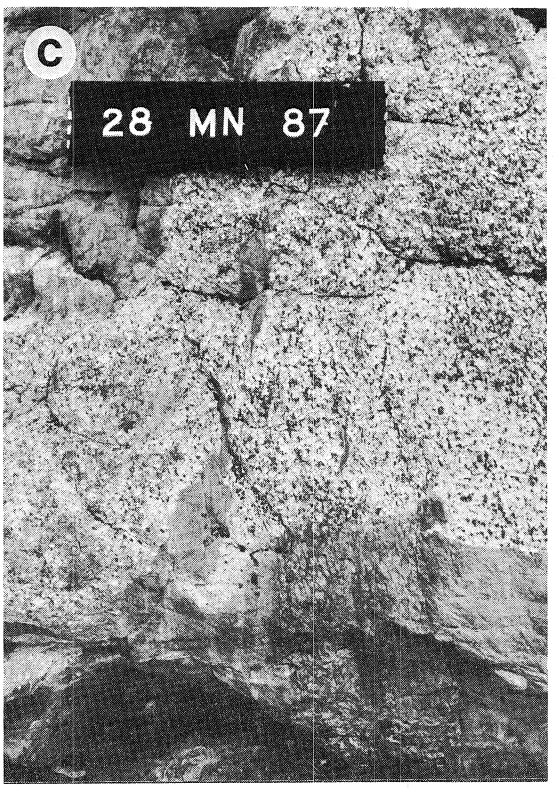


Fig. 15. Contact phenomena around the Värmälä stock. a) $S_1$, clearly visible in metatuffite, continues as a weak foliation into granodiorite at the northeastern contact. Length of code bar 20 cm. b) Granodiorite brecciates metaturbidite at the southwestern contact. c) A detail of Fig. 15b: primary layering is crosscut by granodiorite, but $S_1$ continues across the contact.

They are almost undeformed in areas where $S_1$ is also weak, but tightly to isoclinally folded with $S_1$ in the axial plane where $S_1$ is pronounced. Some apophyses are crosscut by thin quartz veins which in turn are $D_1$ deformed, indicating progressive deformation. In these regimes the apophyses are more intensely deformed than the aplite dikes that protrude into the schists.

The contacts form a rather angular pattern, and the rectilinear northwestern contact suggests a fault and/or fracture control for the pluton. However, the schists near the contact show well preserved primary structures and only moderate schistosity. Neither do the geophysical data support the existence of any linear element that would extend beyond the northwestern contact, although old fractures could have been healed and overprinted by subsequent strain.

On macroscale, within the stock the general pattern of the foliation is lenticular, although there is a concentric component in the center of the pluton (Fig. 14). The foliation is usually penetrative, but in places it occurs as fractures. The lineation associated with the foliation has a radial pattern. The tectonite fabric consists of elongate quartz grains and aggregates as well as biotite flakes. Where the fabric is pronounced, the feldspar phenocrysts are aligned parallel to the fabric. In the diorite, the tectonite fabric is seen as preferred alignment of plagioclase laths and mafic minerals.

A set of fractures usually a few millimeters thick deform the tectonite fabric. Chloritization and epidotization has taken place along the fractures, and at least some of them are faults. Because of the scarcity of observations, no systematics was found in their orientation. The fractures do not parallel $D_2$ or $D_3$ structures in the schists.

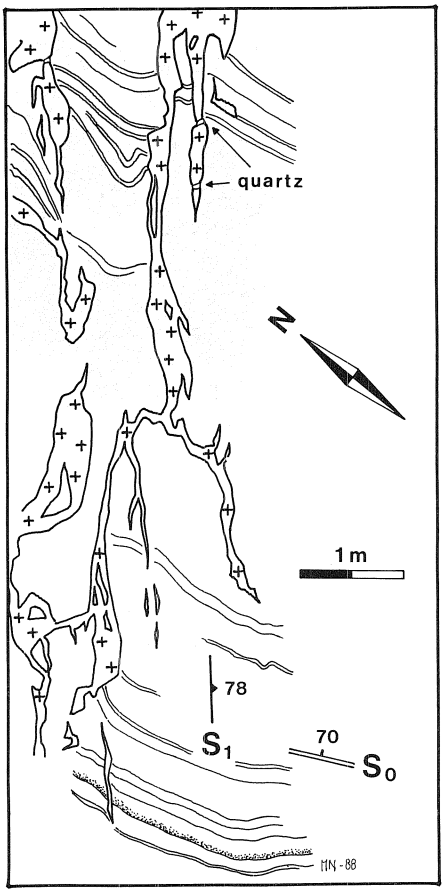


Fig. 16. Detail of the southern contact of the Värmälä stock. Granodiorite apophyses (marked by crosses) have been injected parallel to $S_1$ and slightly boudinaged. Note quartz in boudin necks.

## Quartz fabric study

Local estimates of finite strain were measured from deformed quartz aggregates by the Robin method (see p. 9). An example of two surfaces, each containing two principal axes of the strain ellipsoid, is shown in Fig. 17. The deformed quartz grains and aggregates show that pervasive strain took place (in a solid or nearly-solid state) in the pluton. The grains and aggregates show effects of crystal plastic deformation (undulose extinction, subgrains).

The finite strain ellipsoids range from pure flattening (k=0) to pure constriction (k=38.6;

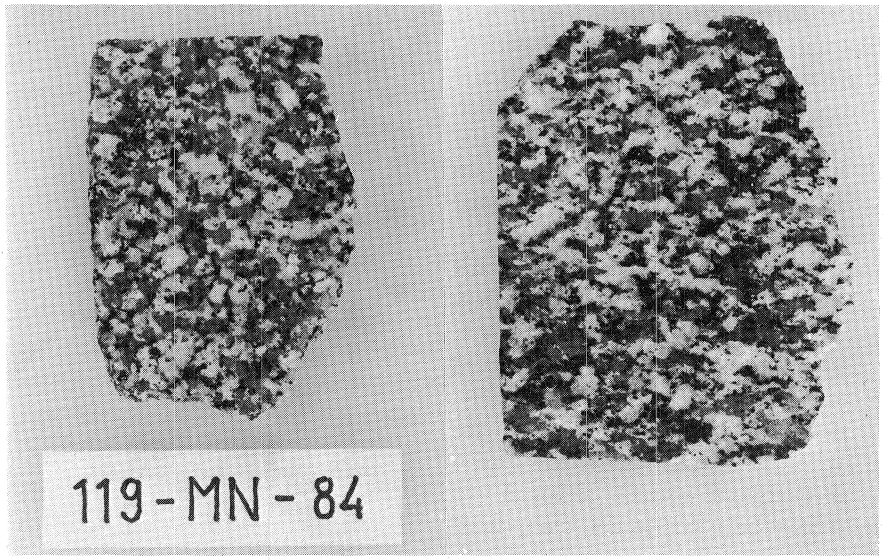


Fig. 17. Two surfaces of a granodiorite sample from the Värmälä stock, with an L>S tectonite fabric. Left: plane perpendicular to foliation and lineation (YZ plane of strain ellipsoid). Right: plane perpendicular to foliation and parallel to lineation (XZ plane). Length of code sign 6 cm.

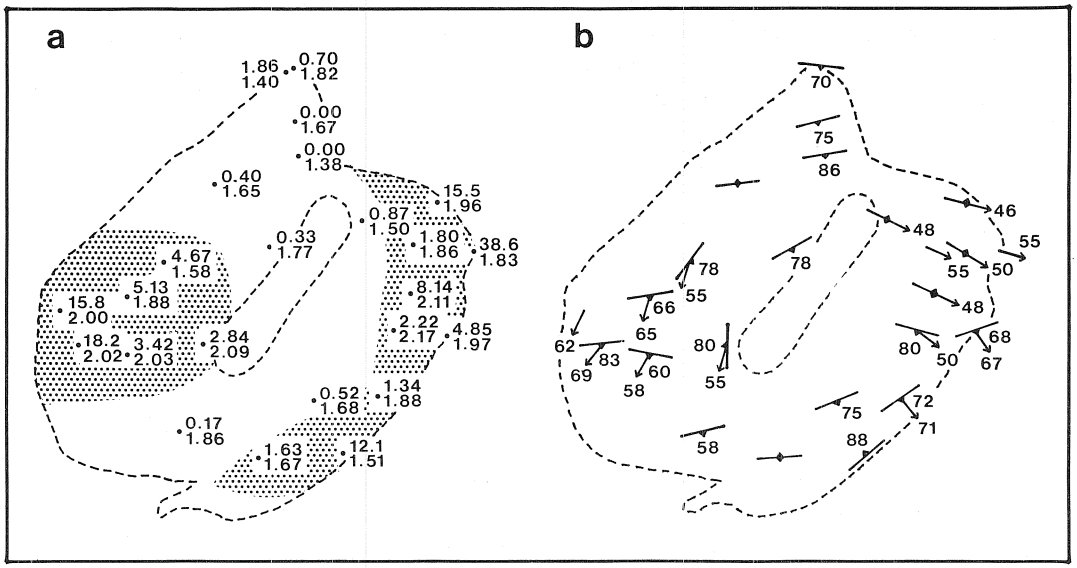


Fig. 18. a) Strain in the Värmälä stock, measured from elongate quartz grains and aggregates. Upper values are k-values, lower ones are r-values. The area of constrictional strain (k>1) is shaded. See Fig. 2 for further explanation. b) Observed tectonite fabric at the sites where the samples for the quartz strain analysis were taken.

Fig. 18). The large scatter is partly due to low strain intensity (r-values from 1.38 to 2.17). As explained earlier (p. 9), the strain determined from quartz aggregates is a minimum estimate. The LS tectonite fabric estimated in the field as well as the data obtained from deformed enclaves are consistent with the results of quartz aggregates. The fabric of the main granodiorite is of the constrictional type at the eastern and western margins, and the k-values rapidly decrease away from these areas. The r-values are slightly higher at the eastern and western margins than elsewhere in the granodiorite-granite. The central quartz monzodiorite is even less deformed, and hence the quartz aggregates did not yield information of strain. In contrast, the diorite at the southern margin contains a distinct L>S tectonite fabric.

## Dikes and veins

Aplite dikes and quartz veins are localized mainly in the marginal areas of the stock, and near the contacts of the central quartz monzodiorite (Fig. 19). Almost without exception, they crosscut their host plutonic rocks with sharp and subplanar contacts. However, some dikes near the contacts have a similar tectonite fabric as their host, indicating that they crystallized before the fabric was formed. The young fractures (p. 31) deform the dikes. The aplite dikes are 2—30 cm thick and often occur in parallel groups. In places they extend into surrounding schists. The quartz veins are of similar thickness as the aplite dikes, and they also appear in parallel arrays. All the dikes and veins as well as the few observed pegmatite dikes strike at high angles to the contacts, although their dip angles vary considerably.

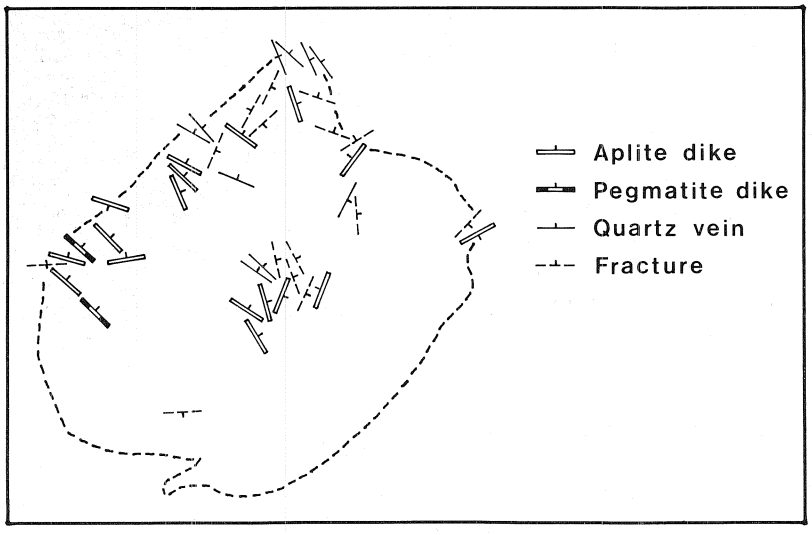


Fig. 19. Orientations of dikes, veins and late fractures in the Värmälä stock.

## Enclaves

Angular, slightly schistose wall rock xenoliths from 5 cm up to 3 m in diameter occur in the immediate vicinity of the contacts of the pluton. The xenoliths are rotated and contain $S_1$ which is not, however, as pronounced as in the wall rock schists.

Dark, fine-grained, roundish or oval-shaped microgranitoid enclaves occur mostly in the marginal areas of the pluton, and in the central quartz monzodiorite. Even in these areas the enclaves are scattered (enclave density at most $2/m^2$). Their longest axes measure from an average of 5—20 cm up to 80 cm. If the host rock has a tectonite fabric, the enclaves retain the same fabric, and they are oriented parallel to the foliation and/or lineation.

## Contact metamorphism

Small, light gray spots are encountered in the schists at several localities around the stock up to 300 m from the contacts. They occur in silty and pelitic units of metaturbidites as well as in felsic and intermediate metatuffites. They are elongate parallel to $S_1$ and $L_1^1$ (Fig. 20a), and their length dimishes away from the maximum of 8 mm near the contacts to 2 mm (at horizontal outcrop). The spots are muscovite-rich with respect to their surroundings. Most probably they are pseudomorphs of andalusite, as Seitsaari (1951, p. 25) suggested. The muscovite flakes in the spots are usually randomly oriented, but in places they are elongate subparallel to $S_1$.

Biotite-rich zones of intensified $S_1$ wrap around the pseudomorphs (Fig. 20b), due to either deformation partitioning around the pre-existing rigid porphyroblasts, deformation of schistosity during syntectonic growth of porphyroblasts, or heterogeneous deformation prior to porphyroblast growth (cf. Prior 1987). The last alternative is improbable, because heterogeneous deformation on such a scale has not been observed outside the contact aureole in the same lithologies. Because pseudomorphism has obliterated inclusion trails, it is impossible to deduce by internal foliation which of the two other possibilities is correct. The fact that the small muscovite flakes in some pseudomorphs are weakly oriented parallel to $S_1$ shows that even the pseudomorphism took place during a late stage of $D_1$. This indicates that both contact metamorphic porphyroblast growth and pseudomorphism took place before the end of progressive $D_1$.

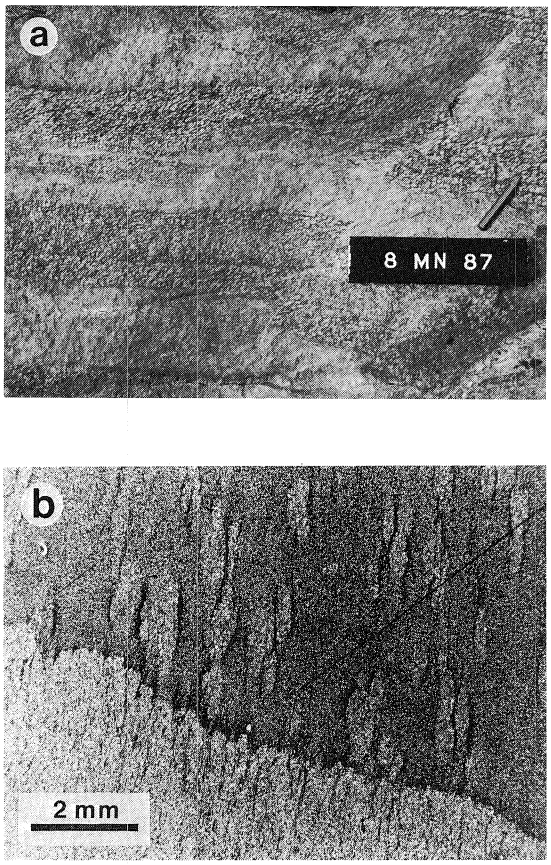


Fig. 20. a) Andalusite pseudomorphs in pelitic units of metaturbidite at the southeastern contact of the Värmälä stock. The pseudomorphs are elongate parallel to $S_1$. Length of code bar 20 cm. b) Photomicrograph of andalusite pseudomorphs at the contact of pelitic and silty units. Intensified $S_1$ around the pseudomorphs is expressed as lenticular, biotite-rich zones. Nicols parallel.

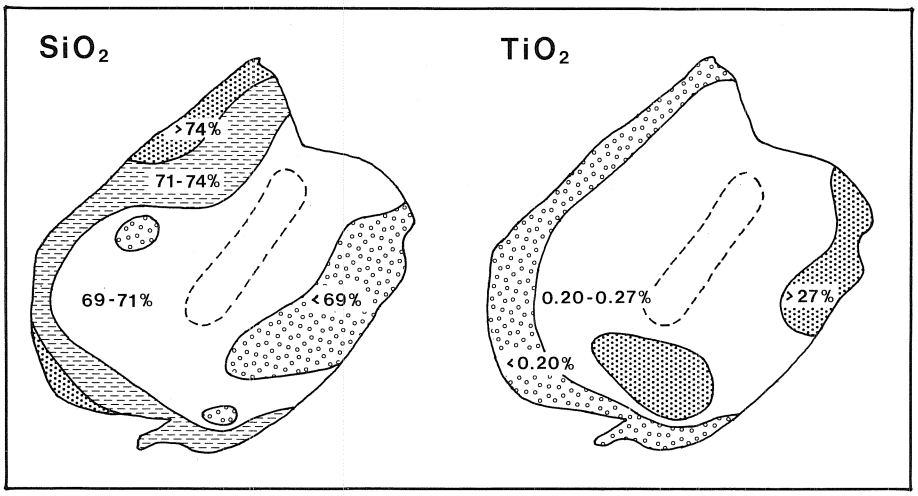


Fig. 21. Variation of $SiO_2$ and $TiO_2$ contents in the granodiorite-granite of the Värmälä stock.

## Geochemistry

The major element distribution exhibits asymmetric zoning within the granodiorite and the granite. The $SiO_2$ content which is over 71 % in the western and northern margins, decreases to around 68 % toward the eastern margin (Fig. 21). Conversely, $TiO_2$, MgO, FeO, and CaO contents are lower in the marginal granite than in the granodiorite (Figs. 21 and 22). The most granitic part at the margin shows that the distribution of the rocks does not correspond to normal zoning.

The central quartz monzodiorite plots between the granodiorite and the granite. In $Na_2O$ versus $SiO_2$, the quartz monzodiorite has the highest values, whereas the granite has the highest $K_2O$ content. The northern porphyritic phase plots in the same manner as the granite. When also the diorite is considered, the $TiO_2$, MgO, FeO and CaO against $SiO_2$ diagrams define negative, slightly curving trends.

In $TiO_2$ versus CaO, the quartz monzodiorite and the northern porphyritic phase plot between the granodiorite and granite. Although the petrological meaning of this diagram is ambiguous, it shows that the phases form distinct groups, and especially that the granodiorite and the marginal granite are separate phases.

Omitting the diorite, SrO has a positive correlation with CaO, the northern porphyritic and western granites having the lowest values. This trend is apparently due to crystallization of feldspars. The SrO content of the central quartz monzodiorite varies considerably. $ZrO_2$ has a similar trend against CaO. In fractional crystallization, Zr would be expected to concentrate in the acid phases. However, the most evolved end members are usually depleted in Zr due to fractionation of zircon. Hence, the decrease of $ZrO_2$ from granodiorite to granite may be due to fractional crystallization. When the possible control by partial melting is considered, experimental studies (Watson 1979, Watson and Harrison 1983) indicate that in an anatectic peraluminous melt, the solubility of Zr increases with increasing temperature and decreasing $SiO_2$ content. The experimental results are supported by observations of leucogranites formed by crustal anatexis, which are strongly depleted in Zr with respect to the unmelted residue (Weber et al. 1985, Wickham 1987). Applying a partial melting model, the granite magma with lower Zr content was extracted first, and the Zr-enriched granodiorite magma later.

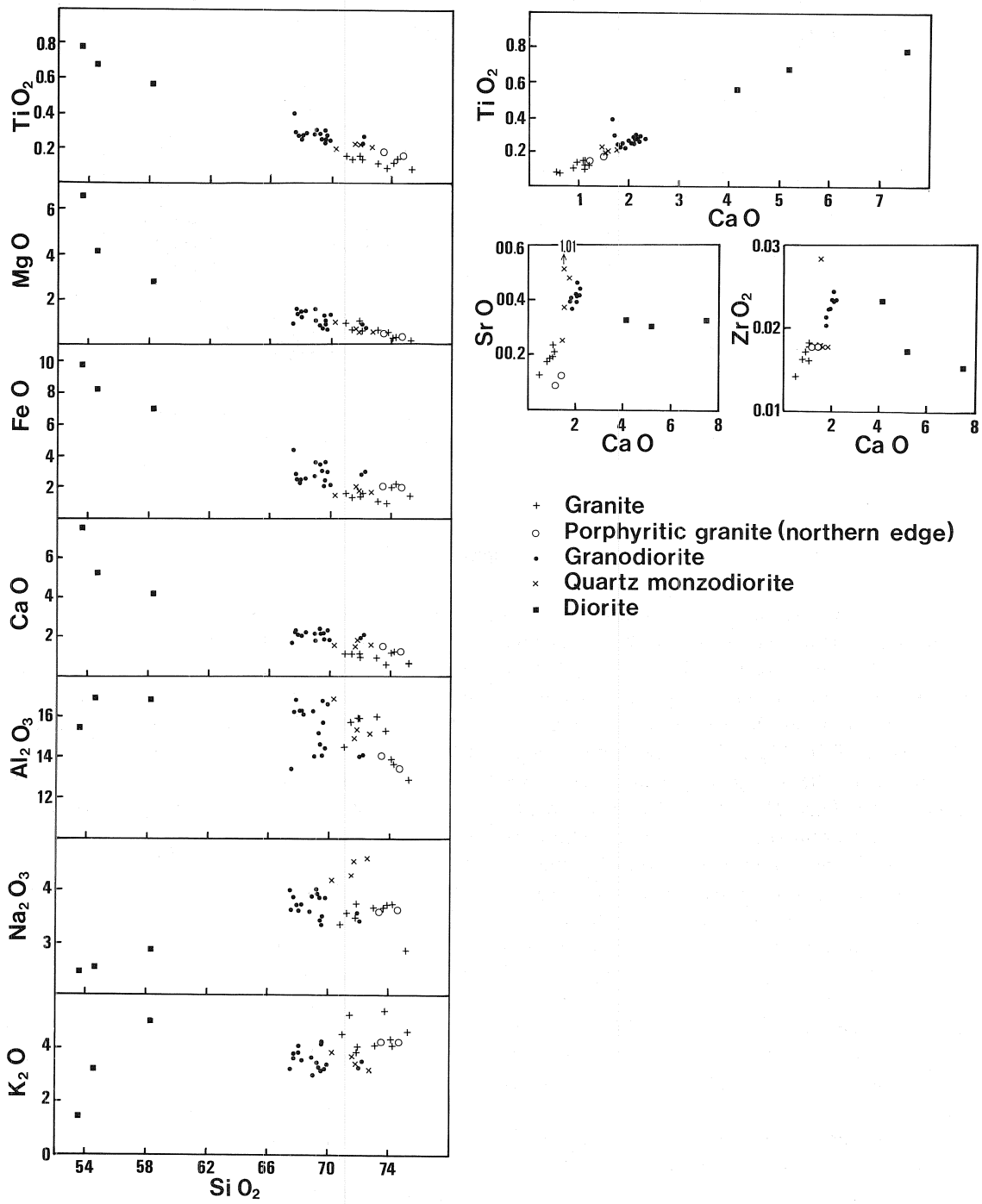


Fig. 22. Variation diagrams for rocks of the Värmälä stock (35 analyses).

## Structural setting and emplacement

Several lines of evidence indicate that the Värmälä stock is syntectonic with respect to $D_1$. These are: 1) $S_1$ continues across the contacts into marginal areas of the pluton; 2) no separate foliation around the pluton overprinting $S_1$ was observed; 3) the granodiorite apophyses are overprinted by $F_1$ folding; 4) the wall rock xenoliths are schistose yet rotated; and 5) the contact metamorphic (andalusite) porphyroblasts were originally syntectonic with respect to $D_1$.

The fact that the wall rock shows weak $S_1$ near the western and northeastern contacts indicates that the emplacement took place after an early stage of progressive $D_1$ deformation, and that these areas acted as strain shadows. The variation in intensity of $D_1$ around the pluton and the wrapping of biotite seams around the pseudomorphs imply that deformation continued during and after the emplacement, i.e. the stock is strictly syntectonic with respect to $D_1$.

The alteration of andalusite into muscovite probably took place in a static state during cooling of the pluton since the muscovite flakes are commonly randomly oriented. As Van den Eeckhout et al. (1986) pointed out, thermal relaxation after emplacement may cause post-tectonic growth of minerals.

The continuation of $S_1$ into the pluton and the slight concentric foliation in the center of the pluton suggest that the bulk strain attained from strain measurements is a combination of regional strain ($D_1$) and emplacement strain. By the fact that the aplite dikes in the interior of the pluton (and also in some marginal areas) are undeformed, it can be inferred that the pluton acted as a rigid body during waning $D_1$ except for its marginal parts. The high strain intensity in the schists at the northern and southern contacts, and the low strain areas around the eastern and western contacts are apparently due to strain partitioning during $D_1$.

Brun and Pons (1981) presented a mathematical model for a syntectonically ballooning pluton, where bulk shortening increases at the contacts parallel to foliation and decreases towards triple points where regional foliation is perpendicular to the contact of the pluton. Approximately at the same site, a change of strain from apparent flattening to apparent constrictional type is to be expected. According to Brun and Pons (1981), foliation triple points are a consequence of interference between a local strain field due to ballooning and a regional strain field. The foliation triple point may be inside a pluton when the strain value of ballooning is low with respect to initial radius of pluton.

The slight concentric foliation, the high (flattening) strain in the schists at the northern and southern contacts of the Värmälä pluton, where $S_1$ is subparallel to the contacts, and the constrictional strain at the eastern and western margins of the pluton are analogous with features predicted for a syntectonic ballooning pluton. The existence of triple points inside the pluton suggest that regional strain was greater than emplacement strain. The approximately radial dike system may be regarded as extensional emplacement fractures. According to Castro (1984), this kind of fractures can be a result of ballooning. However, the weakness of concentric foliation, the fairly constant strain within the pluton and the rather angular contacts are against a major contribution to emplacement by diapirism and favor an initially more passive emplacement.

The Castro Daire granitoid complex in northern Portugal (Oen 1960) is similar to the Värmälä stock in many respects, i.e. the subvertical foliation is partly concentric but in places subparallel to regional foliation. The foliation in the schists is sharply crosscut by the pluton but in places the foliation wraps into parallelism with the contact. Oen (1960) considered the Castro Daire complex as a post-tectonic one that was emplaced first by forceful intrusion and subsequently by major stoping of country rock blocks. The distribution of the rock types of the Värmälä pluton suggests that the emplacement was first passive, and diapiric at a later stage.

Härme and Seitsaari (1950) observed the general southerly plunge of lineations in the Värmälä stock, and concluded that the pluton was tilted to the north during forceful intrusion. Considering the northward thrusting (or reverse faulting) along the

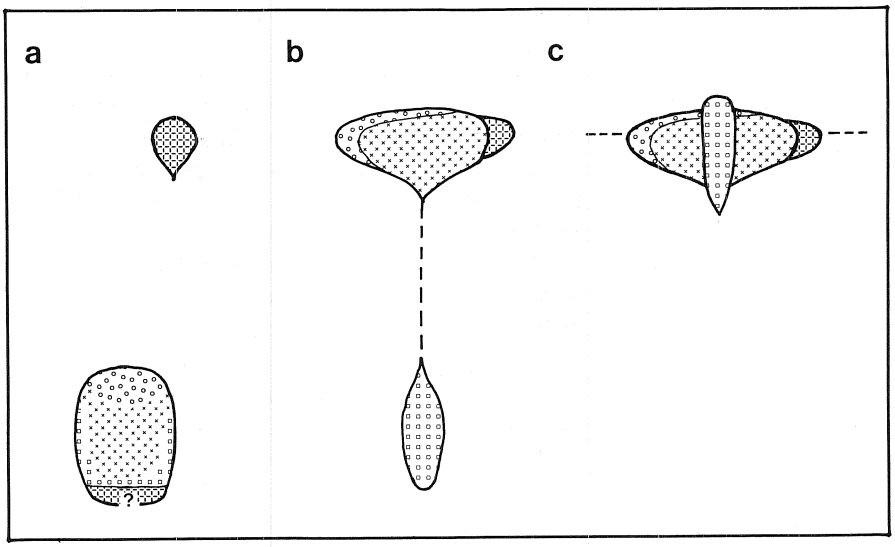


Fig. 23. A model for the emplacement of the reversely and asymmetrically zoned Värmälä pluton. a) A stratified magma chamber existed below the final emplacement level. The diorite was emplaced first, possibly from an external source. b) The fluorine-bearing granitic magma, on top of the chamber, ascended first, and the main granodiorite subsequently. c) The quartz monzodioritic magma with plagioclase cumulates emplaced after the granodiotie had been mostly solidified. The present erosional level is shown by broken line. Symbols for rock types as in Fig. 12.

southern boundary of the belt, tilting during emplacement may have occurred.

The arrangement of $S_1$ around the Värmälä stock is similar to the drag-pattern of foliation obtained in model experiments of simple shear around a rigid spherical body (Ghosh 1975). If the pattern was due to dextral rotation during $D_2$, the strain intensity should be greatest near the northwestern and southeatern contacts, in analogy with the computed strain state (Masuda and Ando 1988). However, $S_1$ is most pronounced near the northern contact. Furthermore, the areas around the eastern and western contacts should be strained, according to the computed strain state around a rigid spherical body.

The position of the quartz monzodiorite in the center of the stock and its almost negligible strain suggest that this phase intruded later than the granodiorite. However, the cumulate-type texture and the fact that the major element compositions plot between the granodiorite and granite are problematic. Considering the high viscosity of granitoid magma, the generation of a cumulus phase by crystal settling is improbable. An alternative segregation model (see Sparks et al. 1984) is that the cumulate-type material crystallized at the bottom and walls of the magma chamber while the residual melt was extracted because of its buoyancy.

Modelling of the emplacement must take into account the asymmetric zoning with a reverse component (the granite at the margin). The position of the quartz monzodiorite and the reverse zoning may be explained by a model modified from Fridrich and Mahood (1984; see also Nabelek et al. 1986). The diorite, not necessarily with a direct genetic relationship to the granitoids, was the first one to intrude. A stratified magma chamber deeper in the crust consisted of granite magma at the top, and granodioritic magma at the bottom of the chamber (Fig. 23a). The mafic enclaves were generated either by magma mingling deeper in the crust, or by mingling between the granodioritic magma and a separate, more mafic magma that existed at the bottom of the stratified magma chamber. Due to crystal fractionation, cumulus-type material accumulated at the bottom and sides of

the felsic magma, generating the quartz monzodioritic magma. The entire magma must have been largely molten for crystal fractionation and vertical stratification to occur. The fluorine-bearing granite ascended to the final level before the granodiorite (Fig. 23b). The quartz monzodiorite intruded when the granodiorite had already mostly solidified (Fig. 23c). The faults that controlled the emplacement were exerted by the ascending quartz monzodiorite. The small porphyritic phase was the last one to intrude.

## SOUTHEASTERN SAVO SCHIST BELT

The Savo Schist Belt is parallel to the NW-SE trending Raahe-Ladoga lineament zone (Fig. 1). The belt, consisting of both schists and migmatitic gneisses, does not comprise a well defined area, and the southeastern termination is especially vague. The author delineated the boundary where sillimanite quartzites occur. Narrow strips of sillimanite-bearing quartzite, observed in the Svecofennian Domain (Eskola and Nieminen 1938, Salaterä 1976, Lehijärvi 1979, Nurmi et al. 1984) are probably parts of a single discontinuous, E-W trending lithohorizon and hence the general E-W structural grain of southern Finland. In contrast, the structural grain north of the quartites is NW-SE. The change in trends is a feature of major tectonic importance (e.g. Park et al. 1984, Vaasjoki and Sakko 1988).

In the southeastern part of the belt (Fig. 24), the

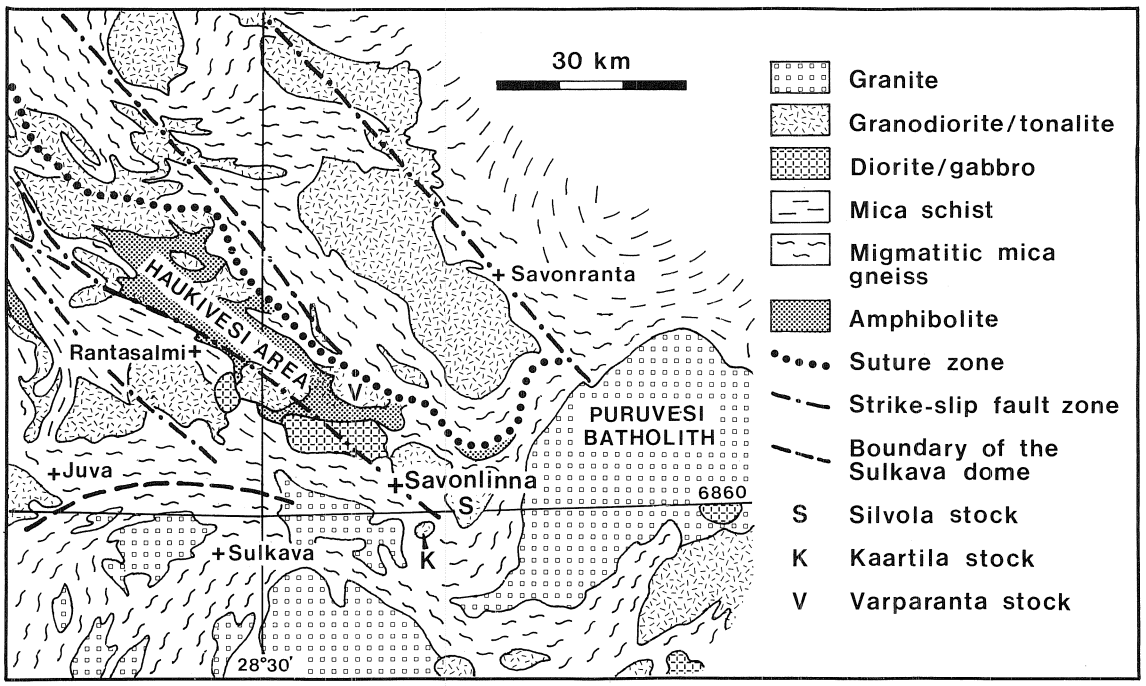


Fig. 24. Generalized geological map of southeastern Savo Schist Belt, showing the location of the Silvola, Kaartila and Varparanta stocks (modified from Gaál and Rauhamäki 1971, Bowes et al. 1984, and Luukkonen and Lukkarinen 1985).

rocks were originally turbiditic sediments (mainly greywackes) with minor mafic volcanics as interlayers (Gaál and Rauhamäki 1971, Korsman 1977). Gaál and Rauhamäki (1971) inferred that the turbidites of the Haukivesi area recrystallized into veined gneisses and cordierite gneisses under upper amphibolite facies conditions, and that volcanics between the turbidites were deformed and recrystallized under granulite facies metamorphism into layered diopside amphibolites. Parkkinen (1975) deduced that also the amphibolites recrystallized under amphibolite facies conditions. In the Rantasalmi-Sulkava area (Fig. 24), the grade of metamorphism in the metaturbidites grew progressively south toward the Sulkava thermal dome (Korsman 1977, Korsman et al. 1984). The peak of metamorphism grew from 645°C to 680°C and from 3.4 kb to 4.8 kb toward the dome, and was 750°C, 4.2 kb within the dome (Korsman et al. 1984).

The geology of the Savo Schist Belt is characterized by complicated tectonics with multiple folding and subsequent faulting which caused a block structure (Korsman et al. 1984, Pajunen 1986). According to Gaál and Rauhamäki (1971), the first deformation in the Haukivesi area produced south verging recumbent folding and thrusting. During $D_2$, subhorizontal compression in the present N-S direction first produced $F_2$ folds with E-W striking, subvertically dipping axial planar $S_2$ schistosity. Due to continued compression, $D_2$ structures were reoriented, and WNW-ESE trending synforms and antiforms were generated within an extensive, NW-SE trending dextral strike-slip fault system. During $D_3$, E-W compression led to the development of domes and basins within the same fault system but with sinistral sense of movement. Parkkinen (1975) divided the $D_2$ deformation of Gaál and Rauhamäki (1971) into two episodes, with the latter defined by strike-slip faulting.

Korsman and Kilpeläinen (1986) and Kilpeläinen (1988) discerned a structural sequence with four deformational phases in the Rantasalmi-Sulkava area (see below). The deformation that produced the dextral strike-slip fault zones and the block structure of the Raahe-Ladoga zone, referred to as $D_2$ by Gaál and Rauhamäki (1971), $D_{2c}$ by Koistinen (1981) and Halden (1982), and $D_3$ by Kilpeläinen (1988), also governs the structure of the Rantasalmi-Sulkava area.

## STRUCTURE OF THE GNEISSES AROUND THE SILVOLA AND KAARTILA STOCKS

The gneisses around the Silvola and Kaartila stocks (Fig. 25) are mainly migmatitic cordierite gneisses, with few diopside amphibolite, quartz-feldspar gneiss, garnet gneiss and metaconglomerate intercalations. The major minerals in the cordierite gneisses are cordierite, K-feldspar, quartz, plagioclase and biotite. Although the primary structures have been obliterated, the mineral compositions of the gneisses suggest that the rocks were originally turbiditic sediments (mainly greywackes), as in the Haukivesi area. The Silvola and Kaartila stocks are surrounded by envelopes of diopside amphibolite, 200—600 m and 30—100 m broad, respectively. The diopside amphibolite contains alternating diopside-rich and hornblende-rich layers a few centimeters wide, and in places fragments strongly elongate parallel to the layering. Geochemically, the rocks resemble modern tholeiitic basalts (Kuusola 1982).

The migmatitic character and the cordierite, garnet and K-feldspar porphyroblasts in the cordierite gneisses suggest peak metamorphic conditions similar to those in the Juva area, 40 km west of the study area (Fig. 24). Korsman et al. (1984) estimated conditions of 680°C and 4.8 kb for the rocks in the Juva area (garnet-cordierite-biotite zone). In the Silvola-Kaartila area, the grade of migmatization increases toward south and east. In the area north of the Kaartila stock, migmatization is weak and the predominant, penetrative foliation is differentiated. In strongly migmatitic cordierite gneisses, e.g. around the two plutons, thin leucocratic veins parallel to the foliation and lithologic layering occur together with

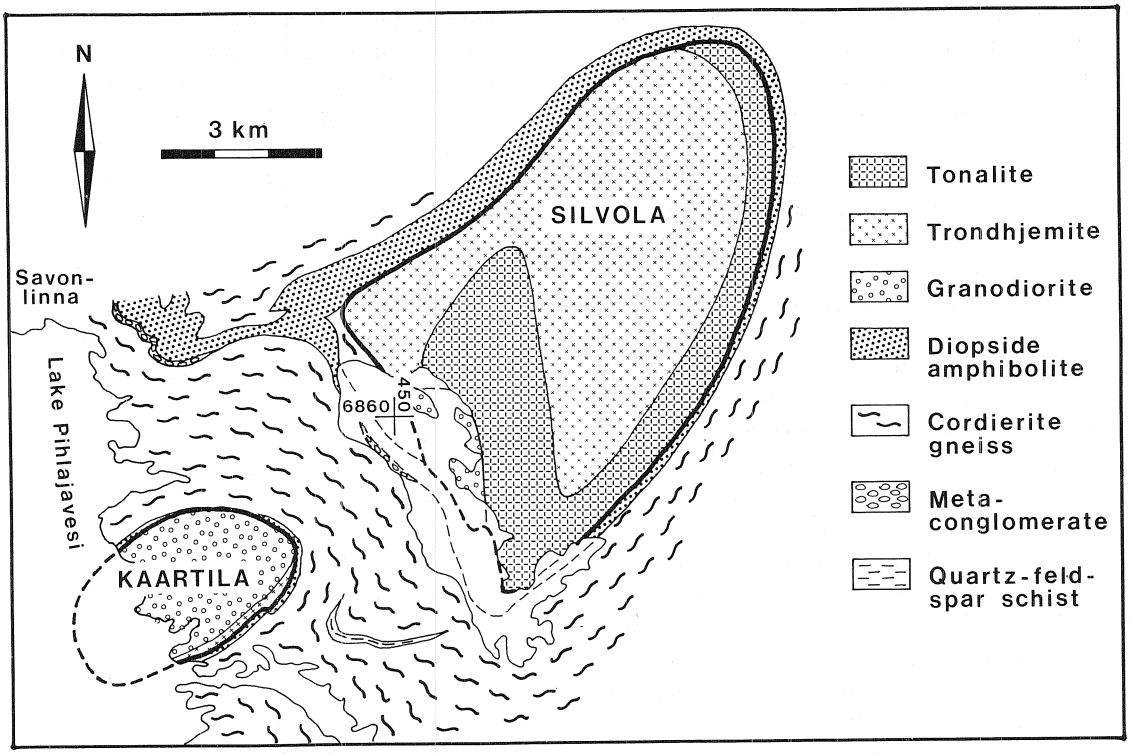


Fig. 25. Geological map of the Silvola and Kaartila stocks and surrounding rocks (based on mapping by G. Gaál, for Outokumpu Exploration, and the author).

thicker, crosscutting ones. These veins suggest both subsolidus segregation and (synchronous or subsequent) anatexis during metamorphism (cf. Sawyer and Robin 1986, Sawyer and Barnes 1988).

Due to intense recrystallization and partial obliteration of early tectonite fabric during high grade metamorphism, the structural sequence in the area cannot be resolved without correlation with studies on deformation and metamorphism in adjacent areas. The problem with correlation in the Savo Schist Belt is that blocks of different tectonothermal history occur side by side (see Korsman et al. 1988).

According to Korsman and Kilpeläinen (1986), a weak $S_1$ cleavage, obliterated in higher grade schists, is visible in metaturbidites of the andalusite metamorphic zone near Rantasalmi (Fig. 24). Further south, the schists in the K-feldspar-sillimanite zone are characterized by $MS_2$ K-feldspar and fibrous $MS_2$ sillimanite as aggregates elongated parallel to the E-W trending, penetrative $S_2$ schistosity. Korsman and Kilpeläinen (1986) concluded that in the K-feldspar-cordierite zone (the Juva area), $MS_3$ biotite masks the $S_2$ schistosity, and $MS_3$ cordierite as well as $MS_3$ K-feldspar formed by the decomposition of $MS_2$ biotite. Kilpeläinen (1988) reconsidered that cordierite and K-feldspar porphyroblasts in the K-feldspar-cordierite zone are $MS_2$, and that $MS_2$ biotite coarsened during progressive $D_2$. $MS_3$ biotite grew in the seams of the NW-SE striking $D_3$ crenulation cleavage, and coarse $MS_3$ biotite is found only futher south, in the garnet-cordierite-biotite zone. $D_4$ deformation with NE-SW trending axial surfaces was not associated with mineral growth.

Halden (1982) defined a structural sequence in medium grade metamorphosed and migmatized gneisses in the Savonranta area (Fig. 24). According to him, porphyroblasts of fibrous sillimanite are elongate parallel to $S_1$ metamorphic banding, and

sillimanite growth continued during the generation of the penetrative $S_2$ schistosity. The discrepancy in the interpretations of Halden (1982) and Korsman and Kilpeläinen (1986) in the timing of sillimanite growth may be due to the location of the Savonranta area in the northeastern (Archean) side of the suture zone (Fig. 24), where the tectonothermal evolution was apparently different from the evolution of the Rantasalmi-Sulkava area.

The dominant tectonite fabric around the Silvola and Kaartila stocks is expressed as a preferred orientation of biotite flakes and cordierite porphyroblasts in cordierite gneisses, and of hornblende grains in amphibolites. The fabric commonly contains both schistosity and mineral lineation. In places where the primary layering of the cordierite gneiss is well preserved and folded (Fig. 26a), biotite flakes define the penetrative, axial planar schistosity which overprints and crenulates an older foliation. Large, poikiloblastic cordierite and K-feldspar porphyroblasts contain biotite flakes which are finer in grainsize but have the same orientation as the matrix biotite. Hence, the porphyroblasts are syntectonic with respect to the axial planar schistosity. Cordierite and, less frequently, garnet contain microfolded sillimanite fibers with axial planes of the microfolds parallel to the penetrative schistosity (Fig. 26b). The sillimanite fibres are recrystallized in the hinges of microfolds. Moreover, microfolded sillimanite partly replaces biotite in some cordierite porphyroblasts. Obviously sillimanite is not in equilibrium with the matrix, because it is preserved only in porphyroblasts.

The features described above may be explained in three ways: 1) sillimanite grew contemporaneously with $MS_1$ biotite, both were crenulated during $F_2$ folding and sillimanite equilibrated during early $D_2$; 2) sillimanite grew mimetically parallel to $S_1$ during an early stage of $D_2$, was microfolded and preserved $D_2$ crenulation while the matrix crenulation was largely destroyed in continued crenulation cleavage development (Bell and Rubenach 1983) or decrenulation (Bell 1986) during progressive $D_2$ deformation; 3) sillimanite grew contemporaneously with the layer-parallel $MS_2$ biotite, and both were microfolded during $D_3$. It is impossible to choose between the first two possibilities, because the microfolding intensity is fairly similar in the sillimanite relics and in the matrix. In both cases, cordierite and K-feldspar would be $MS_2$ or $MS_2$-$MP_2$, whereas in the third case, they would be $MS_3$ or $MS_3$-$MP_3$. The orientation of the axial plane cleavage at high angles to the NW-SE trend of $S_3$ (Fig. 26a) in an area with only minor overprinting by later deformation rules out the third possibility. Hence, the predominant schistosity is $S_2$. Apparently the associated mineral lineation is $L_2^2$, because the older tectonite fabric is largely obliterated.

Leucocratic veins are subparallel with $S_2$ (Figs. 26a and 26c). $S_2$ and $L_2^2$ are well preserved around the Silvola stock (Fig. 27a). In the area between the two plutons, the lithologic layering and $S_2$ strike NW-SE. Considering the strike directions of $S_2$ in adjacent areas (Gaál and Rauhamäki 1971, Halden 1982, Kilpeläinen 1988), the NW-SE trend is due to reorientation of composite $S_2$ in large scale dextral shearing during $D_3$. Dextral $D_3$ shear zones occur in the area, but no large zone of intense $D_3$ deformation can be defined. Consequently, it is difficult to distinguish $MS_3$ biotite from $MS_2$ biotite. The few identified $F_3$ folds show a weak axial planar schistosity (Fig. 26c). In $F_3$ fold hinges, $S_2$ crenulation in sillimanite, visible in cordierite porphyroblasts, is refolded together with coarse $MS_2$ biotite of the matrix (Fig. 26d), and $MS_3$ biotite has overgrown $MS_2$ biotite.

The sharp mutual boundaries between cordierite, garnet and the coarse biotite (possibly coarsened in $D_3$) indicate equilibrium between these minerals. In places the garnet porphyroblasts mimic the microfolded $S_2$ foliation (Fig. 26e). The elongate shape of garnet and the quartz inclusion trails are probably due to crenulation segregation, because no signs of dissolution of garnet are visible. According to Vernon (1987), fibrous sillimanite is the only mineral that can grow in zones of strong noncoaxial deformation such as crenulation limbs. The nucleation of garnet porphyroblasts in crenulation limbs can be explained by growth that postdated or at least spanned $D_2$. Since cordierite and biotite are recrystallized in $F_3$ fold hinges (Fig. 26d), the mineral assemblage cordierite-garnet-biotite equilibrated after $D_3$.

In the Silvola-Kaartila area, the most

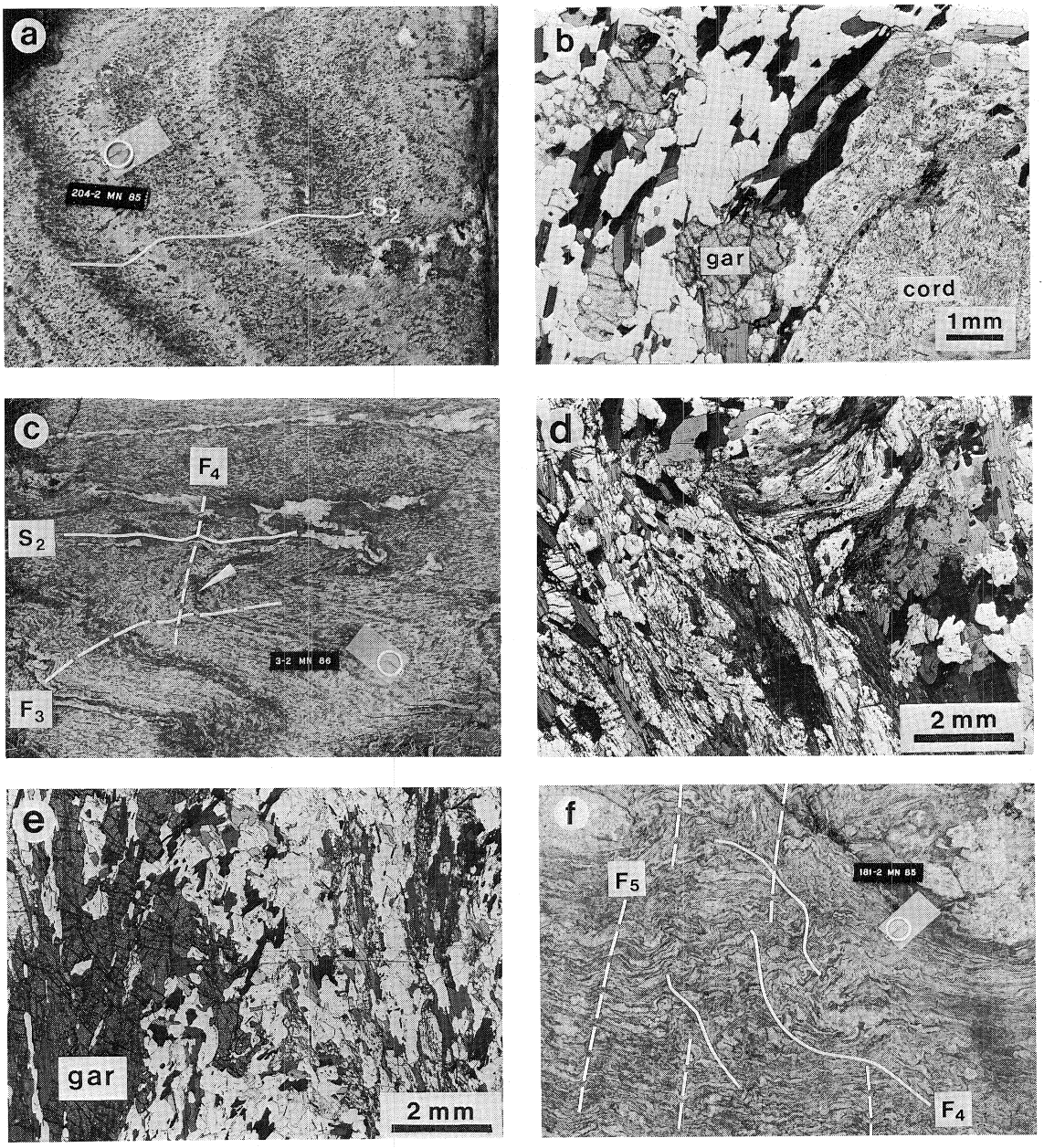


Fig. 26. Structures in the cordierite gneisses between the Silvola and Kaartila stocks. a) $F_2$ folded primary layering, with penetrative $S_2$ foliation. Length of code bar 20 cm. b) Photomicrograph of $S_2$ foliation at the site of Fig. 26a. Garnet (gar) porphyrobasts overgrow $MS_2$ biotite. Crenulated $MS_2$ sillimanite fibres are preserved in a cordierite (cord) porphyroblast. Note the parallelism of crenulation axial trace and external biotite foliation. Nicols parallel. c) $F_3$ fold, overprinted by weak $F_4$ folding. The site of Fig. 26d is shown by arrow. d) Photomicrograph of $F_3$ hinge area. Crenulated $MS_2$ sillimanite, partly replacing biotite, and coarse biotite are microfolded. Note the polygonal arcs by coarse biotite at the upper left corner. Nicols parallel. e) Photomicrograph of $MP_3$ garnet (gar) mimicing $F_3$ microfolding. Nicols parallel. f) $F_4$ folding, overprinted by $F_5$ folding.

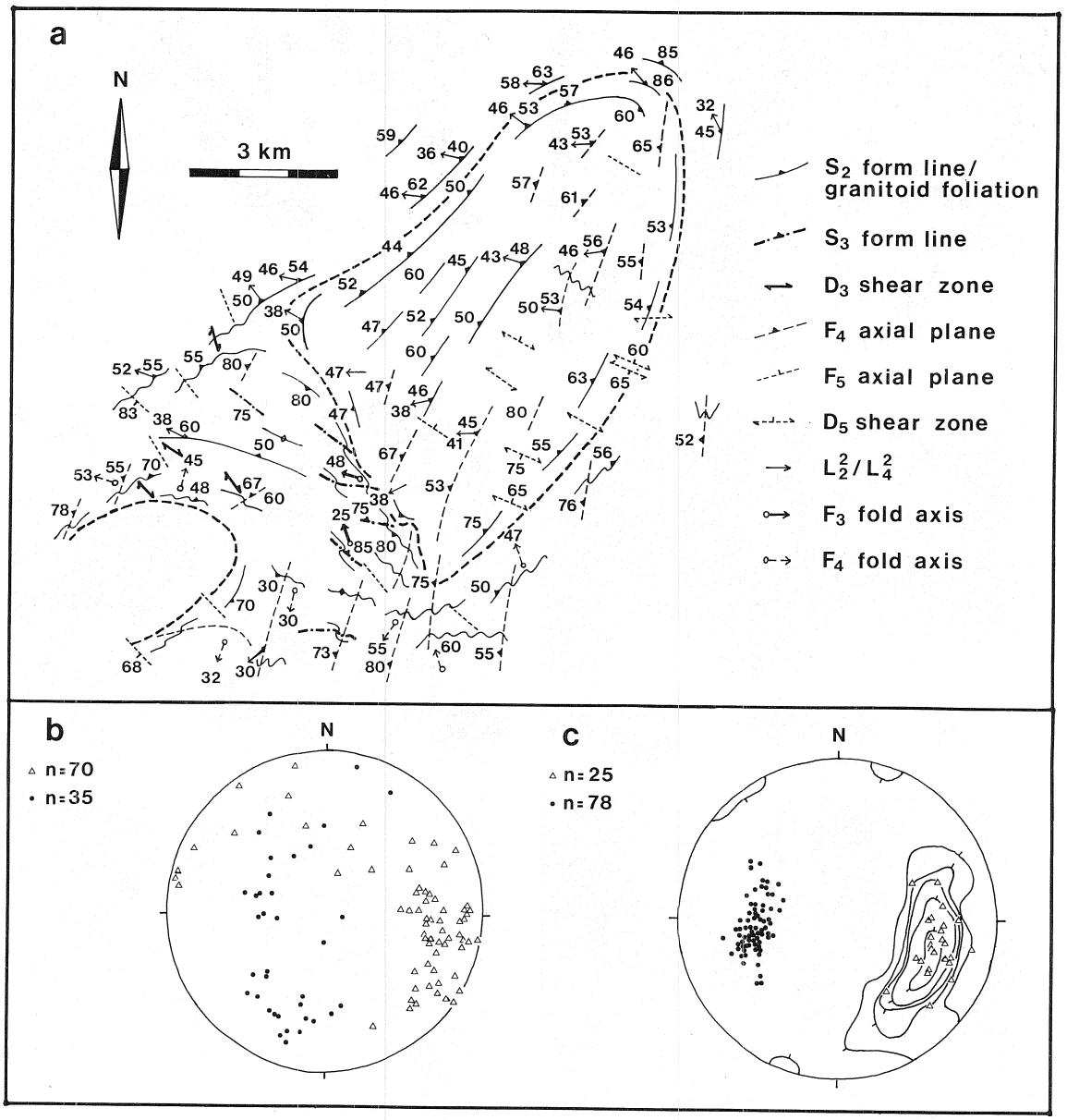


Fig. 27. a) Structural map of the Silvola stock and surrounding rocks. b) Lower hemisphere equal area projections of poles to $F_4$ axial planes (triangles) and $F_4$ fold axes (dots). c) Lower hemisphere equal area projections of structural data in the Silvola stock. Poles to penetrative foliation are expressed as contours (1-2-4-8-16 %; n=174), triangles are poles to crenulation axial planes, and dots are lineations.

characteristic post-$D_2$ structural feature is open to tight $F_4$ folding with NE-SW to NNE-SSW striking axial surfaces (Fig. 27b), corresponding to $D_4$ in the Rantasalmi-Sulkava area (Kilpeläinen 1988). $F_4$ folds are chevron folds in cordierite gneisses, but in diopside amphibolites their hinge zones are more arcuate. The fold axes vary remarkably in orientation. The wavelength of the folds ranges

from a few millimeters to several meters, and the amplitude of the enveloping surface may exceed ten meters.

In the hinge zones of $F_4$ microfolds, biotite flakes are arranged in a polygonal arc pattern, but the undulatory extinction shows that they are strained. Cordierite and K-feldspar are also strained, and garnet is fractured and retrogressed. This implies a considerable drop in metamorphic grade between $D_3$ and $D_4$. Some quartz-feldspar segregations were observed parallel to $F_4$ axial surfaces.

Around the Kaartila stock and further northwest, toward Savonlinna, ductile shear zones overprint $F_4$ folds in cordierite gneisses. The sense of shearing is usually dextral, but often both dextral and sinistral shearing occurs, giving rise to open folding with wavelength of 10 cm to over a meter. The shear zones and fold axial planes, denoted as $D_5$ structures, strike WNW-ESE and dip moderately to steeply SSW (Fig. 27a). In the more competent diopside amphibolites around the Kaartila stock, $D_5$ is seen as small faults with both horizontal and vertical component. The styles of the $F_4$ and $F_5$ folds are much the same (Fig. 26f), and in places the temporal relationship is not clear. Moreover, the microstructures in the hinges of the two fold generations are similar, indicating that also the grade of metamorphism was quite similar. Possibly the two deformational phases were not separated by a long time interval.

Large ovoidal structures with northeastern elongation are prominent in the aeromagnetic gray-tone maps around the study area (1:100 000; maps 4122 and 4211). Some of these were interpreted by Gaál and Rauhamäki (1971) as dome and basin structures due to fold interference. Immediately southeast of the Kaartila stock where the effects of $D_3$ deformation were not observed, there is an ovoidal basin structure due to curving of composite $S_2$ surfaces and $F_4$ axial planes, with $F_4$ fold axes plunging toward the core (Fig. 27a). If this basin is due to fold interference, it must be the result of two post-$D_2$ folding events, because the enveloping surface of the first folding is composite $S_2$. Because $D_3$ structures were not observed in the area, the basin is probably due to an $F_4$ and $F_5$ fold interference. The wide scatter in $F_4$ fold axis plots in Fig. 27b is probably due to both pre-$D_4$ deformation and overprinting by $D_5$.

## THE SILVOLA STOCK

The Silvola stock, which covers a 45 km$^2$ area, is roughly triangular in form (Fig. 25). The contacts of the stock are covered by soil except in the southern part. Petrographically the pluton is homogeneous, and the grainsize of the fairly equigranular rocks is 1—3 mm. In modal composition, the rocks are tonalites, trondhjemites (tonalites with less than 10 % mafic minerals) and granodiorites. Although the composition does not change regularly from margin to center, the eastern margin is slightly more mafic than the rest of the pluton. Internal contacts were not detected, and the tonalite probably changes gradually into trondhjemite. At the southwestern margin there is a fine-grained type with granodioritic composition.

Major minerals are plagioclase, quartz, biotite and hornblende, and K-feldspar in granodiorite. Apatite, magnetite, titanite and metamict allanite occur as accessory minerals. Corundum was identified in X-ray analysis (O. Kouvo 1989, personal communication). Alteration phenomena are minor. The texture varies from hypidiomorphic (primary) to granoblastic (recrystallized). Large quartz grains overgrow plagioclase and occur in intensely deformed rocks as ribbons up to 20 mm in length (Fig. 28a). In rocks with hypidiomorphic texture, plagioclase is weakly zoned whereas in rocks with granoblastic texture, plagioclase is unzoned, and the composition is uniform ($An_{32}$).

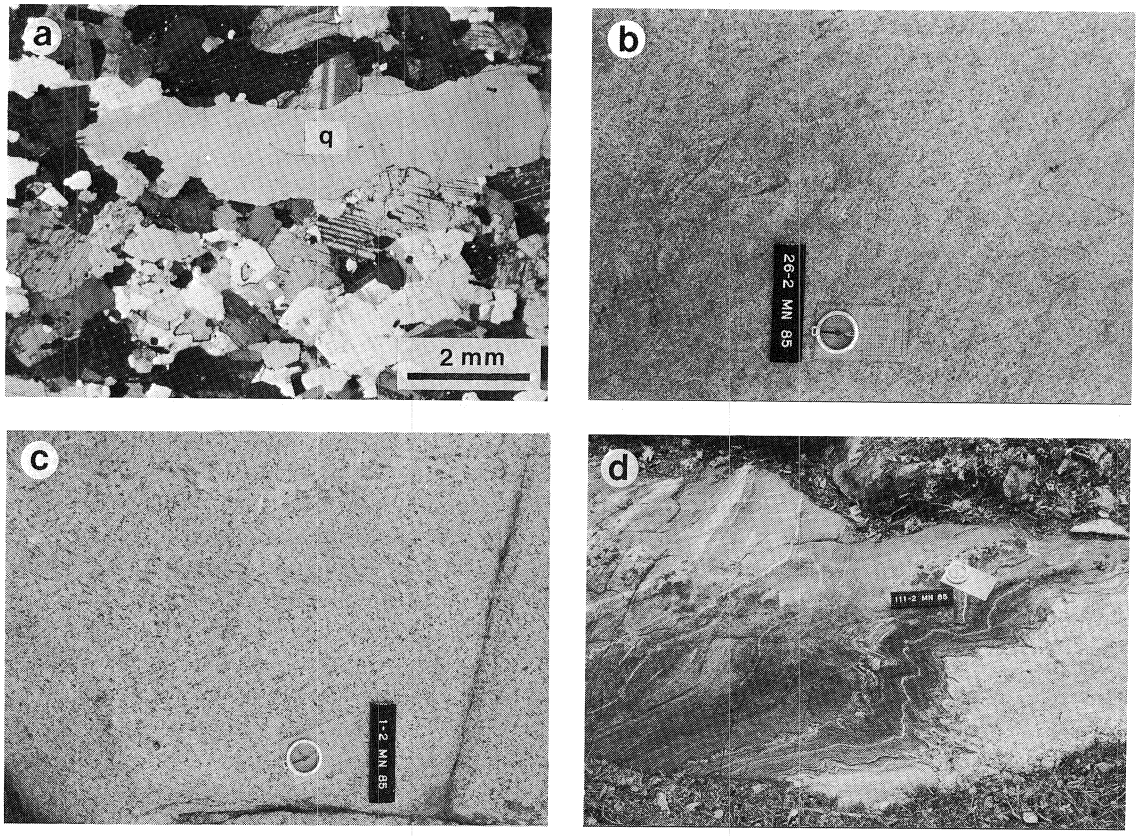


Fig. 28. Structures in the Silvola stock. a) Photomicrograph of trondhjemite. Large, elongate quartz (q) grain has overgrown plagioclase. Note the granoblastic texture. Nicols crossed. b) Hornblende-rich schlieren seams in trondhjemite are $F_4$ crenulated. Length of code bar 20 cm. c) $F_4$ crenulation in trondhjemite, and a pre-$D_4$ shear zone with slightly coarser grain size (at the top). d) Southern contact of the Silvola stock. Both diopside amphibolite and tonalite are $F_4$ folded.

## Structure

Two subparallel foliations occur within the pluton, and the structural complexity is displayed by the LS tectonite fabric which changes even at a single outcrop. Toward the northwestern and southeastern contacts, S fabric becomes pronounced, but no such pattern is found elsewhere in the Silvola stock.

The penetrative foliation, denoted as $S_2$, is conformable to the contacts and $S_2$ in country rocks at the margins of the pluton, although it is barely discernible at the southwestern margin (Fig. 27a). It is expressed as preferred orientation of biotite, quartz and hornblende aggregates. Although the large quartz grains are strongly elongate, they exhibit subgrain formation but no dynamic recrystallization. The other minerals are almost strain-free. In the center of the pluton there are a few thin, hornblende-rich schlieren seams parallel to the foliation (Fig 28b). If the seams are due to segregation of mafic minerals in the crystallizing magma during emplacement, $S_2$ was formed during emplacement.

In the central part of the stock, $S_2$ is deformed by parallel zones 3—15 cm wide and 0.5—2 m long. The zones may be 20—50 cm apart, but usually they are more widely distributed. They consist of slightly coarser and more felsic material than the surrounding rock (Fig. 28c). The zones

are interpreted as shear zones where last fractions of melt crystallized. The difference in strain intensity between the shear zones and non-sheared rock could not be determined because of later recrystallization (see below). The relation of shearing in the pluton to $D_3$ deformation in the country rocks is not known.

The penetrative $S_2$ foliation is crenulated, especially in the center of the pluton. Also the shear zones were folded and rotated toward parallelism with the axial plane of crenulation. The crenulation is open to tight, asymmetric similar-type folding with wavelengths of 1—10 cm (Figs. 28b and 28c). The crenulation axial plane coincides with the axial plane of $F_4$ folds in the supracrustal rocks (Fig. 27), indicating that the former is also a $D_4$ structure. The best evidence is in the contact at the southern edge, where both the tonalite and the amphibolite are $F_4$ folded (Fig. 28d). Within the stock, the crenulation axial plane and $S_2$ are generally subparallel, and in places the two cannot be distinguished. Toward the eastern margin the intensity of crenulation increases, and the contact-parallel composite foliation occurs both as a penetrative fabric and fractures. The change in LS tectonite fabric is due to the effect of $D_4$ on $D_2$ structures, and the west plunging mineral lineation (Fig. 27c) is an $L_4^2$ intersection lineation. Although the timing of recrystallization is complicated because of the subparallelism of $S_2$ and crenulation axial plane, the granoblastic texture in crenulation zones and the hypidiomorphic texture and zoned plagioclase in less deformed rocks suggests that recrystallization was associated with $D_4$ deformation.

A set of ductile shear zones overprint all the above described structures, including $D_4$ crenulation. The zones strike E-W to ESE-WNW, and dip north or south with highly variable angles (Fig. 27a). The shear zones are 5—30 cm wide and 3 m long at a maximum, dextral or less commonly sinistral, and give the penetrative foliation a wavy appearance. Some of these zones contain unoriented, fine-grained quartz-feldspar material with vague margins, suggesting remobilization along them. Because the zones strike subparallel to $D_5$ shear zones and fold axial traces in the gneisses, they are inferred as $D_5$ structures.

## Magnetic fabric study

The rocks in the Silvola stock contain titanomagnetite as an abundant accessory mineral. The euhedral to subhedral grains are elongated subparallel to biotite, hornblende and quartz which define the tectonite fabric. The relatively high susceptibility of the rocks, bulk susceptibility ranging from 110 up to 29000 $10^{-6}$ SI (median value 15470 $10^{-6}$ SI), is reflected as a dark-toned anomaly on the aeromagnetic gray-tone maps (1:100 000; maps 4122 and 4211).

The anisotropy of magnetic susceptibility was measured from 34 samples (1—3 measurements per sample). The magnetic foliations (the planes containing maximum and intermediate susceptibility) and lineations (the maximum susceptibility) correspond well with structural measurements made at each site (Fig. 29). The parallelism of magnetic foliation with $F_4$ axial plane is obvious at the southern contact: in the zone of intense $F_4$ folding (Fig. 28d), foliation in both the tonalite and the diopside amphibolite is parallel to $F_4$ axial plane, whereas 50 meters away, it is parallel to the contact and $S_2$ in the tonalite. The magnetic fabric may be due to reorientation of magnetite grains, or crystallization of secondary magnetite during $D_4$. The grains are in places surrounded by titanite which may be due to exsolution of Ti during recrystallization. Thus the magnetic fabric generally records $D_4$ deformation rather than magmatic flow or emplacement strain.

At the northern contact, the magnetic foliation is parallel to the contact rather than $F_4$ axial plane. Here, also the petrofabric is parallel to the contact. Apparently the marginal zone cooled earlier than the rest of the pluton; when the magnetite grains in the inner parts were recrystallized or reorientated during $D_4$, the grains at the contact retained the emplacement (syn-$D_2$) fabric.

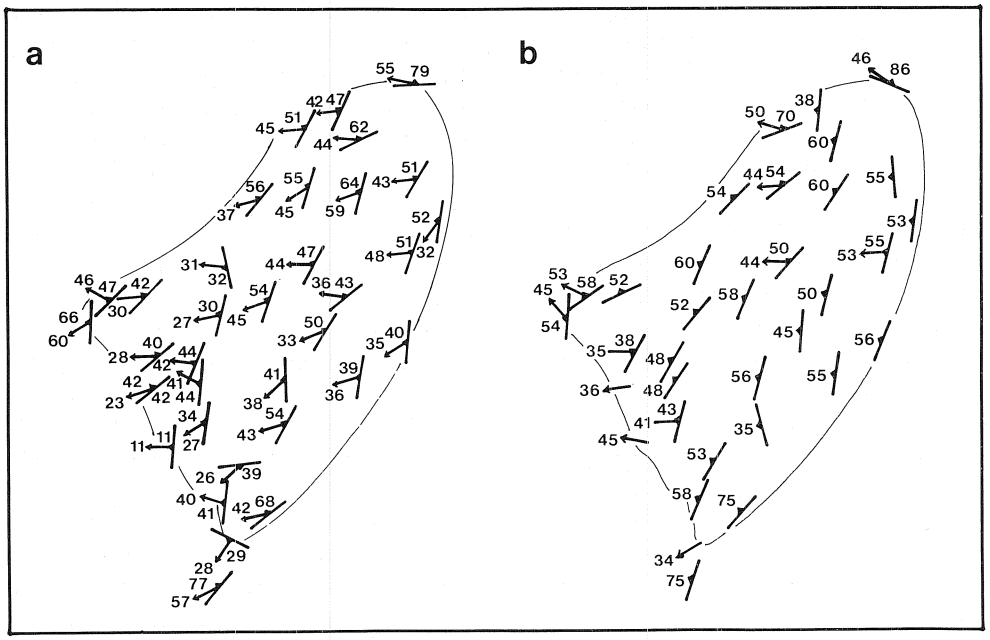


Fig. 29. a) Magnetic foliations (planes containing maximum and intermediate principal axes of the magnetic fabric ellispoid) and lineations (maximum principal axis) measured in the Silvola stock. b) Petrofabric of the sites where the samples for the magnetic fabric study were taken.

## Dikes

Both pegmatite and aplite dikes, usually 2—20 cm in width, occur in the Silvola stock, but the former are far more common. A group of pegmatite and aplite dikes crosscut the $S_2$ fabric but are overprinted by $D_4$. Rectilinear, undeformed dikes are encountered in the marginal areas of the pluton, and they strike at high angles to the contacts.

## Enclaves

Roundish microgranitoid enclaves with slightly varying compositions occur in the Silvola pluton, with a maximum density of one per 2 $m^2$. They are strongly elongate parallel to $S_2$, with longitudinal dimensions in horizontal section from a few centimeters to some tens of centimeters. The effects of $D_4$ crenulation are clearly visible in some enclaves. The few amphibolite xenoliths observed are strongly elongated, and occur parallel to the southern contact.

## Contact metamorphism

Within 500 m from the southern contact of the Silvola stock, the cordierite gneiss contains roundish garnet porphyroblasts 1—4 mm in diameter (Fig. 30a). In places both elongate garnet porphyroblasts (see Fig. 26e) and roundish ones can be seen at the same outcrop. Hence, the latter may

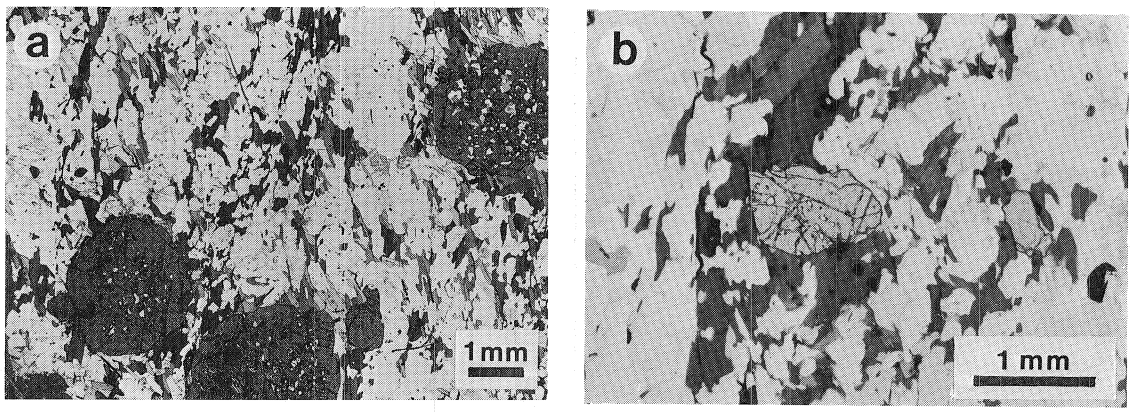


Fig. 30. a) Photomicrograph of contact metamorphic (?) garnet porphyroblasts in biotite gneiss near the southern contact of the Silvola stock. Note the small biotite inclusions in garnet. Nicols parallel. b) Garnet is partly dissolved against coarse biotite of the matrix.

be contact metamorphic. The porphyroblasts contain small, poorly oriented biotite inclusions. The coarse biotite flakes in the matrix wrap around garnet, but in places the garnet is dissolved against biotite (Fig. 30b; cf. Bell and Rubenach 1983). The biotite inclusions and dissolution against the coarse biotite in the matrix suggest that the garnet grew during $D_2$, or at least before the end of $D_3$, if the matrix biotite is $MS_3$.

## Geochemistry

The major element variation diagrams show differentiation within the tonalite-trondhjemite (Fig. 31). There is a distinct scatter in the granodiorite plots. $TiO_2$, MgO, FeO and $Al_2O_3$ have continuous, negative correlations with $SiO_2$ (from 64 % to 73 %). $Na_2O$ has fairly constant values along the $SiO_2$ range. The differentiation mechanism cannot be deduced from the major element trends. The $SiO_2$ distribution and some major element ratios (e.g. FeO/MgO) form curious N-S trending zones, especially one extending north from the southern edge of the pluton (Fig. 32). Although the sample density is fairly low, the zones seem to be parallel with $F_4$ fold axial plane. The zones of low $SiO_2$ content and low FeO/MgO ratio may represent less fractionated levels of a stratified pluton which are exposed as antiformal crests of large scale $F_4$ folds. The geochemical variation is slightly different from the lithological variation (Fig. 25) in the pluton.

## Structural setting and emplacement

The concordance of the Silvola stock with the $D_2$ structures in the supracrustal rocks, and the probably contact metamorphic ($MS_2$) garnet porphyroblasts suggest that the emplacement of the pluton was synchronous with $D_2$. Relationship to $D_3$ is not clear, because effects of $D_3$ deformation could not be identified within the pluton. Possibly the effects of $D_3$ were restricted to a relatively narrow zone, and the Silvola stock remained almost undeformed during this event.

Stoping must be rejected as an emplacement mechanism because of the paucity of wall rock

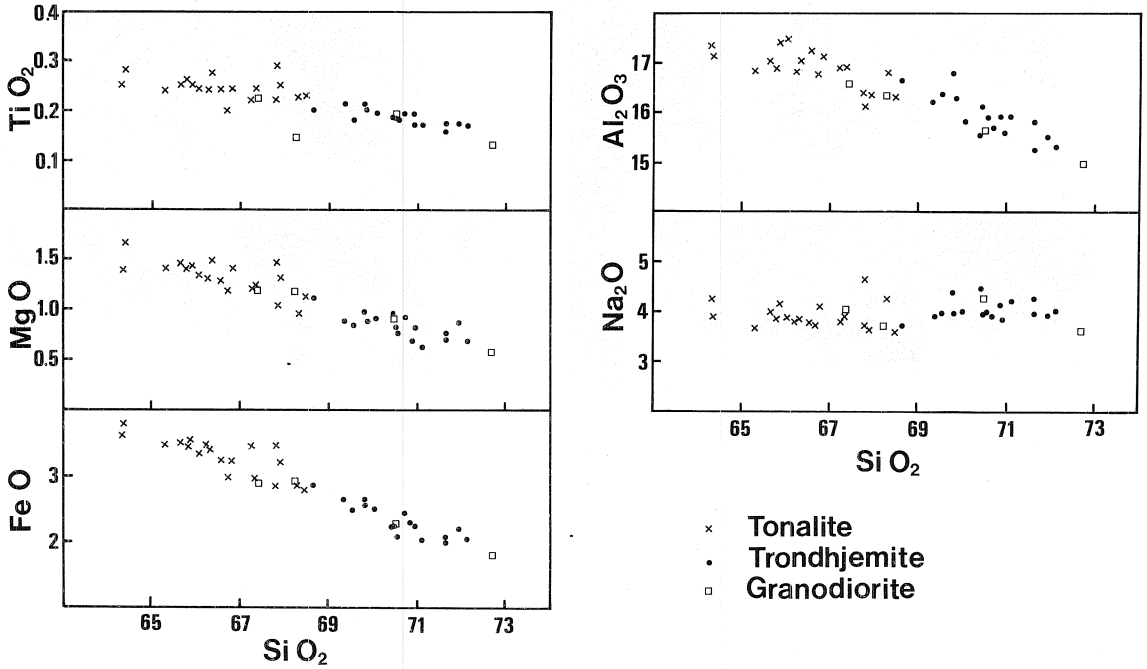


Fig. 31. Variation diagrams for rocks of the Silvola stock (40 analyses).

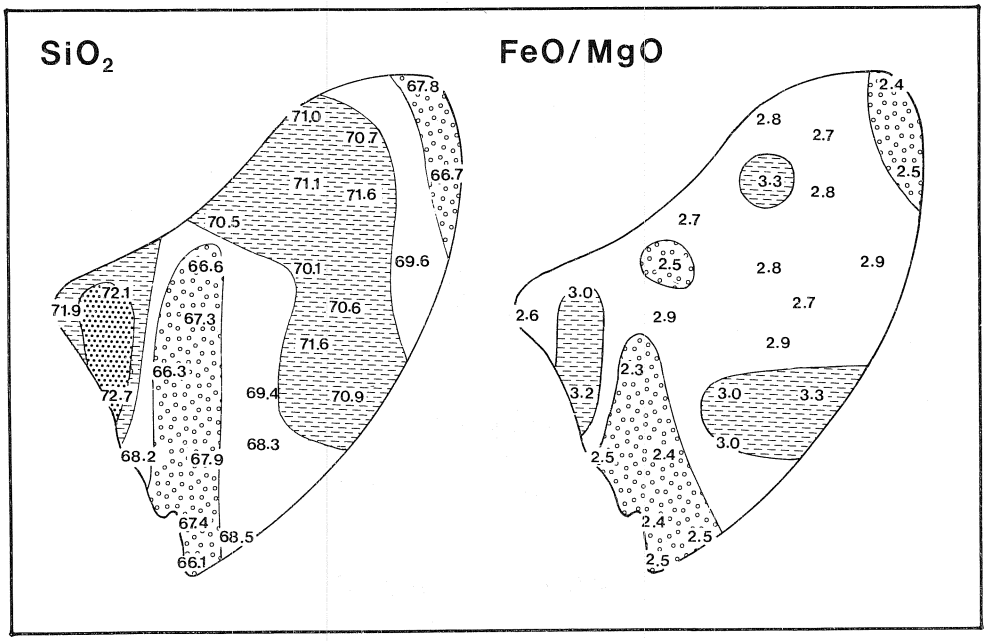


Fig. 32. Variation of $SiO_2$ contents and FeO/MgO ratio in the Silvola stock.

xenoliths. The emplacement mechanism cannot be inferred from the LS tectonite fabric, because the emplacement fabric is overprinted by later deformation. The contact-parallel $S_2$ foliation which can be discerned also within the pluton, suggests diapiric emplacement. The rectilinear pegmatite and aplite dikes which are at high angles to contacts cannot be used to infer ballooning, because the pluton was intensely deformed after the emplacement.

The pluton was not entirely crystalline when the older, pre-$D_4$ shear zones were formed. The crenulation, recrystallization and possibly major scale folding during $D_4$ indicate that the pluton was still fairly hot. The ductile pattern of the post-$D_4$ shear zones, and the unoriented leucocratic material in the middle of these zones, possibly due to remobilization, suggest that the pluton was still relatively warm during this late stage ($D_5$?) deformation.

It is suggested that the pluton was emplaced during $D_2$ as a diapir, remained almost undeformed during $D_3$, and was deformed into its present triangular form during $D_4$ when it was crystalline but still fairly hot. This interpretation is essentially the same, although with a different nomenclature of deformational events, as the one presented by G. Gaál (1984, personal communication).

## THE KAARTILA STOCK

The western part of the Kaartila stock is covered by water (Fig. 25), but by aeromagnetic maps the stock is inferred to be oval-shaped and cover a 8 km$^2$ area. Modal compositions, ranging from monzogranite to tonalite, do not show any regular distribution of the different rock types. The prevailing rock type is granodiorite. Main minerals are plagioclase ($An_{16-14}$), quartz and K-feldspar. The quartz grains show undulatory extinction but no recrystallization, even in distinctly foliated rock. Perthitic exsolution texture is typical for K-feldspar. Both biotite and hornblende are present. Rare garnet was observed as small anhedral grains.

The rocks vary from a fairly homogeneous, fine-grained type occuring mostly in the central part of the stock, to the prevailing heterogeneous type (Fig. 33a). In the latter, abundant mica-rich streaks and leucocratic (quartz-feldspar and quartz) veins with vague margins give a streaky and migmatitic texture (Fig. 33b). The leucocratic veins are usually 0.5—2 cm wide but some pegmatitic ones are up to 15 cm wide. The mica-rich streaks are always parallel to the penetrative foliation but the leucocratic veins occur also as subparallel ones. The foliation-parallel veins may be primary flow structures formed during emplacement, due to metamorphic segregation or to partial melting in situ. In the streaky rock type with foliation-parallel veins, there are small patches of coarse, unfoliated material with irregular margins. If the patches were due to late crystallization of melt, then the mica-rich streaks and foliation-parallel leucocratic veins were formed during emplacement.

Effects of contact metamorphism were not observed in the gneisses around the Kaartila stock.

### Structure

The penetrative foliation within the pluton, denoted as $S_2$, is concentric and conformable with the contacts and composite $S_2$ foliation in the country rocks (Fig. 34), and it dips steeply outward in the marginal areas. Although the dip angles generally decrease toward the center, the change of dips is not regular.

The tectonite fabric is planar except in the center of the stock where a weak, subhorizontal mineral lineation occurs. The fabric is displayed by the preferred orientation of biotite and hornblende, and by an elongation of quartz grains. Intensive flattening strain is seen at the southern contact, where granodiorite and amphibolite layers alternate

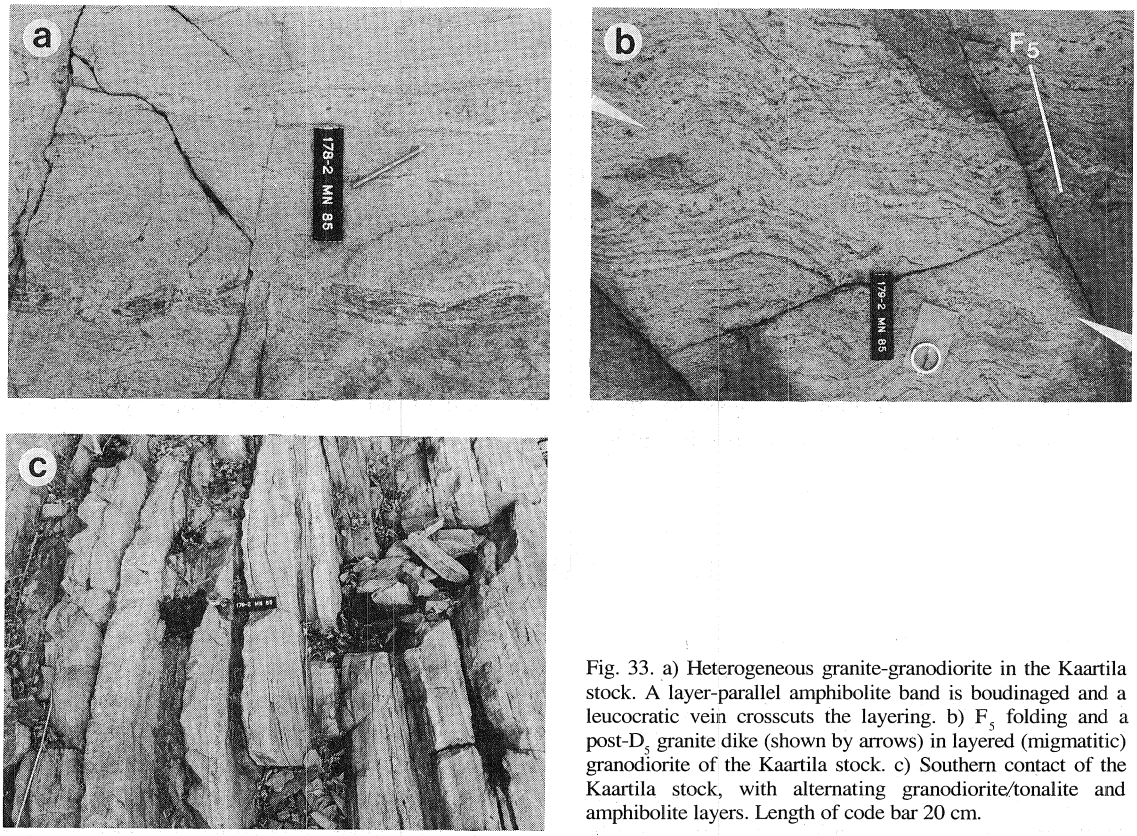


Fig. 33. a) Heterogeneous granite-granodiorite in the Kaartila stock. A layer-parallel amphibolite band is boudinaged and a leucocratic vein crosscuts the layering. b) $F_5$ folding and a post-$D_5$ granite dike (shown by arrows) in layered (migmatitic) granodiorite of the Kaartila stock. c) Southern contact of the Kaartila stock, with alternating granodiorite/tonalite and amphibolite layers. Length of code bar 20 cm.

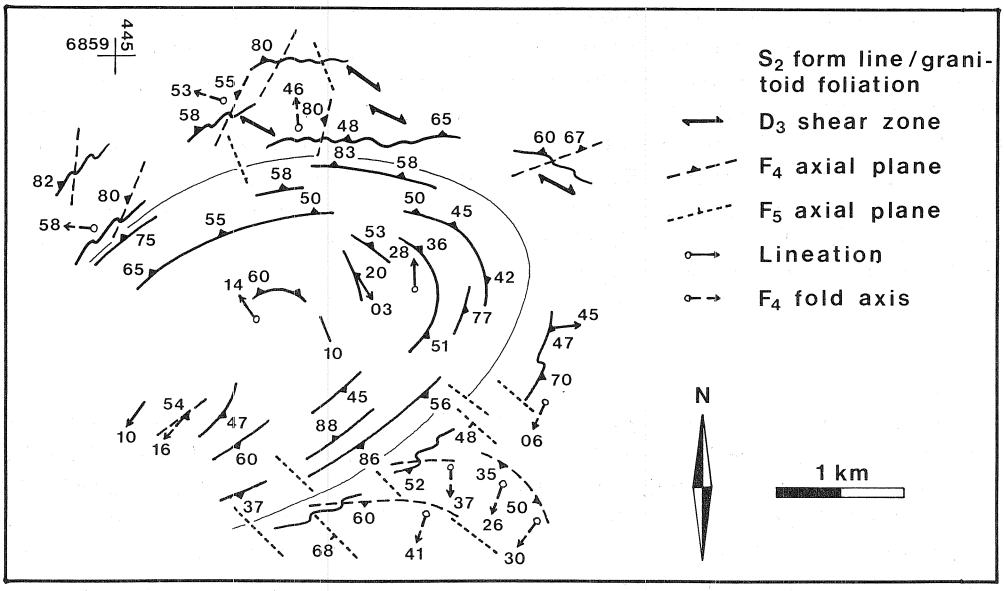


Fig. 34. Structural map of the Kaartila stock and surrounding rocks.

(Fig. 33c). Moreover, the crosscutting leucocratic veins have been folded and rotated toward parallelism with $S_2$.

Within the pluton, there are a few zones of high strain, several meters wide, trending NNE-SSE. They exhibit a L<S fabric with a gently WSW plunging lineation. In places $S_2$ is folded, and the gently plunging fold axes are parallel to the lineation seen in the zones of high strain. These structures are interpreted as contemporaneous with the $F_4$ folds rather than $D_3$ structures in the surrounding supracrustal rocks on the basis of subparallel fold axial planes. The tight $F_4$ folds in the wall rocks are dextral near the northwestern contact, sinistral near the southeastern contact, and symmetric near the northern contact. The $F_4$ fold axes plunge away from the contacts.

A set of NW-SE striking, moderately to steeply southwest dipping $D_5$ shear zones 5—15 cm wide overprints the structures described above (Fig. 33b). They have both dextral and sinistral shear sense, as in the surrounding gneisses.

## Dikes

Abundant pegmatite dikes crosscut the $S_2$ foliation trend within the pluton but are deformed themselves, and some deformed dikes crosscut earlier dikes. At the southern margin there is a set of undeformed granite dikes a few centimetres wide which crosscut $D_5$ structures (Fig. 33b).

## Enclaves

Microgranitoid enclaves are lacking, but xenoliths of supracrustal rocks occur sporadically in the pluton, mostly near the contacts. Small biotite-rich xenoliths with vague margins and larger mica gneiss xenoliths are elongate parallel to the foliation. Their length ranges from less than a meter to over 10 meters, the largest xenolith covering more than 30 m x 40 m. The gneisses are strongly assimilated, and there are abundant leucocratic segregation veins with mafic selvedges (Sawyer and Robin 1986) in the gneisses. The number and size of amphibolite xenoliths is less. At the southern margin, the amount of sheet-like amphibolite xenoliths increases gradually over a few tens of meters toward the contact, and the granitoid becomes more mafic. At the contact there are alternating amphibolite and granitoid (granodiorite/tonalite) layers (Fig. 33c).

## Geochemistry

It is difficult to discern any variation in the major element compositions against $SiO_2$ in the rocks of the Kaartila stock, largely due to the restricted range of $SiO_2$ content (71 % to 77 %; Fig. 35a) of the samples. $SiO_2$ contents are slightly higher and MgO contents lower in the center of the pluton than in the margins (Fig. 35b). A characteristic feature is that $K_2O$, Ba, Rb and Th contents vary considerably. When plotted against each other, these elements show fairly clear trends. The distribution of these elements in the pluton is clearly concentric (the pattern of Ba and Rb shown in Fig. 35b), the highest values being in the center. These features indicate that the pluton is somewhat differentiated (mainly in incompatible elements), and that it increasingly evolved toward the center.

## Structural setting and emplacement

The emplacement of the Kaartila stock is interpreted as synchronous with $D_2$ because of the continuation of conformable foliation ($S_2$ in wall rocks) across the contacts. If the folded $S_2$ fabric and zones of high strain were due to $D_4$, the pluton was still warm enough to deform in a ductile

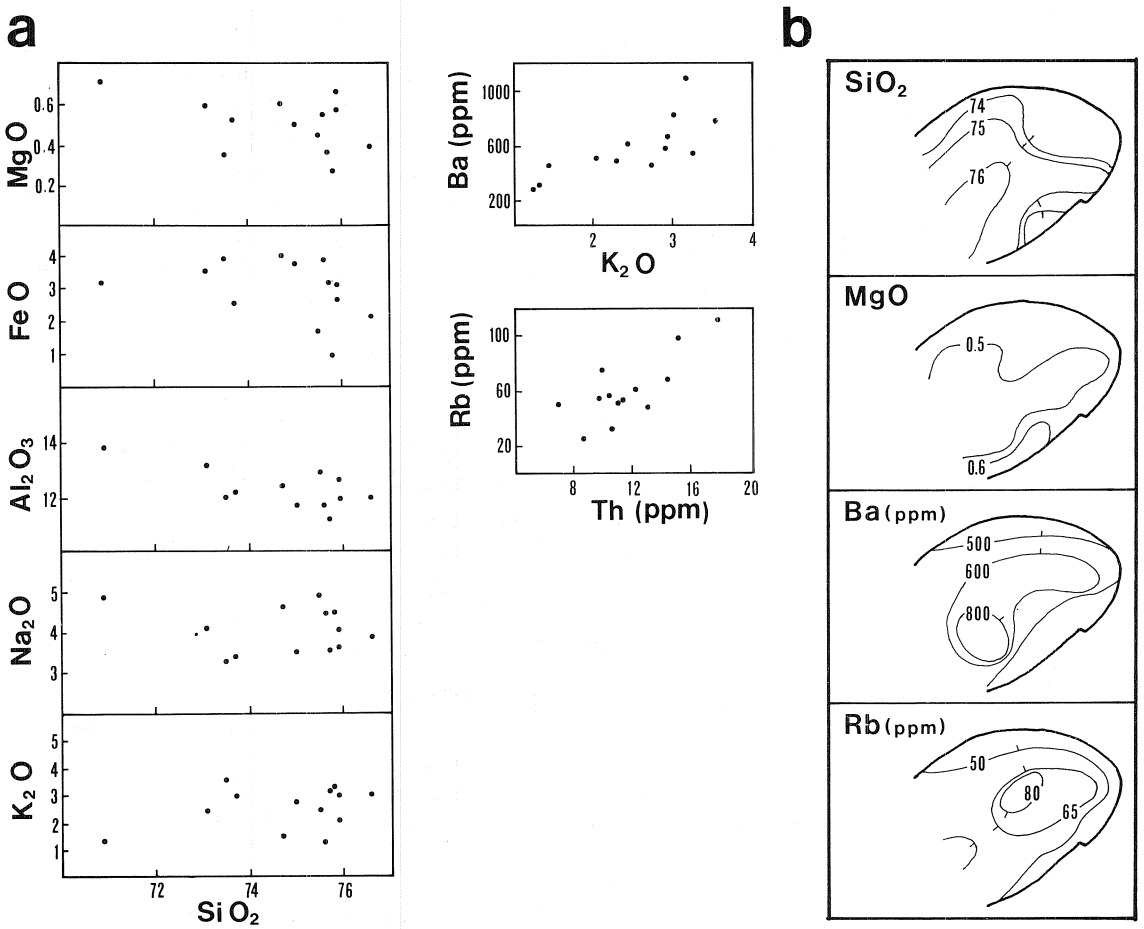


Fig. 35. a) Variation diagrams for rocks of the Kaartila stock (13 analyses). b) Variation of $SiO_2$, MgO, Ba and Rb contents in the Kaartila stock.

manner, although deformation concentrated in narrow zones.

The high $SiO_2$ content, the relatively large amount of mica gneiss xenoliths and the general heterogeneity of the rocks suggest that the pluton was formed by partial melting of metasedimentary rocks (cf. Flood and Vernon 1978, Wickham 1987). The xenoliths may be regarded as unmelted restite material, and the accessory garnets as remnants of almost totally resorbed restite. However, the abundant hornblende in the granitoids, and the amphibolite xenoliths indicate a mafic component, i.e. the pluton probably has a mixed origin. Such a source could be a mixture of metagreywackes and mafic metavolcanic rocks. The concordance and conformity of the granitoid foliation and foliation in the wall rocks, the general flattening strain in the marginal areas, and the subhorizontal lineations in the center of the pluton suggest diapiric emplacement. If the magma was generated by partial melting of supracrustal rocks, with a substantial volume of metasedimentary rocks, it probably was rather hydrous. The abundance of pegmatite dikes and leucocratic veins in the Kaartila stock is consistent with such an origin. The hydrous magma could not ascend far from the source area (Cann 1970, Hyndman 1981); possibly it only expanded the overlying strata as an immature diapir.

The slight differentiation, mostly in incompatible elements, may be the result of progressive partial melting, and/or fractional crystallization during ascent. Partial melting, ascent of the magma and final emplacement probably occurred during progressive $D_2$, contemporaneously with prograde metamorphism in the area.

## MODEL FOR THE STRUCTURAL EVOLUTION OF THE GNEISSES AND THE SILVOLA AND KAARTILA STOCKS

Since $D_1$ structures are mostly obliterated in the gneisses, their original orientation cannot be deduced. Although the orientation of $F_2$ folding and the penetrative $S_2$ foliation were mostly transposed during subsequent deformation, compression in the present N-S direction is inferred. Both plutons were emplaced as diapirs during $D_2$ (Fig. 36a). The Silvola tonalite ascended from a deeper structural level than the Kaartila granite-tonalite which only expanded the overlying strata as an immature diapir. A NW-SE trending zone of noncoaxial deformation was generated in the gneisses, in which dextral $D_3$ folds and shear zones developed and earlier structures were transposed

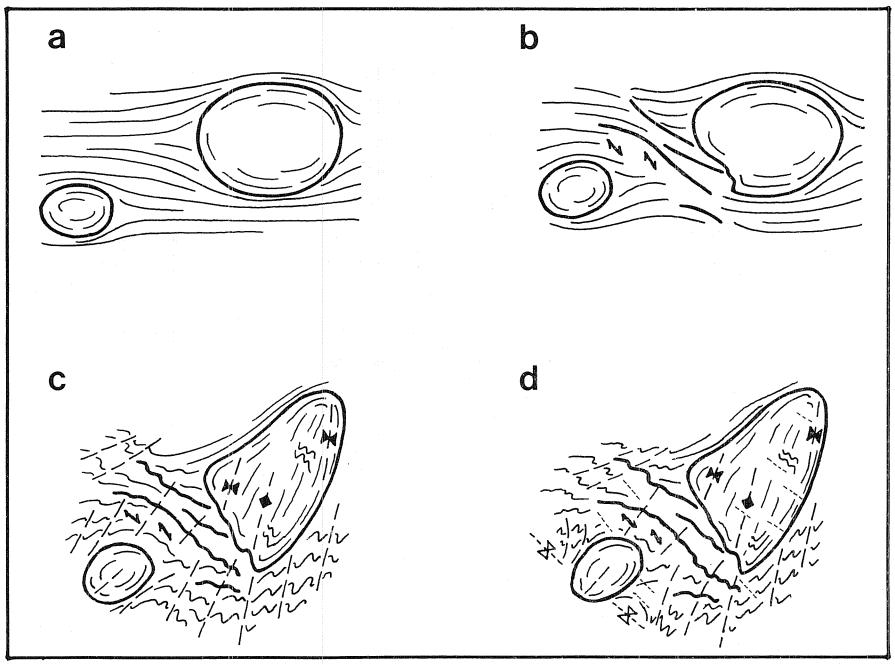


Fig. 36. Model for the structural evolution in the Silvola-Kaartila area. a) The plutons were emplaced diapirically during $D_2$. b) During subsequent $D_3$ dextral shear, $D_2$ structures were reoriented in the area between the plutons. c) The gneisses were intensely $F_4$ folded, and the penetrative foliation in the Silvola stock was crenulated. The Silvola stock was deformed into its present triangular form. d) During $D_5$, minor open folding was generated, but in the western part of the area (and further west), large dome and basin structures were generated due to $D_4$—$D_5$ fold interference.

(Fig. 36b). During $D_4$, WNW-ESE compression lead to folding with roughly NNE trending axial trace. The Silvola tonalite was folded and attained its present triangular form (Fig. 36c). $D_4$ deformation was probably essentially coaxial, because $F_4$ folding developed asymmetrically around the Kaartila stock, and $F_4$ folds are symmetrical further away from the plutons. Although the intensity of $D_4$ grew toward ESE, the plutons behaved as semirigid bodies. Hence, the area between the plutons was a strain shadow and $F_4$ folding was weak.

During $D_5$, $D_4$ synforms and antiforms were deformed into domes and basins in the southwestern part of the study area (Fig. 36d). The intensity of $D_5$ seems to have been greater in the southwestern part of the study area. There is no evidence of doming of the Kaartila pluton during this late stage.

A peculiar feature is the occurrence of the diopside amphibolite rims around the plutons. A similar envelope occurs also around another granitoid pluton, the Käkövesi batholith, in high grade metamorphic environment of southeastern Finland (Nurmi et al. 1984). Because amphibolites are scarce in the surrounding supracrustal rocks, their existence around the plutons is apparently related to the emplacement of the latter. In centrifuge experiments of domal structures, a ring of denser material, originally overlying the upwelling lighter material, formed around the domal structure (Ramberg 1967, Fig. 88). In analogy, the rims may be part of overlying volcanics that vertically collapsed during the diapiric emplacement of the plutons. Another possibility is that the amphibolites were dragged along the ascending diapirs from a deeper crustal level.

## THE VARPARANTA STOCK

The Varparanta stock is about 20 km north from Savonlinna and about 20 km northwest from the Silvola and Kaartila stocks (see Fig. 24). The exposed part of the pluton is roughly 45 km$^2$ in area, but the western part is covered by water (Fig. 37). Aeromagnetic data (gray-tone map 4211, 1:100 000) suggests an additional 4 km$^2$ area, and a lensoid shape for the pluton.

The northern part of the stock is surrounded by migmatitic cordierite gneisses with thinly laminated felsic schists and amphibolites as interlayers. The cordierite gneisses were probably originally turbidites, and the interlayers were felsic and mafic tuffites. The cordierite, garnet and K-feldspar porphyroblasts in the cordierite gneisses suggest peak metamorphic conditions similar to those in the Silvola-Kaartila area. To the south of the stock, the host rocks are diopside amphibolites of volcanic origin. Diopside-rich parts occur as layers less than 10 cm in thickness, or as fragments. Pillow lavas have been encountered in the same succession (Gaál and Rauhamäki 1971).

The main rock type of the pluton is tonalite. It is equigranular or slightly porphyritic, with subhedral plagioclase phenocrysts (5—12 mm in size) in a medium-grained matrix. Plagioclase ($An_{32—28}$) is unzoned. Biotite is more abundant than hornblende. Hornblende, K-feldspar titanite, apatite, magnetite and zircon occur as accessory minerals. In the center of the two domal structures (see below), the rocks are trondhjemitic, with slightly more albitic plagioclase ($An_{25—17}$). The trondhjemites are characterized by small, roundish or elongate quartz grains and aggregates 2—5 mm in size.

Toward the margins of the domes the rock becomes banded in such a way that lenses, 2—50 cm thick and up to several meters long, of quartz dioritic composition alternate with tonalite (Fig. 38a). In places the banded rock grades into a patchy type (Fig. 38b).

In the southern part of the stock, there is a separate trondhjemite (labelled as magnetite-rich trondhjemite in Fig. 37) which intersects the main tonalite with sharp contacts. It has a smaller grain size and higher magnetite content than the surrounding tonalite. At the southern contact against diopside amphibolite, a foliated, porphyritic tonalite with fine-grained matrix crosscuts the amphibolite

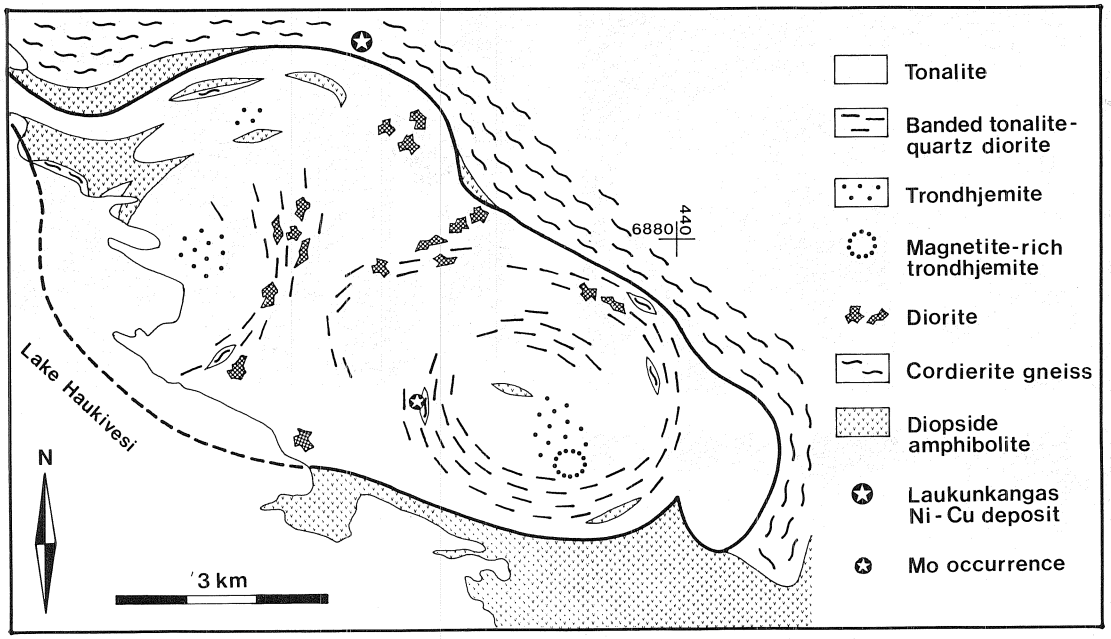


Fig. 37. Geological map of the Varparanta stock (based chiefly on mapping by the author, with data of Outokumpu Exploration).

(Fig. 38c). The unzoned plagioclase phenocrysts, 1—3 mm in size, are more altered and slightly more calcic ($An_{16}$) than the matrix plagioclase ($An_{13}$). The porphyritic tonalite is crosscut by an unfoliated, porphyritic granodiorite dike. In the granodiorite, both phenocryst and matrix plagioclase are zoned ($An_{17—10}$).

Pegmatite and aplite dikes 3—10 cm in width occur sporadically within the pluton. There are pegmatite dikes both crosscutting and parallel to the foliation of the tonalite. The few observations preclude any orientation analysis. In the center of the pluton (Fig. 37), there is a small, lenticular Mo occurrence which consists of mineralized and silicified tonalite, crosscut by mineralized quartz veins.

## Structure of the gneisses and amphibolites

In the cordierite gneisses, the oldest foliation is defined by the preferred orientation of biotite and cordierite. In places the cordierite, garnet and plagioclase porphyroblasts contain fibrous sillimanite as crenulated relics, similar to the sillimanite in the Silvola-Kaartila area. The crenulation demonstrates the existence of an older tectonite fabric, and hence the penetrative foliation is denoted as $S_2$. The development of $S_2$ was associated with growth of cordierite and K-feldspar porphyroblasts, and metamorphic differentiation, which generated foliation-parallel leucocratic segregation veins. Moreover, abundant granitic and pegmatitic dikes, 0.5—5 cm in thickness, crosscut $S_2$ at small angles. Isoclinal folding of the dikes, with $S_2$ in the axial surface, shows that they were deformed in $D_2$. In the diopside amphibolites, $S_2$ and $L_2^2$ stretching lineation are seen as preferred orientation of hornblende grains (c axes). The compositional layering in the diopside amphibolites is at least partly due to deformation and differentiation during $D_2$.

The composite $S_2$ foliation is overprinted by tight to isoclinal $F_3$ folds. $F_3$ folding, with moderately

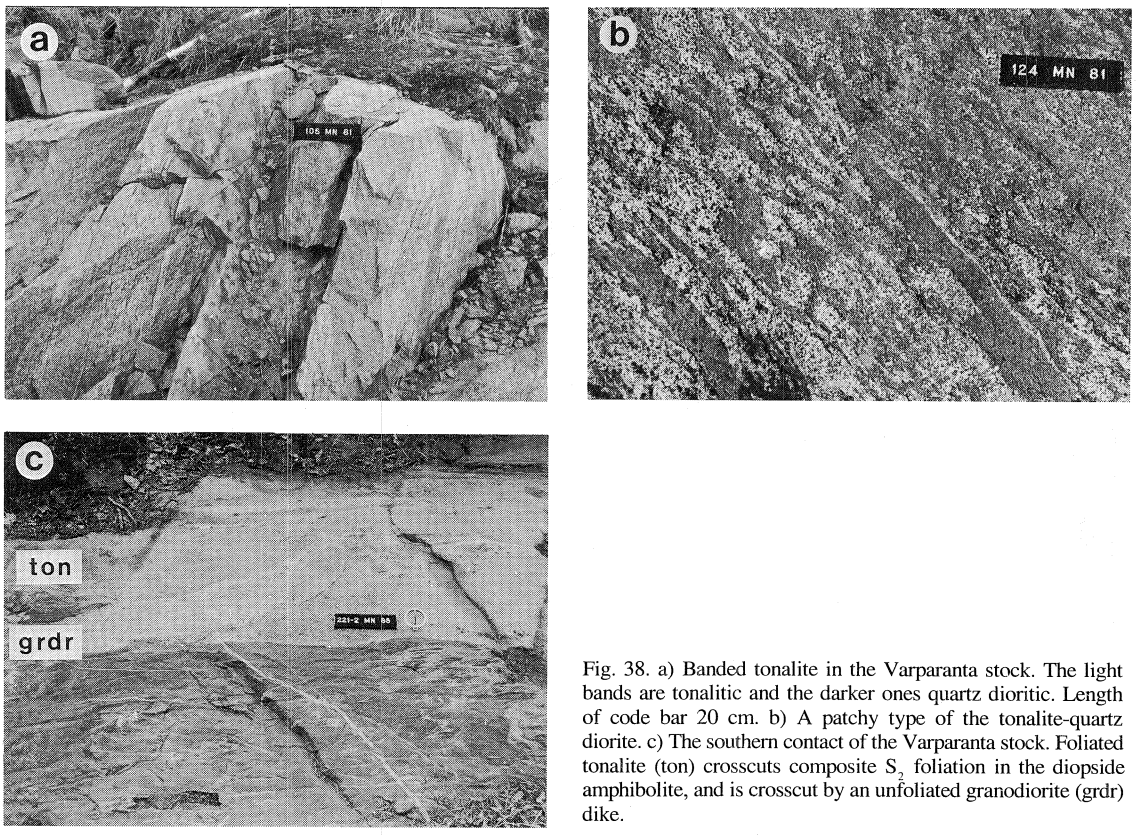


Fig. 38. a) Banded tonalite in the Varparanta stock. The light bands are tonalitic and the darker ones quartz dioritic. Length of code bar 20 cm. b) A patchy type of the tonalite-quartz diorite. c) The southern contact of the Varparanta stock. Foliated tonalite (ton) crosscuts composite $S_2$ foliation in the diopside amphibolite, and is crosscut by an unfoliated granodiorite (grdr) dike.

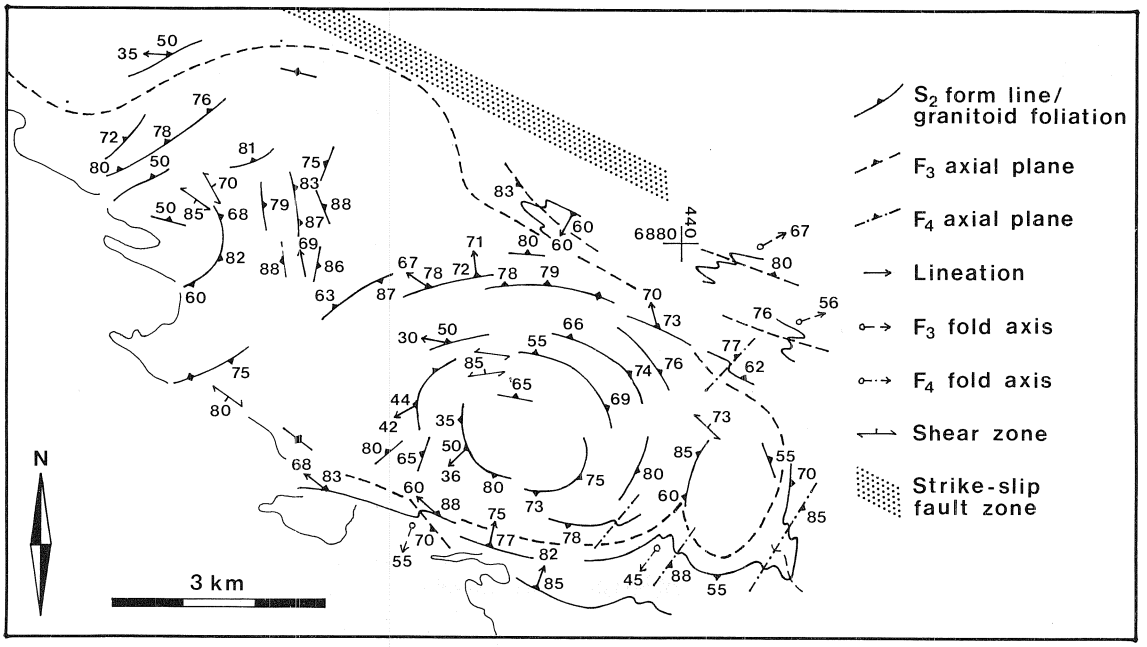


Fig. 39. Structural map of the Varparanta stock (based chiefly on mapping by the author, with data of Outokumpu Exploration).

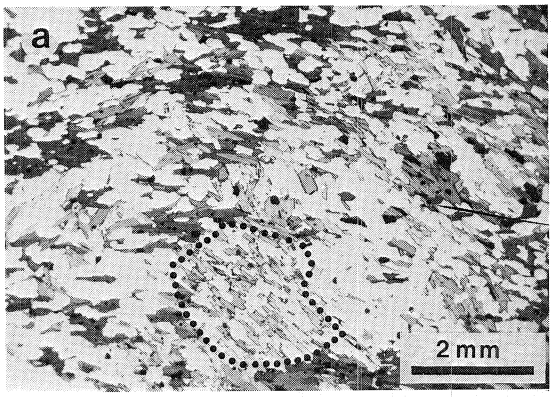


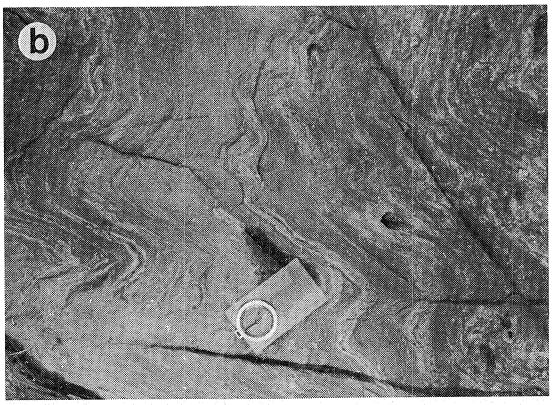


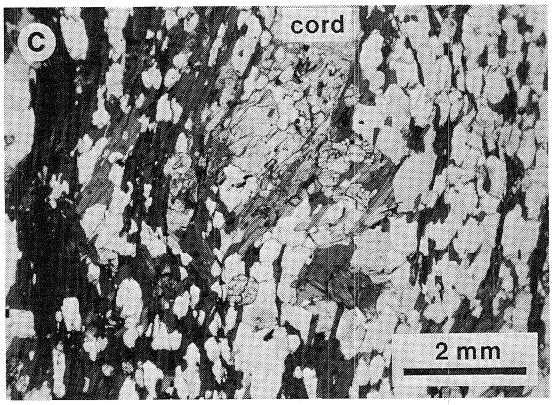


Fig. 40. a) Photomicrograph of $F_3$ crenulation in cordierite gneiss near the northeastern contact of the Varparanta stock. Coarse $MS_3$ biotite overgrows $MS_2$ biotite. $MS_2$ biotite is preserved in K-feldspar (rimmed by points) Nicols parallel. b) $F_4$ folding in diopside amphibolite near the southern contact of the Varparanta stock. Length of compass 12 cm. c) Photomicrograph of cordierite gneiss at the northeastern contact of the Varparanta stock. Roundish garnet porphyroblasts overgrow $S_3$ differentiated foliation. Cordierite (cord) is strongly pinitized. Nicols partly crossed.

plunging fold axes and subvertical, WNW-ESE striking axial surfaces, govern the structure of the gneisses north of the Varparanta stock (Fig. 39). The folds are similar or chevron-type, both symmetric and asymmetric, with wavelengths and amplitudes ranging from 10 cm to over a meter. The wavelengths of enveloping surfaces are probably much greater. In silty layers, $S_2$ is crenulated, and in $F_3$ fold hinges the $S_3$ foliation is distinctly differentiated (Fig. 40a). Cordierite is strongly pinitized in $F_3$ microfold hinges. In the diopside amphibolites, neither foliation nor fracturing, overprinting $S_2$ layering, was observed.

Gaál and Rauhamäki (1971) delineated a strike-slip fault zone along the northern margin of the Varparanta stock. It trends WNW-ESE, parallel to $F_3$ axial trace. A pipelike body of layered gabbro, hosting the Laukunkangas Ni-Cu deposit (Grundström 1980) is within the fault zone (Fig. 37). The zone is part of the strike-slip fault system that controls the emplacement of the Ni-Cu occurrences and their mafic-ultramafic host plutonic rocks along the Raahe-Ladoga zone (Gaál 1972). $D_3$ structures are not overprinted by a foliation or a fracture system. Thus the fault zone may be a zone of intensified $D_3$ strain.

$F_4$ folding is open to tight, with axial surfaces striking NE-SW (Fig. 39). In crenulated layers of cordierite gneisses, hinges of $F_4$ microfolds exhibit growth of large biotite grains in the axial plane, and retrogression of cordierite into muscovite. In diopside amphibolite, $F_4$ occurs as similar folding (Fig. 40b) without mineral orientation parallel to the axial plane.

## Structure of the Varparanta stock

Macroscopically, the Varparanta stock is concordant to $S_2$ in the country rocks (Fig. 39). On outcrop scale, the plutonic rock brecciates wall rocks or occurs as layer-parallel sheets. At the southern contact, tonalite sheets from a few centimeters up to over a meter wide occur subparallel to layering and $S_2$ in diopside amphibolite. The contact zone is about 20 m wide, and the amount of tonalite sheets gradually diminishes away from the pluton. The porphyritic tonalite (Fig. 38c) brecciates the foliated diopside amphibolite, but contains rather weak $S_2$ foliation.

In the stock, the foliation defines two domal structures with weakly foliated centers. Foliation is expressed as preferred orientation of biotite flakes, and of quartz grains and aggregates. The intensity of foliation grows toward the margins where the banded rock type prevails. Foliation dips gently outward in the center of the eastern dome, and gradually steepens until near the contacts it is subvertical and parallel to $S_2$ in the supracrustal rocks. In the western dome the gradation is not as clear as in the eastern one.

The tectonite fabric grades from S type in the center of the domes to L<S in the marginal areas. The gradation is not regular, however, because near the northeastern contact, the fabric changes from S type to L<S within 200 meters. The tectonite fabric is similar in the plutonic rock and in the country rocks at the contact. Hence, the concentric foliation is defined as $S_2$ and the mineral lineation as $L_2^2$. $L_2^2$ plunges anticlockwise with respect to the foliation dip directions. This feature is more distinct in the eastern dome than in the western one.

The lenticular Mo occurrence strikes N-S and dips moderately to the west. The author studied the quartz vein pattern of the Mo occurrence (Nironen 1985). It consists of at least three overlapping extensional en echelon vein arrays which were formed during sinistral transpression, probably at a late stage of emplacement of the pluton.

A set of WNW-ESE trending shear zones, overprinting the banding as well as the foliation and associated lineation, were observed in the pluton. The zones are a few centimeters in width, and they have dextral and sinistral shear senses in horizontal section. They are similar in style and orientation to the $D_5$ structures around the Silvola and Kaartila plutons.

## Contact metamorphism

At the northeastern contact of the Varparanta stock, cordierite gneiss contains small, roundish garnet porphyroblasts which overgrow the differentiated $S_3$ foliation (Fig. 40c). The garnet can be distinguished from the abundant anhedral garnet, and hence it may be contact metamorphic.

## Enclaves

Numerous wall rock xenoliths occur mainly near the contacts and between the domes. They are large diopside amphibolite and mica gneiss xenoliths oriented subparallel to $S_2$, and $S_2$ crosscuts the contact between the xenoliths and the host rocks. The mica gneiss is garnet-bearing and contains a distinct foliation, expressed as elongated biotite flakes. In the northwestern part of the pluton, the amount and extent of the xenoliths is partly inferred from geophysical maps.

Roundish microgranitoid enclaves are rather scarce in the Varparanta pluton, occuring mainly in the center of the eastern dome. The enclaves become more elongated toward the margins of the dome, where the banded tonalite-quartz diorite prevails.

Fragments of diorite, with variable sizes and shapes, occur irregularly within the pluton, mainly between the two domes. Some fragments are foliated and oriented subparallel to $S_2$, but the more

hornblende-rich ones are irregularly shaped and brecciated by tonalite. Major minerals are hornblende and plagioclase ($An_{45-27}$; Saltikoff 1965). According to Saltikoff (1965), some fragments are exceptionally apatite-rich (8.6% of total mineral composition), consisting of euhedral hornblende laths and plagioclase as an interstitial mineral. It is quite possible that there is a gradation from separate microgranitoid enclaves through banded tonalite-quartz diorite (Fig. 38a) and the patchy type (Fig. 38b) to diorite fragments.

## Geochemistry

In the major element variation diagrams, $TiO_2$ and CaO define linear, straight trends with a negative slope against $SiO_2$ (Fig. 41). In MgO and FeO versus $SiO_2$, the trends are straight from the quartz diorite to the $SiO_2$-enriched trondhjemites. The magnetite-rich trondhjemite plots at the most evolved end. Considering the low FeO content of the rock type, most Fe must be in magnetite. $Al_2O_3$, $Na_2O$ and $K_2O$ contents are fairly constant in the tonalite-trondhjemite.

Field evidence (banded quartz diorite grading into the patchy type, microgranitoid enclaves possibly grading into banded quartz diorite) and compositional differences in the diorites indicate that there may be a gradation from diorite to quartz diorite. Although the analyses of mafic rocks are few, the data allows some petrogenetic consideration. The deviation of the trends from straight line in the MgO and FeO versus $SiO_2$ diagrams makes partial melting / restite unmixing improbable. The homogeneous tonalites are more $SiO_2$-rich than the enclave-bearing tonalites and the tonalites of the banded type. Moreover, one analysis of a tonalite ($SiO_2$ 57.5 %) which brecciates a diorite fragment, plots between the tonalites and the quartz diorite. In the SrO versus CaO diagram, the same tonalite has the highest SrO value and plots to the intersection of the two trends of the tonalites-trondhjemites and the mafic rocks. These characteristics may be explained by mixing and mingling between a quartz dioritic and a felsic magma. The quartz diorite was the fractionation product of a dioritic/gabbroic magma. The felsic magma was either trondhjemite, from which the tonalites were generated by mixing with quartz diorite, or tonalite, from which the trondhjemites were generated by fractional crystallization in situ.

## Structural setting and emplacement

Gaál and Rauhamäki (1971) suggested that the Varparanta pluton was emplaced as sheets into the supracrustal rocks during $D_1$ and was folded into an antiform during $D_2$, with subsequent fold interference formed during $D_3$. This kind of emplacement mechanism implies the existence of wall rocks in the center of the domes. However, the central areas of the domes consist of fairly homogeneous, weakly foliated tonalite. The continuation of the LS fabric across the contacts, the concordance of the pluton with $D_2$ structures in the country rocks, the mica gneiss xenoliths with a well developed tectonite fabric ($S_2$?) suggest that the pluton intruded during $D_2$. If the foliation in the porpyritic tonalite at the southern contact was generated during a late stage of $D_2$, the pluton had been emplaced by the end of $D_2$. The granodiorite dike expresses post-$D_2$ magmatic activity. Assuming that the small garnet porphyroblasts at the northeastern contact are contact metamorphic, their post-$D_3$ growth suggests close temporal relationship between $D_2$ and $D_3$.

The occurrence of mafic rock as variable patches in a more felsic one has commonly been ascribed due to magma mixing/mingling (e.g. Bayer et al. 1987, Frost and Mahood 1987, Barbarin 1988). In contrast, banding in igneous bodies is a peculiar feature rarely described in geological literature. Callegari and Dal Piaz (1973) described banding and hornblende-rich fragments in the contact zones

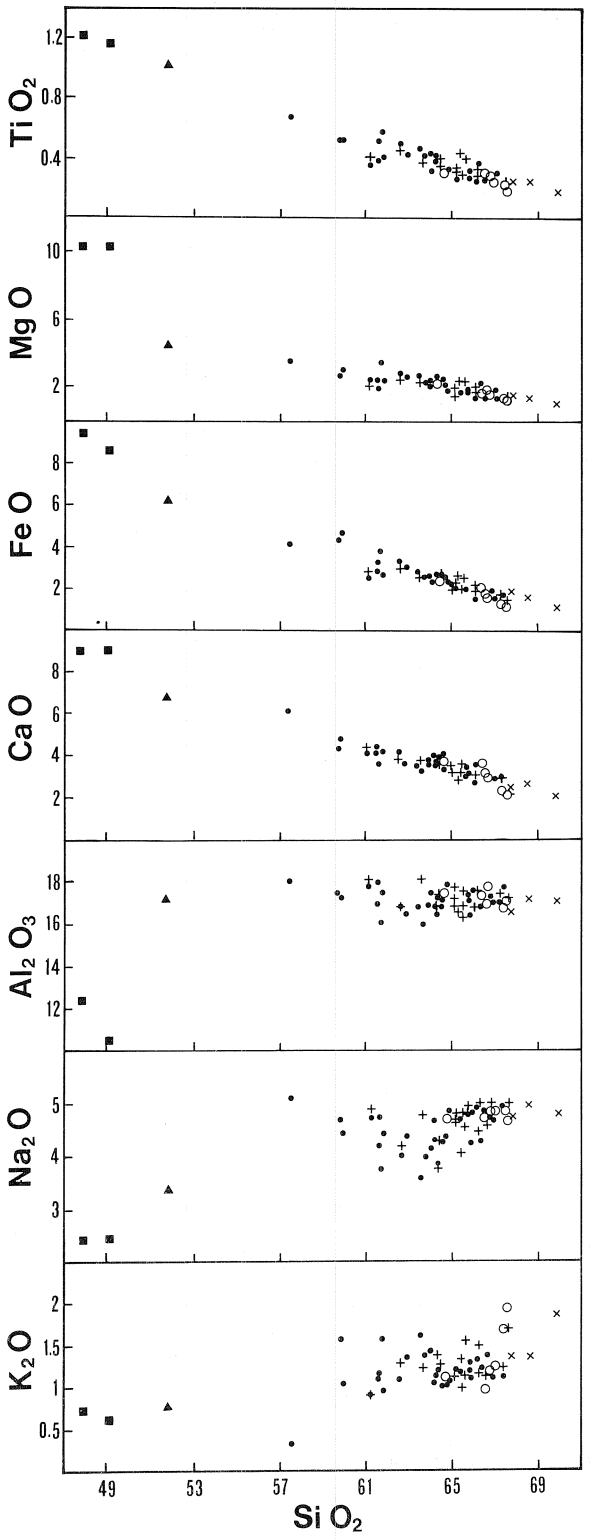


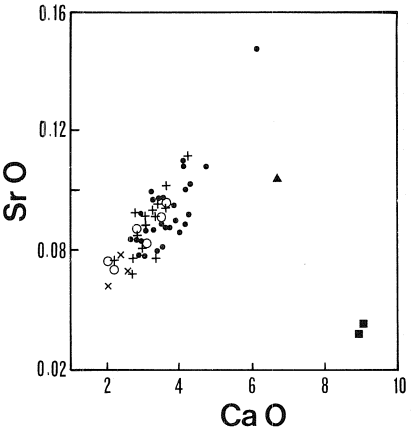


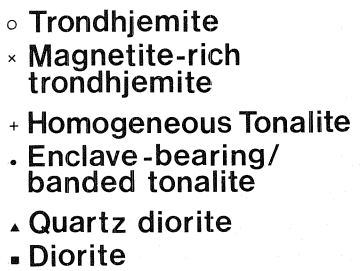


Fig. 41. Variation diagrams for rocks of the Varparanta stock (61 analyses).

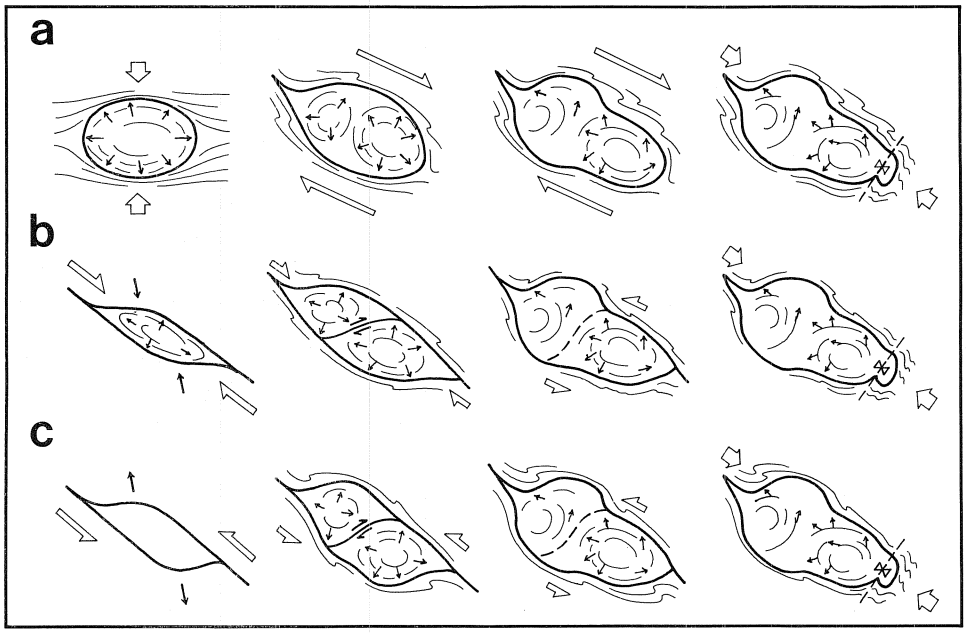


Fig. 42. Emplacement models for the Varparanta stock. a) The pluton was emplaced diapirically during $D_2$ deformation. The whole body was rotated in dextral shear ($D_3$), and was refolded ($D_4$). b) Magma intruded forcefully in a contractional duplex within a strike-slip fault zone ($D_{2-3}$). Two domal structures were generated during dextral shear and subsequent sinistral shear. After shearing had ceased, the pluton was refolded ($D_4$). c) Magma was emplaced passively by pull-apart into a sinistral strike-slip fault zone. During continued sinistral shear, the emplacement became forceful, and the two domal structures were generated. After shearing had ceased, the pluton was refolded ($D_4$).

between successive intrusive bodies of the the Adamello intrusive complex, in northern Italy. According to R. Bateman (1987, personal communication), banding also occurs within the intrusive bodies of Adamello, like in the Varparanta pluton. Pitcher and Berger (1972, p. 251) interpreted similar banding in the Main Donegal granite pluton, in Ireland, as due to mechanical segregation of partly crystalline magma during emplacement of the pluton as a series of coalescing vertical sheets. Hutton (1982) agreed with the concept of shearing of partly consolidated material as the cause for banding, although he rejected the emplacement model of Pitcher and Berger (1972). Banded lavas have been interpreted as due to mingling between silicic and more mafic magma (Bacon 1983).

In the Varparanta pluton, mingling and (minor) mixing occurred between the tonalitic/trondhjemitic magma and the most evolved part of the mafic phase (quartz dioritic magma). The patchy and the banded type formed due to shearing of incompletely crystalline material, consisting of two intermingled magmas, during emplacement. The magnetite-rich trondhjemite, the porphyritic tonalite and the granodiorite dikes were the last ones to intrude.

The structural sequence in the country rocks is analogous to the one presented by Parkkinen (1975) for the cordierite gneisses 10 km south of the Varparanta stock. In that area, $D_3$ deformation was ductile shearing (mainly dextral strike-slip faulting) during the culmination of metamorphism. On the basis of map analysis, Parkkinen (1975) concluded that the Varparanta stock is within a NW-SE striking dextral strike-slip fault zone (see also Bowes et al. 1984, Fig. 2). The author observed intense nonaxial deformation with dextral sense of shear in a paragneiss immediately north of the Varparanta stock. However, contrasting interpretations have been made about the location and shear sense of the strike-slip faults (cf. Gaál 1972,

Parkkinen 1975, Talvitie 1975). Gaál and Rauhamäki (1971) inferred that a fault zone with sinistral sense of movement developed along the northern margin of the Varparanta pluton after dextral faulting.

When the emplacement and deformation of the pluton is delineated, the location within a strike-slip fault system, the anticlockwise rotation of the lineations in the domal structures, and the sinistral transpression during Mo mineralization have to be considered. The domal structures, the conformable foliation, the gradual growth of foliation intensity toward the margins and the outward plunging lineations suggest forceful emplacement for the tonalite. Three models are presented. In the first one (Fig. 42a), the Varparanta pluton was emplaced diapirically in a compressional regime ($D_2$). The whole body, hot enough to deform ductilely, was rotated and deformed within a strike-slip fault zone ($D_3$), and the lineations rotated contemporaneously. The southeastern part of the pluton was subsequently refolded ($D_4$). The problem with this model is the double doming of the pluton. Centrifuge models (Ramberg 1970, Plate 14) suggest that a diapir may decay into several domal structures in the mature stage. In analogy, the Varparanta pluton may have separated into two domal structures during emplacement.

In the two other models, a progressive syn $D_{2-3}$ deformation is considered rather than two separate episodes. In the model of Fig. 42b, the pluton was emplaced forcefully along a transpressional fault in a contractional duplex (Woodcock and Fischer 1986) of the dextral strike-slip fault zone. Doming and dextral shearing occurred contemporaneously within the duplex, and the lineations were rotated. In this model, the rotation direction of the lineations is not consistent with dextral shear; perhaps the shear sense changed at a late stage of emplacement. In natural examples of plutons emplaced syntectonically into subhorizontal shear zones (Brun and Pons 1981, Guineberteau et al. 1987), the plunge directions and angles of stretching lineations in and around the plutons vary considerably.

In the third model (Fig. 42c), the pluton was emplaced by pull-apart within a sinistral strike-slip fault zone (Rodgers 1980, Woodcock and Fischer 1986). In continued sinistral shear, a synthetic sinistral shear zone and two domal structures were formed in the pluton, and the lineations were rotated anticlockwise. An analogous model was presented by Guineberteau et al. (1987) for the emplacement of the Mortagne granite, located in the South Armorican Shear Zone, France. However, the emplacement into an extensional pull-apart basin is passive rather than forceful, and thus the doming and outward plunging lineations in the Varparanta stock pose a problem. The emplacement may have been first passive, and subsequently more forceful during waning sinistral shear.

## COMPARISON OF THE GRANITOIDS

### Emplacement mechanism

None of the studied granitoid plutons contain structures that would unequivocally show the emplacement mechanism, but some possibilites can be ruled out; the ones that remain are the most probable, either as sole mechanisms or as combinations. The fact that the plutons are multiphase except for Kaartila and possibly Silvola, has to be taken into account when the emplacement mechanisms are considered.

The scarcity of wall rock xenoliths makes stoping an improbable mechanism except in marginal areas of Varparanta, Värmälä and Hämeenkyrö. The Varparanta stock is within a horizontal shear zone system like the granitoids in the Savonranta area (Fig. 24). However, the shape of the Varparanta pluton is totally different from the ones in Savonranta, the latter being sigmoidal in plan. Hence, pure passive emplacement along a vertical tensional area in the shear zone (cf. Halden 1982) is improbable.

Although the characteristics of a diapir are controversial (see discussion of Van den Eeckhout et al. 1986), the following criteria have been used to distinguish diapiric plutons and gneiss domes

(Coward 1981, Schwerdtner 1981, Bateman 1984):

1) Less dense material with circular or oval shape is surrounded by more dense material;
2) There should be structures such as foliation, cleavage and lineations conformable to the contact. Structures due to diapirism diminish in intensity away from the contact;
3) The strain distributions should involve subhorizontal extension in the crestal area of the less dense material. In the trunk region, the long axes of prolate strain ellipsoids should be vertical;
4) Lineations should form radial or tangential patterns;
5) An approach to concordancy with the contact of pre-emplacement structures (e.g. bedding and regional foliation) should be present;
6) There should be no repetition of layers by folding of the overlying strata, unless earlier deformation phases are involved;
7) The bodies of less dense material should not form any regular pattern such as would be produced by cross folding.

Considering these criteria, diapirism is the most probable emplacement mechanism for the Silvola and Kaartila plutons. They contain a conformable, circular foliation, and the main regional foliation is concordant to the contacts. In Kaartila, the foliation intensity decreases toward the center. Subhorizontal extensional structures in crestal area of a pluton, as in the Kaartila stock, are typical for immature diapirs (Schwerdtner et al. 1978) and high levels of mature diapirs (Dixon 1975). In Silvola, overprinting of contact-parallel structures by later regional deformation complicates the interpretation. In Varparanta, the contact-parallel granitoid foliation and regional foliation, and the decrease of foliation intensity toward the center of the domes suggest diapirism. Presumably the lineation pattern in the Varparanta pluton was originally radial, and rotated during emplacement in noncoaxial regional deformation. The migmatitic character of the gneisses around the three plutons, with abundant anatectic veins, indicates low viscosity contrast during emplacement between the plutons and their wall rocks.

The deformation of the primary layering toward concordance at the eastern contact of the Hämeenkyrö batholith might be due to diapiric emplacement of the pluton. However, the angularity of the eastern contact, the general lenticular foliation pattern with an S tectonite fabric, the fact that the granitoid foliation and the regional foliation are partly contact-parallel, and that the strain intensity diminishes toward the center only in these areas suggest that the emplacement was first passive and subsequently more forceful when the younger phases intruded. Likewise, the rather angular contacts of the Värmälä stock, the low strain intensity in the entire pluton, and the concentric foliation around the later phase (quartz monzodiorite) suggest passive emplacement at first, and more forceful at a later stage. The bulk strain in these plutons is apparently a combination of regional and (minor) emplacement strain.

## Structural setting

The criteria for a syntectonic diapir have been that the regional foliation and the one created by the emplacing intrusion (aureole foliation) are coeval (Pitcher 1979, p. 646), and that contact metamorphic porphyroblasts around the intrusion have grown synchronously with respect to the diapiric foliation (Bateman 1984). The growth may continue after emplacment due to thermal relaxation (Van den Eeckhout et al. 1986).

In addition, Bateman (1984) presented the following criteria for syntectonic diapiric plutons:

1) There should be a decrease in the k value of the strain ellipsoid toward and into the pluton, unless passing near the triple point (point of constrictional strain);
2) The regional foliation should be identical to the aureole foliation where they are subparallel in trend, and it should overprint the aureole foliation in the vicinity of the triple point (in ballooning plutons);
3) The younger aureole foliations should form closed trends which are more circular than the ellipsoidal plan of the pluton.

It should be noted that these criteria are based

on mathematical modelling of Brun and Pons (1981). In an example of triple points, Brun et al. (1981) assumed that the fabric in the supracrustal rocks between the domal structures at Kuopio, eastern Finland, were due to diapirism. According to Park (1981), however, the domes are due to fold interference, and the tectonite fabric has a composite (partly earlier) origin.

Although $S_1$, the main regional foliation in the Tampere Schist Belt, partly crosscuts the contacts of the Hämeenkyrö and Värmälä plutons, the lack of an aureole foliation overprinting the regional one, and the pseudomorphs of syntectonic contact metamorphic minerals around the Hämeenkyrö and Värmälä plutons indicate that the plutons are syntectonic sensu stricto with respect $D_1$. Moreover, the constrictional areas in the Värmälä stock are in accordance with the first criterion above.

Although the evidence is not as definite as above, the concordance of the contacts of the Silvola, Kaartila and Varparanta plutons with $D_2$ structures, and the pre-$D_3$, possibly contact metamorphic garnet in Silvola suggest that these plutons are syntectonic with respect to $D_2$.

The internal structures of the plutons ranges from lenticular (Hämeenkyrö, Värmälä) to concentric (Kaartila). The lenticular structures in the plutons of the Tampere Schist Belt are due to the dominance of regional strain over emplacement strain. In the plutons of the Savo Schist Belt, the conformable foliations near the triple point areas are intrusion induced, but the strain pattern in the plutons may be the combination of regional and emplacement strain. The difference in internal structures may reflect the difference in metamorphic grade of the country rocks during emplacement, and hence the viscosity contrast rather than intensity of regional deformation. Because of the difference in metamorphic grade, it is difficult to deduce if the plutons in the Tampere Schist Belt were emplaced during an earlier or later stage of regional deformation than the ones in the Savo Schist Belt.

In the classification of Buddington (1959), the Hämeenkyrö batholith and Värmälä stock have both epizonal (passive emplacement) and mesozonal (diapirism, concentric foliation, medium/high grade metamorphism) characteristics, whereas the plutons of the Savo Schist Belt are mesozonal.

## Geochemistry and petrogenesis

Variation diagrams can be used to infer the most probable differentiation mechanism during crystallization at or near the final emplacement level, or to eliminate the impossible mechanisms. Field evidence of major wall rock contamination is minor in all plutons. In the Hämeenkyrö batholith, simple fractional crystallization in situ cannot account for the concentric zoning in the pluton, although it probably occurred within each phase. The rather simple variation trends in Silvola may be due to fractional crystallization or partial melting. The Kaartila pluton was generated by partial melting, and during crystallization mainly the incompatible elements fractionated. The reversely zoned Värmälä pluton was differentiated before final intrusion. The quartz monzodiorite is possibly the result of sidewall crystallization. In Varparanta, differentiation probably involved fractional crystallization, but the banded tonalite-quartz diorite must have a more complicated origin. The diorite fragments, enclaves, and the banded and patchy quartz diorite may represent different degrees of magma mingling and (minor) mixing.

Roundish or oval-shaped microgranitoid enclaves are characteristic of the Hämeenkyrö, Värmälä and Silvola plutons but are scarce in Varparanta and lacking in Kaartila. The lack of trace element evidence makes it impossible to infer the origin of the enclaves; they may be the result of magma mingling, fragments of synplutonic dikes, and/or fragments of igneous wall rocks that were incorporated into the magma during ascent. The most common explanation for microgranitoid enclaves is magma mingling (e.g. Vernon 1983, Bacon 1986, Sparks and Marshall 1986). The relative volumes of felsic and mafic magma

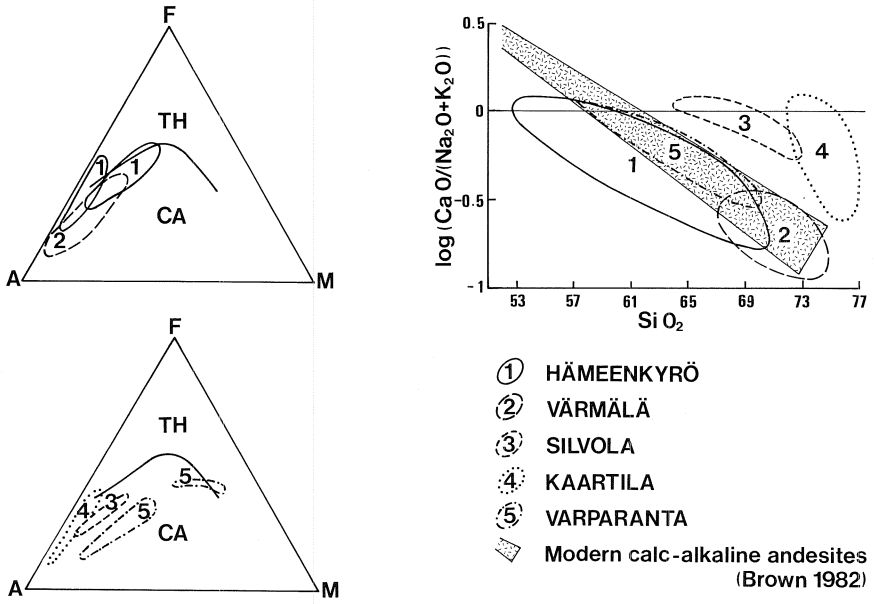


Fig. 43. Composition of the plutons in an AFM diagram and a calc-alkali ratio — $SiO_2$ diagram. The analyses of each pluton plot within the closed lines. The curved line in the in the AFM diagram divides the area into tholeiitic (TH) and calc-alkaline (CA) fields (after Irvine and Baragar 1971).

determines the interaction process; large volumes of felsic magma promote mingling rather than mixing, and conversely (Barbarin 1988).

Geochemical data of all five plutons were plotted on several diagrams to define the magmatic affinities of the plutons and differences between the plutons of the Tampere and Savo Schist Belts. On the AFM diagram (Fig. 43), the plutons plot in the calc-alkaline field, except for the granite phase of Hämeenkyrö which is partly in the tholeiitic field. In the calc-alkali ratio versus $SiO_2$ diagram, Varparanta, Värmälä and partly Hämeenkyrö plot in the field of Phanerozoic calc-alkaline andesites, whereas Silvola and Kaartila define a distinctly different trend. Brown (1982) plotted data from Paleozoic magmatic arcs on this diagram, and concluded that the maturity of the arcs increases toward the origin. Applied to the present data, the diagram suggests a slightly more primitive source for the Silvola and Kaartila plutons relative to the other three.

In the two other diagrams generally used to delineate magmatic affininties (Fig. 44), Värmälä, Silvola and Varparanta are clearly calc-alkaline, whereas Kaartila shows a tholeiitic affinity. When the affinities of the plutons and adjacent metavolcanics are compared, the magmatic rocks of the Tampere Schist Belt are calc-alkaline. In the Savo Schist Belt, the metavolcanics, surrounding the plutons, and the Kaartila stock show tholeiitic affinities, whereas Silvola and Varparanta are calc-alkaline.

In the $Na_2O$ versus $K_2O$ diagram and alumina saturation versus $SiO_2$ diagram (Fig. 45), used to distinguish whether the granitoids have an I-type (igneous) or S-type (sedimentary) source (Chappell and White 1974), the plutons plot in the field of I-type rocks, except for Varparanta and Värmälä in the latter diagram. The plutons are peraluminous except for the Hämeenkyrö batholith which is mildly metaluminous. In the $K_2O$ versus $SiO_2$ diagram (Fig. 46), Hämeenkyrö and Värmälä form a high-K trend distinct from the lower trend of plutons of the Savo Schist Belt, suggesting a more evolved source for the rocks in the Tampere Schist Belt.

The geochemistry of the Kaartila pluton is somewhat problematic, considering the inter-

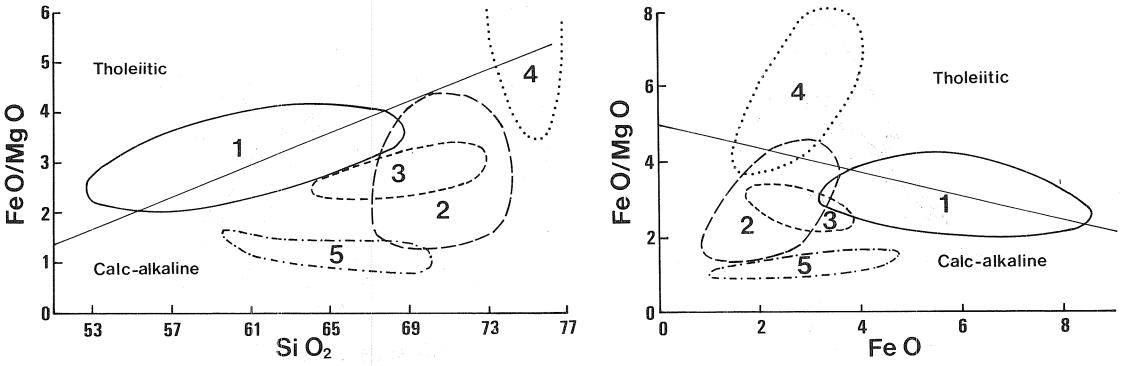


Fig. 44. Composition of the plutons in FeO/MgO ratio versus $SiO_2$ and FeO diagrams. The area is divided into tholeiitic and calc-alkaline fields (after Miyashiro 1974). Line markings as in Fig. 43.

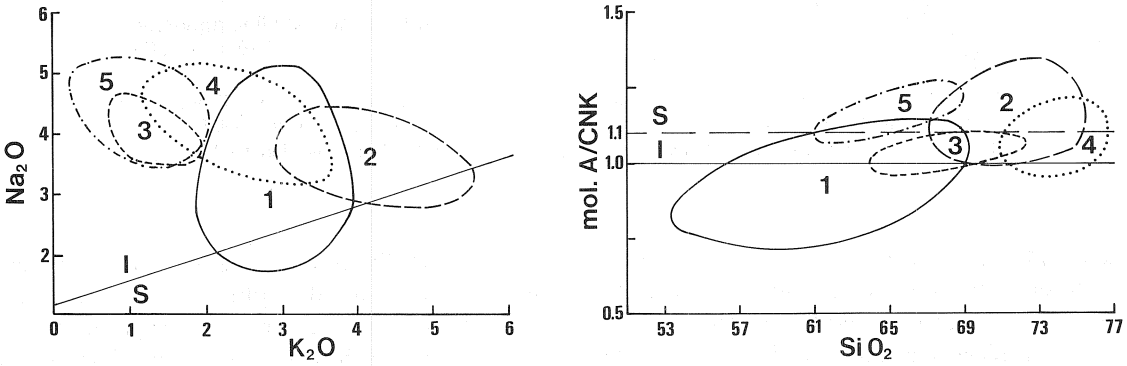


Fig. 45. Composition of the plutons in a $Na_2O$ versus $K_2O$ diagram and an alumina saturation versus $SiO_2$ diagram. The area is divided into I-type and S-type granitoid fields (after Chappell and White 1974, White and Chappell 1983). The solid line in the latter diagram separates the peraluminous (upper) and metaluminous (lower) fields. Line markings as in Fig. 43.

pretation of its origin. A mixed source, with both metagreywackes and mafic metavolcanics, should be reflected in the diagrams as elevated $SiO_2$ and $K_2O$ contents, with respect to plutons derived from melting of solely mafic/intermediate igneous material (the paucity of felsic metavolcanics in the Savo Schist Belt makes them an improbable source). Indeed, the Kaartila stock has a tendency of maturity in the $K_2O$ versus $SiO_2$ diagram (Fig. 46), relative to the other plutons of the Savo Schist Belt. A mixture of shales and greywackes were interpreted as the source of the S-type granites in the original type area, the Lachlan Fold Belt of southeastern Australia (White and Chappell 1983).

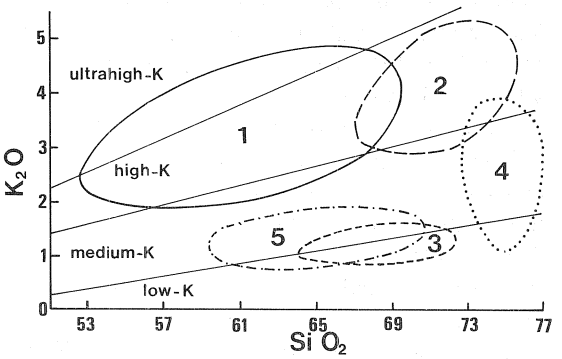


Fig. 46. Composition of the plutons in a $K_2O$ versus $SiO_2$ diagram (boundary lines slighlty modified from Kähkönen 1987). Line markings as in Fig. 43.

Sm-Nd isotopic studies of igneous, metavolcanic and metasedimentary rocks in the Svecofennian Domain (Huhma 1986, Patchett and Kouvo 1986, Huhma 1987) indicate a major source of newly mantle-derived material, mixed with a small amount of material derived from Archean crust. Considering that crustal growth rate in the early Precambrian was faster than at present (Patchett and Arndt 1986), rapid evolution is likely to produce immature sediments such as volcanogenic greywackes. As Barker (1981) pointed out, granitoids derived from such immature sediments may be metaluminous to mildly peraluminous and have I-type characteristics. Hence, the plotting of the analyses of the Kaartila stock in the I-type field in the diagrams may be due to an igneous source component, and/or the possibility that the I-type/S-type classification cannot be applied to granitoids of rapidly evolved Precambrian terrains as readily as to Phanerozoic ones. Moreover, the authors who introduced the classification point out that the S-type granites of the original type area are not associated with regional metamorphic rocks (White et al. 1986).

If the differentiation processes during crystallization at the final stage are difficult to interpret, it is far more difficult to deduce the processes that generated the magmas. Some general points may be presented. Experimental studies on granitoids or simulating granitoid melts (Wyllie 1977, 1983) favor a crustal origin for granodioritic-granitic magmas, either by anatexis, or by more complicated processes with an addition of mantle-derived heat, volatiles or magma. Partial melting in the crust may be a multiphase process (Pitcher 1979, p. 644) which may produce concentric multiphase plutons such as the Hämeenkyrö batholith. In contrast, the studies indicate that tonalitic melt cannot be generated in crustal anatexis under conditions of normal regional metamorphism. Models involving fractional crystallization of mantle-derived magma (Condie and McCrink 1982), a mixture of mantle magma and crustal re-melt (Barker et al. 1981, Hyndman and Foster 1988), and partial melting of subducted oceanic slab with subsequent crustal assimilation (Anderson and Cullers 1987, Defant et al. 1988) have been presented for the origin of tonalites.

The synkinematic Svecokarelian granitoids of Finland are mainly calc-alkaline and have generally I-type characteristics (Nurmi et al. 1984). The tonalites are geochemically more homogeneous than the granodiorites and granites, suggesting a more homogeneous source for the former. Front and Nurmi (1987) proposed partial melting of basaltic source rocks for the origin of the tonalites, and inferred the microgranitoid inclusions as restites.

According to Didier (1987), a variety of microgranitoid enclaves in a pluton suggest several mixing/mingling events. Barbarin (1988) noted the scarcity of microgranitoid enclaves in mainly crustal-derived, potassic granitoids. He concluded that the abundance of the enclaves in I-type granitoids is directly related to the abundance of mantle-derived magma which caused re-melting of crust and the generation of the enclosing granitoids. The conclusion is consistent with the inferred crustal origin of the Kaartila stock, which does not contain microgranitoid enclaves. The existence of enclaves in the plutons of this study is not dependent on composition of the pluton, because the rock types containing enclaves range from quartz diorite to granite. The tonalitic plutons may have originated through mixing and mingling between crustal magma and either mantle-derived magma or magma generated by partial melting of subducted oceanic slab. Further interaction between the mixed/mingled magma and crustal rocks, by partial melting and/or assimilation, produced the more granodioritic and granitic derivatives. Hence, magma mixing and mingling probably occurred repeatedly in the crust, e.g. in stratified magma chambers.

## EVOLUTION OF THE TAMPERE AND SAVO SCHIST BELTS

The U-Pb zircon ages date the crystallization of zircon. Theoretical calculations suggest ascending velocities of tens of centimeters per year for granitic magma in the crust, which means that the magma body would traverse a 30 km thick crust in a few million years (Marsh 1982). Because the limits of experimental error of high-precision U-Pb zircon dating is of the same order, the ages can be considered as emplacement ages.

### Age data of the Tampere Schist Belt

The U-Pb ages determined for the non-sedimentary rocks of the Tampere Schist Belt form a rather restricted group. The zircon ages of the metavolcanic rocks range from 1904 Ma (Intermediate Volcanic Unit, Orivesi) through 1898 Ma (Lower Volcanic Unit, Ylöjärvi) to 1889 Ma (Upper Volcanic Unit, Ylöjärvi; Kähkönen et al., in press).

New analyses yielded U-Pb zircon ages of 1885 Ma and 1878 Ma for the Hämeenkyrö batholith and the Värmälä stock, respectively (Figs. 47a and 47b) The ages are typical of the Svecofennian synkinematic granitoids. An U-Pb age of about 1880 Ma was dated earlier for titanite in the Hämeenkyrö batholith (Patchett and Kouvo 1986). U-Pb data of uraninite from the tourmaline breccia of the Ylöjärvi deposit has been presented previously (Himmi et al. 1979). In spite of the small amount of uraninite, preserved in tourmaline, recalculation of the data yielded a rather concordant result. Hence, the radiometric age of 1.86 Ga (see Fig. 47a and Appendix 2), may be considered as the age of the uraninite.

The result for the Nokia batholith, immediately south of the Hämeenkyrö batholith (Fig. 3), is ambiguous. The batholith consists of porphyritic granodiorite, and contains large, abundant mica schist xenoliths (for description of the sample, see Kouvo and Tilton 1966). The clear, long zircons (see Appendix 2) give an age of 1898 Ma (Fig. 47c), but the short, turbid ones yield an older age. The latter may be restites of almost totally melted older material. A mixture of two zircon generations, or an inheritage of lead may explain the 1898 Ma age which is slightly higher than the typical synkinematic age.

In his classical study on the Tampere Schist Belt, Sederholm (1897) described clasts of igneous rocks in the metaconglomerates at several localities in the Tampere Schist Belt. U-Pb zircon data of igneous clasts from four sites near the eastern shore of Lake Näsijärvi, west of the Värmälä stock, are presented in Fig. 47d. Recalculated old data, added with new analyses, give a 1890 Ma age for an igneous boulder (A90) near the northwestern contact of the Värmälä stock (for description of the sample, see Kouvo and Tilton 1966). The other three samples were collected by Sederholm (see Appendix 2 and Sederholm 1897, Fig. 5). The "syenite" cobbles are granodioritic to quartz monzodioritic in modal composition. Sederholm (1897, p. 27—34) described the "micropegmatitic" texture of these cobbles. They contain euhedral oligoclase grains, and in the interstices of the grains there is micrographic, in places granophyric, intergowth between oligoclase and quartz. The analyses give a U-Pb zircon age of 1884 Ma for one of these cobbles (A26). If all the three samples are treated as a (cogenetic) group, they yield an age of 1887 Ma. However, the cobbles probably do not have a common provenance, because one of the samples (A393) represents another lithohorizon than the other two.

The schists in Lavia, about 60 km west of Tampere, contain an intercalation of meta-conglomerate, with clasts of darkish igneous rock (for description, see Sederholm 1915). The boulder sample from Välimäki has a U-Pb zircon age of 1888 Ma (Fig. 47e; courtesy of O. Kouvo). In modal composition, the boulder is tonalitic.

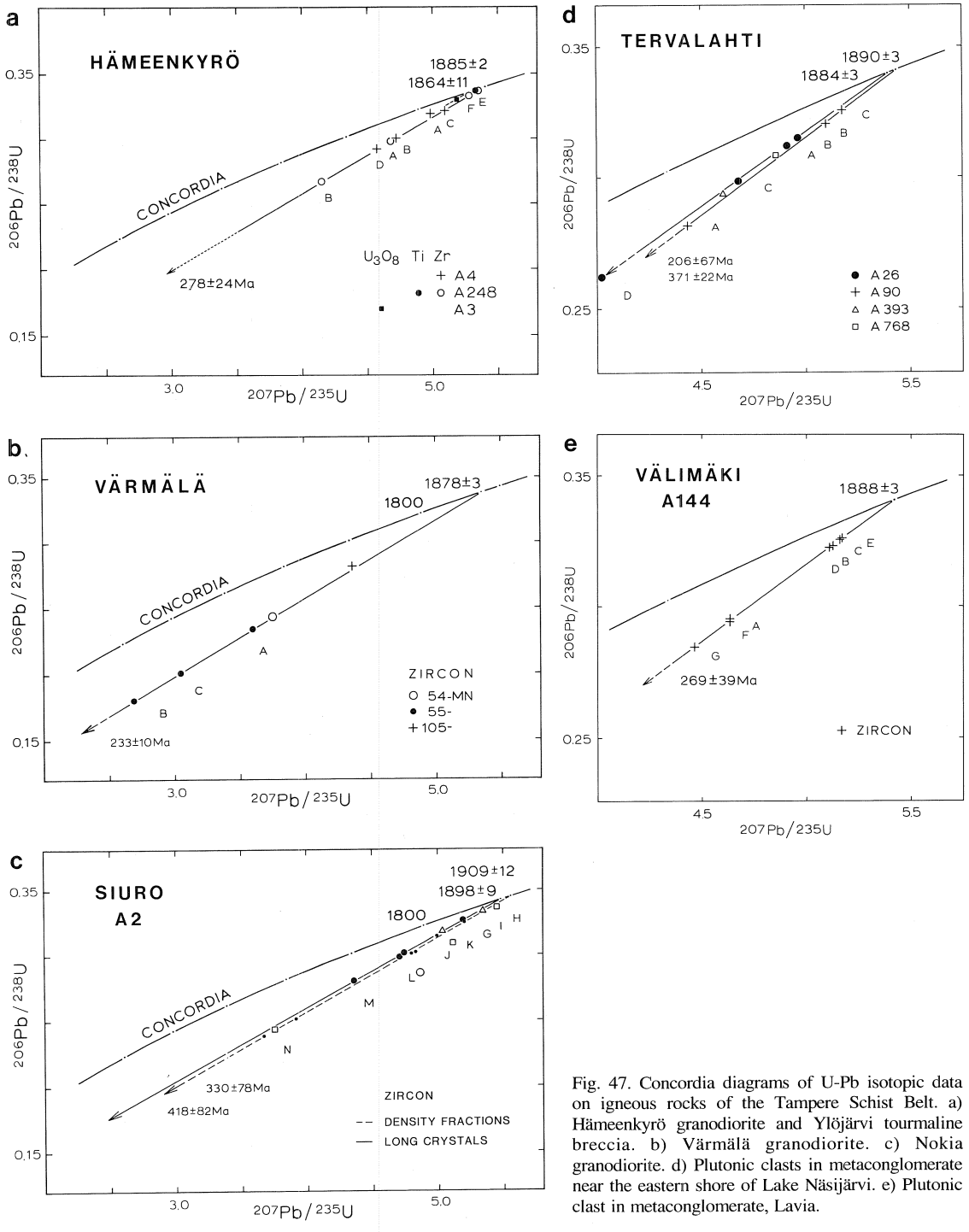


Fig. 47. Concordia diagrams of U-Pb isotopic data on igneous rocks of the Tampere Schist Belt. a) Hämeenkyrö granodiorite and Ylöjärvi tourmaline breccia. b) Värmälä granodiorite. c) Nokia granodiorite. d) Plutonic clasts in metaconglomerate near the eastern shore of Lake Näsijärvi. e) Plutonic clast in metaconglomerate, Lavia.

## Evolution of the Tampere Schist Belt

The dated metavolcanic rocks in the Tampere Schist Belt generally give somewhat higher ages than the plutonic rocks and the igneous clasts in metaconglomerates. The metaconglomerates at the eastern shore of Lake Näsijärvi may be considered as a continuation of the conglomerate interlayer between the Upper and Lower Volcanic Units in the Ylöjärvi-Takamaa area (see p. 14 and Figs. 3, 7 and 12). The micrographic and granophyric textures in these cobbles suggest near-surface crystallization conditions. They may have been derived from dikes which originated from underlying plutonic bodies such as the Värmälä stock.

The plutonic clasts in the metaconglomerates have been in the center of the debate around the existence of an unconformity between the Bothnian schists (the Tampere Schist Belt) and a distinctly older crust, i.e. the gneisses to the south of the schists. Sederholm (1897) considered the metaconglomerates as weathering products of the older rocks. The general opinion has been against the existence of such a hiatus (see discussion in Simonen 1953b). The age data proves that the igneous clasts in the Tampere Schist Belt do not represent a considerably older crust.

The restricted age range between the metavolcanics, the granitoid plutons and the igneous clasts indicate rapid cycling between magmatism, uplift, erosion and sedimentation. Similar ages for synkinematic granitoids and igneous clasts of metaconglomerates have been obtained elsewhere in the Svecofennian Domain (Vaasjoki and Sakko 1988, Korsman et al. 1988).

A closure temperature exceeding 550°C has been estimated for titanite of a regionally metamorphosed tonalite (Cliff and Cohen 1980). Since the estimations for temperature during peak metamorphism in the Tampere Schist Belt are of the same order (see p. 13), the 1.88 Ga age of titanite in the Hämeenkyrö batholith does not tell whether the batholth was subjected to regional metamorphism or not.

The metavolcanic rocks of the Tampere Schist Belt resemble volcanics in mature island arcs or volcanic arcs at active continental margins (Kähkönen 1987). According to Ojakangas (1986), the metaturbidites were probably deposited in a forearc basin. Thus the inference of Simonen (1953b, p. 35), that the Tampere Schist Belt is part of an ancient volcanic arc, is still valid.

The age data indicates that magmatic activity started before 1.90 Ga ago. The tectonothermal events, including the emplacement of the granitoid plutons, culminated 1.90—1.88 Ga ago, and uplift, erosion and redeposition of material occurred roughly simultaneously. The plutons cooled rather rapidly and acted as rigid bodies during the late stage of $D_1$ deformation. Since tourmalinization and mineralization were interpreted as synchronous with $D_2$ deformation, the 1.86 Ga old uraninite from the tourmaline breccia dates the retrogressive tectonothermal stage.

## Evolution of the Savo Schist Belt

The U-Pb zircon age of the Silvola tonalite is 1886 Ma, whereas the age of titanite is distinctly younger, 1829 Ma (Fig. 48). The similar U-Pb zircon age of the Tuusmäki tonalite, near Rantasalmi (1888 Ma; Korsman et al. 1984), indicates that the two plutons were emplaced coevally. The tectonothermal evolution in the Silvola-Kaartila area generally corresponds to the evolution in the Rantasalmi-Sulkava area. However, $D_2$ deformation initiated before the emplacement of the Silvola and Kaartila stocks, whereas the emplacement of the tonalites preceded $D_2$ in the Rantasalmi-Sulkava area (Korsman et al. 1984).

Kilpeläinen (1988) inferred that $D_3$ occurred 1.83—1.80 Ga ago, because $D_3$ overprints the metamorphic zones. The age for $D_3$ was obtained from zircon and monazite in the neosome and paleosome of migmatite within the Sulkava dome

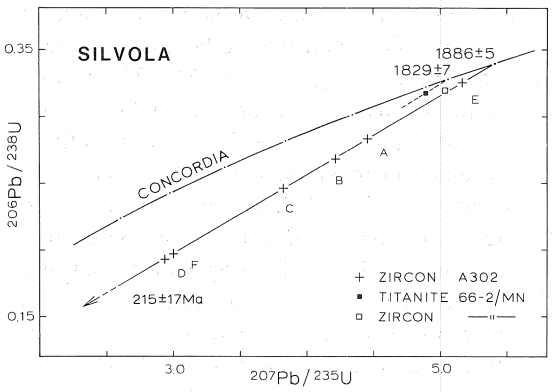


Fig. 48. Concordia diagram of U-Pb isotopic data on the Silvola tonalite.

(Korsman et al. 1984). Korsman et al. (1984) concluded that the Sulkava area was uplifted through the effect of gravity, i.e. it is also a structural dome. Since the metamorphism was progressive, it may have culminated earlier outside the thermal dome, and the Sulkava area may have evolved separately during the final stage of progressive metamorphism. The configuration of metamorphic zones and zones of $D_3$ deformation in the Rantasalmi-Sulkava area (Korsman et al. 1988, Fig. 2) suggests that the $D_3$ zones wane toward the Sulkava dome. Melt-enhanced deformation during advanced anatexis (Hollister and Crawford 1986) may have caused uplift of the thermal dome and overprinting of $D_3$ structures. If this was true, the zircons date the anatexis and uplift about 1.83 Ga ago; $D_3$ deformation occurred after the metamorphic culmination outside the Sulkava dome, but earlier than the updoming.

The large Puruvesi granite batholith, covering some 1000 km$^2$ area (Nykänen 1975a, 1980), has its western margin 5 km east of the Silvola stock (see Fig. 24). The U-Pb zircon age of the batholith is about 1.80 Ga (Nykänen 1983). The batholith is largely homogeneous and weakly foliated, but gneissic varieties with wall rock xenoliths occur in places, especially in the marginal areas (Nykänen 1975b). The Puruvesi granite crosscuts all structures in the surrounding schists and gneisses (Halden 1982), but on macroscale the dominant, composite fabric strikes subparallel to the contacts and dips steeply away from the batholith. East of the Silvola stock, the $F_4$ axial surfaces are subparallel to the contact of the Puruvesi granite. Since the age relationship between $D_4$ and the emplacement of the batholith is not known, there are two possibilities: 1) The emplacement post-dated $D_4$. The structures in the gneisses, including $F_4$, were reoriented, and the shape of the Silvola stock changed during the emplacement of the granite. In this case, 1.80 Ga would be the minimum age for $D_4$; 2) $D_4$ postdated the emplacement, or $D_4$ occurred synchronously but outlasted the emplacement. Because $D_4$ structures in the Rantasalmi-Sulkava area crosscut 1.80 Ga old granitoids (Kilpeläinen 1988), the latter possibility is more probable.

Considering the small volume of the Silvola pluton, the 1.83 Ga age of titanite cannot date mere cooling of the body. Rather, it indicates that the pluton was subjected to the progressive regional metamorphism. Although the zircons yield a typical synkinematic age, the subhedral shape of the crystals suggests that zircon was unstable during metamorphism. Assuming that $D_4$ deformation was active about 1.80 Ga ago, the pluton was deformed ductilely 90 Ma after its emplacement.

In the northwestern part of the Savo Schist Belt, $D_{1-2}$ deformation and associated progressive metamorphism preceded the emplacement of the 1.88 Ga old (synkinematic) granitoids (Korsman et al. 1988). In contrast, the southeastern part (the Rantasalmi-Sulkava area) represents another block which evolved later: the synkinematic granitoids were emplaced before $D_2$ (different from $D_2$ in the northwestern part). According to Korsman et al. (1988), the Rantasalmi-Sulkava area was thrust over the northwestern part about 1.84 Ga ago, when $D_2$ deformation and associated progressive metamorphism were still going on. The fragmentation of the belt mainly occurred during $D_3$.

In spite of the similarity in microstructures and metamorphic grade around the Varparanta stock and the Silvola-Kaartila area, the complicated, fault-controlled structure of the southeastern Savo Schist Belt makes structural correlation between the areas and the timing of emplacement of the Varparanta pluton problematic. Gaál and Rauhamäki (1971) concluded that N-S compression generated NW-

SE trending, dextral vertical faults, and subsequent E-W compression led to reactivation of some faults with a sinistral sense of movement in the Haukivesi area. Parkkinen (1975) inferred similar reactivation for the strike-slip faults in the northeastern (Archean) side of the suture zone.

Gaál and Rauhamäki (1971) inferred that the tonalites/trodhjemites are the oldest intrusives in the Haukivesi area. The Ni-Cu bearing mafic-ultramafic rocks intruded subsequently, and the porhyritic hypersthene granodiorites were the last ones to intrude. However, the U-Pb age of the Laukunkangas gabbro, hosting the Ni-Cu deposit, is 1880 Ma (Huhma 1986), whereas the Voinsalmi hypersthene granodiorite has a slightly older age of 1887 Ma (Patchett and Kouvo 1986). Thus there is some discrepancy between the age data and the inferred intrusion sequence, although the limit of error for the latter age is ± 11 Ma. The isotopic data indicates that the Varparanta tonalite intruded 1.89—1.88 Ga ago, i.e. fairly coevally with the Silvola and Tuusmäki tonalites. If $D_3$ was active in the southeastern Savo Schist Belt about 1.84—1.83 Ga ago, (or 1.83—1.80 Ga ago, as Kilpeläinen (1988) concluded), the faulting which controlled the emplacement of the Varparanta pluton was considerably older. Hence, the isotopic data and structural interpretations indicate that the Haukivesi area is an old fault zone along the margin of the Archean continent which was reactivated repeatedly.

## IMPLICATIONS FOR THE EVOLUTION OF THE SVECOFENNIAN CRUST

In the Svecofennian Domain, fragments of 1.93—1.92 Ga old crust, in the form of gneissic tonalites, have been identified within the Raahe-Ladoga zone, to the southwest of the suture zone (Helovuori 1979, Korsman et al. 1984), and of crust older than 1.90 Ga in the Kalanti area, southwestern Finland (Fig. 1; Patchett and Kouvo 1986). In the northwestern part of the Raahe-Ladoga zone, magmatic activity started 1.90 Ga ago, and tectonothermal activity had ceased 40 Ma later, and possibly after no more than 25 Ma (Vaasjoki and Sakko 1988). In the migmatites at the southern coast of Finland, near Helsinki, major tectonothermal events initiated 1.90 Ga ago and lasted less than 20 Ma (Hopgood et al. 1983).

U-Pb isotopic data of the Tampere and Savo Schist Belts are summarized in Fig. 49. In the Tampere Schist Belt, the major tectonothermal activity started about 1.90 Ga ago and lasted less than 40 Ma. In regard of this age range and the ones presented above, the evolution in the southeastern Savo Schist Belt was exceptionally long, intiating 1.90 Ga ago and lasting up to 1.80 Ga ago, i.e. 100 Ma.

The areas of late (1.84—1.81 Ga) metamorphic culmination, i.e. southeastern Savo Schist Belt and southwestern Finland (Hölttä 1986) are in a broad zone characterized by late-kinematic granites and post-kinematic granitoids. The spatial association suggests a major crustal process (cf. Front and Nurmi 1987, Vaasjoki and Sakko 1988). Isotopic data on monazites and titanites in the Svecofennian Domain yield ages around 1.80 Ga, probably indicating a late thermal event (Patchett and Kouvo 1986).

Nowadays there is a general agreement that processes resembling modern plate tectonic processes operated in the early Proterozoic. In the most comprehensive models presented so far, the Svecofennian Domain was formed by sequential accretion of two (Gaál 1986) or more (Park et al. 1984) island arcs to the present north or northeast. Although the Precambrian crustal growth rate was considerably faster than modern crustal growth (Patchett and Arndt 1986, Reymer and Schubert 1986), the U-Pb zircon ages of the metavolcanics in the Svecofennian Domain are so uniform that a simple accretionary system is improbable. Moreover, early deformation structures identified in the Svecofennian Domain of Finland and central Sweden, with differing vergence directions (Nironen, in press), suggest a more complicated history.

There is a general 'softening' and waning of

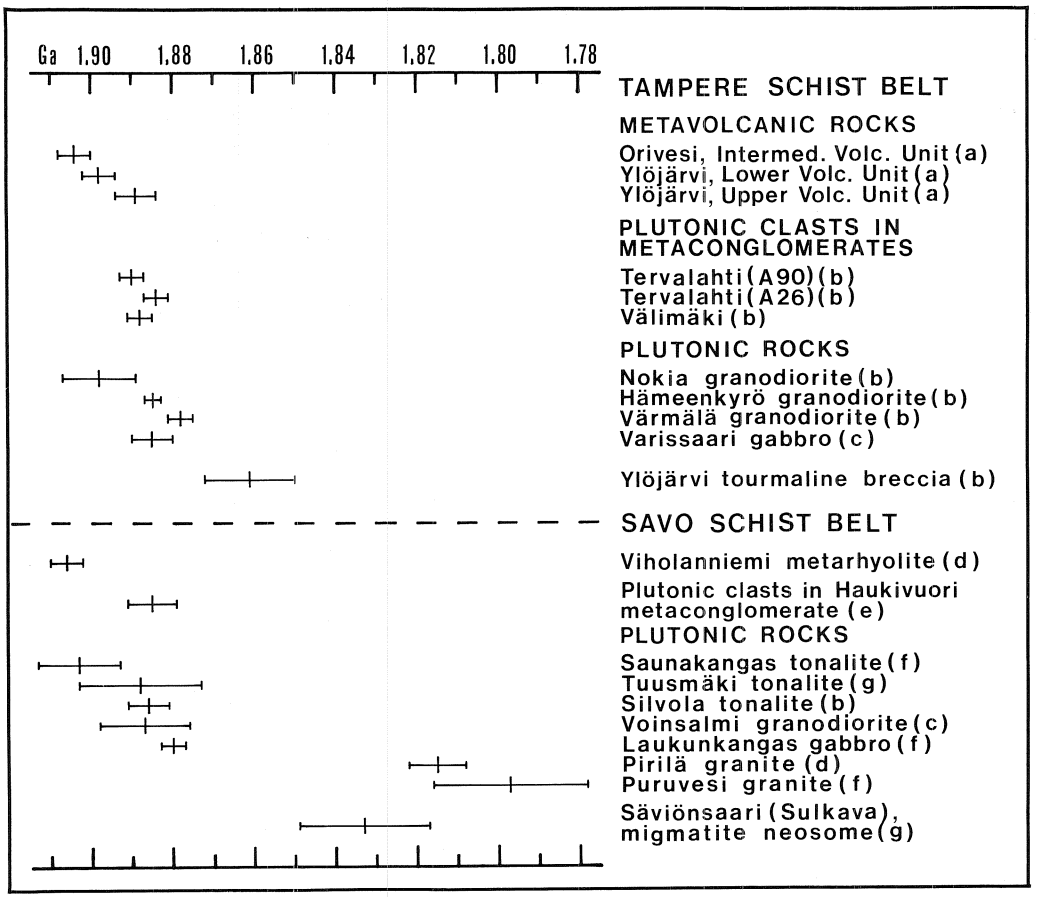


Fig. 49. Summary of U-Pb isotopic ages of the Tampere Schist Belt and southeastern Savo Schist Belt, with 2 sigma error bars. The ages are zircon ages except for the Ylöjärvi tourmaline breccia which is from uraninite. References: a) Kähkönen et al., in press; b) This study; c) Patchett and Kouvo 1986; d) Vaasjoki and Sakko 1988; e) Korsman et al. 1988; f) Huhma 1986; g) Korsman et al. 1984.

faulting toward southeast in the Raahe-Ladoga zone. In the northwestern part of the Savo Schist Belt, deformation was brittle-ductile in style and separated the crust into distinct blocks (Korsman et al. 1984, Pajunen 1986), whereas in the Rantasalmi area it was ductile. In the Silvola-Kaartila area, the older foliations were mainly reoriented ductilely during $D_3$ deformation.

Korsman et al. (1984) proposed tectonic thickening of the crust for the development of the progressive deformation in the Rantasalmi-Sulkava area. Analogous situations are in the Alps (e.g. England 1978) and in the Himalayas (e.g. Hodges et al. 1988) which are both continental collision regimes. Front and Nurmi (1987) suggested that the late-kinematic granites were generated as the result of collision of two continents of similar or different ages. Recently, Korsman et al. (1988) concluded that the rocks of the Rantasalmi-Sulkava area were thrust over the northwestern Savo Schist Belt.

When the evolution of an old shield area is delineated, one faces the fact that it is only the fragments of the possible arc systems etc. that we see at present. Considering the orientations of the volcanic-sedimentary belts in the Svecofennian Domain and the varying vergence directions in them, several microplates, subduction zones as well as extensional regimes probably existed. In a tentative model it is suggested that the vigorous

accretion of volcanic arcs toward the Archean craton and small early Proterozoic nuclei (gneissic tonalites) produced new crust about 1.90-1.87 Ga ago. At this time, the boundary between the Archean craton and the newly formed Proterozoic crust (the suture zone) was an active fault zone. Two newly formed larger plates collided along a WSW-ENE trending zone so that the southern one was partly thrust over the northern one, and the NW-SE trending fault zone (the Raahe-Ladoga zone) was reactivated. The collision occurred after the main tectonothermal events within the two plates had largely ceased, i.e. after 1.87 Ga ago. The collision led to tectonic thickening of the crust and emplacement of the late-kinematic granites 1.84—1.81 Ga ago. The late $D_4$ folding in the Savo Schist Belt was due to the collision. The emplacement of the post-kinematic granitoids and the large-scale thermal event 1.80 Ga ago marks the cratonization of the Svecofennian crust.

## CONCLUSIONS

The five studied granitoid plutons, belonging to the synkinematic (1.90—1.87 Ga) age group, range in composition from tonalite to granite. The plutons show internal structures ranging from lenticular, due to a combination of regional and emplacement strain (Hämeenkyrö, Värmälä), to concentric (Varparanta, Silvola, Kaartila). The differences may not reflect the effect of regional strain in the plutons, but differences in metamorphic grade in the country rocks, and hence the viscosity contrast during emplacement.

Emplacement of plutons at or close to the culmination of tectonothermal activity may be diapiric when the host rocks are migmatitic and melt present has lowered their viscosity, as in the Savo Schist Belt. Emplacement into lower grade metamorphic environment such as the Tampere Schist Belt may take place first rather passively via faults and/or fractures, and change into ballooning during continued injection of magma. Moreover, strike-slip faulting may control the emplacement of a pluton, e.g. the Varparanta stock.

Each pluton has distinct geochemical characteristics. The two multiphase plutons, the Hämeenkyrö batholith and the Värmälä stock, show normal and reverse horizontal zoning, respectively. The zoning suggests injection of magma as separate pulses. There is no field evidence for major magma mixing or wall rock contamination to account for the differentiation in the plutons, but the typical microgranitoid enclaves indicate that some magma mingling occurred. In the Varparanta stock, mingling and mixing between a mafic and a felsic magma during emplacment produced compositional banding. Differentiation during final emplacement involved at least some fractional crystallization in the plutons. The Kaartila stock is an exception: it is not distinctly differentiated, and instead of microgranitoid enclaves, it contains xenoliths of supracrustal rocks. Probably the Kaartila stock is the result of partial melting of supracrustal rocks not far below the emplacement level.

The granodioritic-granitic plutons and adjacent metavolcanic rocks in the Tampere Schist Belt are calc-alkaline. The metavolcanics surrounding the plutons in the Savo Schist Belt are tholeiitic, whereas the tonalitic plutons have both tholeiitic and calc-alkaline affinities. The plutons have mainly I-type characteristics. The apparent inconsistency between geochemical (I-type) affinity and inferred crustal origin of the Kaartila pluton may be due to partial melting of (immature) greywackes and metavolcanics.

The tonalitic plutons possibly originated through mixing and mingling between crustal and mantle-derived magma, or magma derived by partial melting of subducted oceanic slab. Further interaction between the mixed magma and crustal rocks, by partial melting and/or assimilation, generated the granodioritic and granitic magmas. As a consequence of repeated mixing and mingling, microgranitoid enclaves exist in rocks ranging in composition from quartz diorite to granite.

The Hämeenkyrö batholith and the Värmälä stock are syntectonic with respect to $D_1$ in the Tampere Schist Belt. The tectonothermal evolution

culminated 1.90—1.88 Ga ago, with simultaneous rapid erosion and redeposition of material. The plutons cooled rather rapidly, and acted as rigid bodies at the late stage of $D_1$ deformation. The 1.86 Ga age of $D_2$ deformation records the waning stage of evolution.

In the Savo Schist Belt, the plutons were emplaced 1.89—1.88 Ga ago. The Silvola and Kaartila stocks are syntectonic with respect to $D_2$. The culmination of progressive metamorphism about 1.83 Ga ago led to slow cooling of the Silvola stock. The pluton was deformed ductilely as late as about 1.80 Ga ago, during $D_4$ deformation.

Inference of the emplacement mechanism and structural setting of the Varparanta stock is complicated by the location of the pluton within a strike-slip fault system. The $D_{2-3}$ faulting which controlled the emplacement of the stock probably occurred considerably earlier than the $D_3$ deformation in the Rantasalmi-Sulkava and Silvola-Kaartila areas.

The Tampere Schist Belt is interpreted as a forearc of an early Proterozoic volcanic arc system. For the Savo Schist Belt, the evidence is limited. It is suggested that the belt consists of several arcs which were accreted and faulted along the Archean craton. Both belts evolved simultaneously with other convergent margins, possibly against small nuclei of early Proterozoic crust. Subsequent collision of newly formed microplates led to reactivation of the NW-SE trending strike-slip faults 1.84—1.83 Ga ago, thickening of the crust, generation of the late-kinematic granites, and late ($D_4$) folding.

If the crustal evolution was as complicated as hypothetically presented above, it means that the supracrustal belts represent areas of different crustal evolution. Hence, correlation between structures in isolated supracrustal domains such as the Tampere and Savo Schist Belts or even within a single belt may lead to erroneous interpretations. The granitoids are coeval, but they are related to different tectonic events in the two belts. Subsequent faulting has brought areas of originally different crustal levels to the present level.

## ACKNOWLEDGEMENTS

This study was financed principally by the Academy of Finland, for which I worked as a researcher. Financial support was also provided by the Emil Aaltonen Foundation.

I am grateful to Professor Ilmari Haapala for giving me the opportunity to work and use the facilities of the Deparment of Geology, University of Helsinki. I thank Dr. Risto Puranen who helped me to use the equipment in the Petrophysical Laboratory of the Geological Survey of Finland, and Dr. Martti Lehtinen, of the Department of Geology, who provided X-ray data. Especially I want to thank Dr. Olavi Kouvo and the staff of the Unit for Isotope Geology, Geological Survey of Finland, for their contribution at the final stage of this work.

Professor Gabor Gaál, of the Geological Survey of Finland, and my friend Kai Front provided their personal geological material for this study. Basically, Gabor Gaál is responsible for my interest to the scope of this study.

I owe special thanks to Dr. Roger Bateman for constructive criticism on the earlier versions of the manuscript, for checking the English of the manuscript, and for his Australian sense of humor. I also appreciate discussions with Dr. Kalevi Korsman, and the comments of Ilmari Haapala and Kai Front on the manuscript. I thank Riitta Virtanen and Liisa Siren who drew the illustrations of geochemical data and isotopic data, respectively.

And last but not least, I want to thank my fellow students in the Department of Geology for good vibes: rock is here to stay!

## REFERENCES


**Anderson, J.L. & Cullers, R.L., 1987.** Crust-enriched, mantle-derived tonalites in the early Proterozoic Penokean orogen of Wisconsin. J. Geol. 95, 139—154.

**Bacon, C.R., 1983.** Eruptive history of Mount Mazama and Crater Lake caldera, Cascade Range, U.S.A. J. Volcanol. Geotherm. Res. 18, 57—115.

**Bacon, C.R., 1986.** Magmatic inclusions in silicic and intermediate volcanic rocks. J. Geophys. Res. 91, 6091—6112.

**Bailey, D.K., 1970.** Volatile flux, heat-focusing and the generation of magma. *In:* G. Newall & N. Rast (Editors), Mechanism of Igneous Intrusion. Gallery Press, Liverpool, 177—186.

**Balk, R., 1937.** Structural behavior of igneous rocks. Geol. Soc. Am. Mem. 5, 177 p.

**Balsey, J.R. & Buddington, A.F., 1960.** Magnetic susceptibility anisotropy and fabric of some Adirondack granites and orthogneisses. Am. J. Sci. 258A, 6—20.

**Barbarin, B., 1988.** Field evidence for successive mixing and mingling between the Piolard Diorite and the Saint-Julien-la-Vêtre Monzogranite (Nord-Forez, Massif Central, France). Can. J. Earth Sci. 25, 49—59.

**Barker, F., 1981.** Introduction to special issue on granites and rhyolites: a commentary for the nonspecialist. J. Geophys. Res. 86, 10131—10135.

**Barker, F., Arth, J.G. & Hudson, T., 1981.** Tonalites in crustal evolution. Philos. Trans. R. Soc. Lond. A301, 293—303.

**Barriere, M., 1977.** Deformation associated with the Ploumanac'h intrusive complex, Brittany. J. Geol. Soc. Lond. 134, 311—324.

**Bateman, P.C. & Chappell, B.W., 1979.** Crystallization, fractionation, and solidification of the Tuolumne Intrusive Series, Yosemite National Park, California. Geol. Soc. Am. Bull. 90, 465—482.

**Bateman, R., 1984.** On the role of diapirism in the segregation, ascent and final emplacement of granitoid magmas. Tectonophysics 110, 211—231.

**Bateman, R., 1985a.** Aureole deformation by flattening around a diapir during in situ ballooning: the Cannibal Creek Granite. J. Geol. 93, 293—310.

**Bateman, R., 1985b.** Progressive crystallization of a granitoid diapir and its relationship to stages of emplacement. J. Geol. 93, 645—662.

**Bates, R.L. & Jackson, J.A., 1980.** Glossary of Geology. American Geological Institute, Falls Church, Va., 751 p.

**Bayer, P., Schmidt-Thomé, R., Weber-Diefenbach, K. & Horn, H.A., 1987.** Complex concentric granitoid intrusions in the coastal mobile belt, Espirito Santo, Brazil: the Santa Angélica Pluton — an example. Geol. Rundsch. 76, 357—371.

**Bell, T.H., 1986.** Foliation development and refraction in metamorphic rocks: reactivation of earlier foliations and decrenulation due to shifting patterns of deformation partitioning. J. Metamorph. Geol. 4, 421—444.

**Bell, T.H. & Duncan, A.C., 1978.** A rationalized and unified shorthand terminology for lineations and fold axes in tectonites. Tectonophysics 47, T1—T5.

**Bell, T.H. & Rubenach, M.J., 1983.** Sequential porphyroblast growth and crenulation cleavage development during progressive deformation. *In:* M. Etheridge & S. Cox (Editors), Deformation Processes in Tectonophysics. Tectonophysics 92, 171—194.

**Berthé, D., Choukroune, P. & Jegouzo, P., 1979.** Orthogneiss, mylonite and non coaxial deformation of granites: the example of the South Armorican Shear Zone. J. Struct. Geol. 1, 31—42.

**Bowes, D.R., Halden, N.M., Koistinen, T.J. & Park, A.F., 1984.** Structural features of basement and cover rocks in the eastern Svecokarelides, Finland. *In:* A. Kröner & R. Greiling (Editors), Precambrian Tectonics Illustrated. E. Schweizerbart'sche Verlaagsbuchhandlung, Stuttgart, 147—171.

**Brown, G.C., 1982.** Calc-alkaline intrusive rocks: their diversity, evolution, and relation to volcanic arcs. *In:* R.S. Thorpe (Editor), Andesites, Orogenic Andesites and Related Rocks. John Wiley & Sons, Chichester, 437—461

**Brun, J.P. & Pons, J., 1981.** Strain patterns of pluton emplacement in a crust undergoing non-coaxial deformation, Sierra Morena, Southern Spain. J. Struct. Geol. 3, 219—229.

**Brun, J.P., Gapais, D. & LeTheoff, B., 1981.** The mantled gneiss domes of Kuopio (Finland): interfering diapirs. Tectonophysics 74, 283—304.

**Buddington, A.F., 1959.** Granite emplacement with special reference to North America. Geol. Soc. Am. Bull. 70, 671—747.

**Burg, J.-P., 1987.** Regional shear variation in relation to diapirism and folding. J. Struct. Geol. 9, 925—934.

**Callegari, E. & Dal Piaz, G., 1973.** Field relationships between the main igneous masses of the Adamello intrusive massif (Northern Italy). Mem. Inst. Geol. Miner. Univ. Padova 29, 38 p.

**Campbell, D.S., 1978.** Structural and metamorphic studies in the Svecokarelides, Tampere, Finland. Unpubl. Ph. D. thesis, Glasg. Univ., 146 p.

**Campbell, D.S., 1980.** Structural and metamorphic development of migmatites in the Svecokarelides, near Tampere, Finland. Trans. R. Soc. Edinb., Earth Sci. 71, 185—200.

**Cann, J.R., 1970.** Upward movement of granitic magma. Geol. Mag. 107, 335—340.

**Castro, A., 1984.** Emplacement fractures in granite plutons (Central Extremadura batholith, Spain). Geol. Rundsch. 73, 869—880.

**Castro, A., 1987.** On granitoid emplacement and related structures. A review. Geol. Rundsch. 76, 101—124.

**Chappell, B.W. & White, A.J.R., 1974.** Two contrasting granite types. Pac. Geol. 8, 173—174.

**Choukroune, P. & Gapais, D., 1983.** Strain pattern in the Aar Granite (Central Alps): orthogneiss developed by bulk inhomogeneous flattening. J. Struct. Geol. 5, 411—418.

**Cliff, R.A. & Cohen, A., 1980.** Uranium-lead isotope systematics in a regionally metamorphosed tonalite from the Eastern Alps. Earth Planet. Sci. Lett. 50, 211—218.

**Cobbold, P.R., Cosgrove, J.W. & Summers, J.M., 1971.** Development of internal structures in deformed anisotropic rocks. Tectonophysics 12, 23—53.

**Condie, K.C. & McCrink, T.P., 1982.** Geochemistry of Proterozoic volcanic and granitic rocks from the Gold Hill — Wheeler Peak area, northern New Mexico. Precambrian Res. 19, 141—166.

**Courrioux, G., 1987.** Oblique diapirism: the Criffel granodiorite/granite zoned pluton (southwest Scotland). J. Struct. Geol. 9, 313—330.

**Coward, M.P., 1981.** Diapirism and gravity tectonics: report of a Tectonic Studies Group conference, Leeds Univ. 1980. J. Struct. Geol. 3, 89— 95.

**Defant, M.J., Drummond, M.S., Arthur, J.D. & Ragland, P.C., 1988.** An example of trondhjemite petrogenesis: the Blakes Ferry pluton, Alabama, U.S.A. Lithos 21, 161—181.

**Didier, J., 1973.** Granites and Their Enclaves. Elsevier, Amsterdam, 393 p.

**Didier, J., 1987.** Contribution of enclave studies to the understanding of origin and evolution of granitic magmas. Geol. Rundsch. 76, 41—50.

**Dixon, J.M., 1975.** Finite strain and progressive deformation in models of diapiric structures. Tectonophysics 28, 89—124.

**Duncan, I.J., 1984.** Structural evolution of the Thor-Odin gneiss dome. Tectonophysics 101, 87—130.

**Ehlers, C., 1978.** Gravity tectonics and folding around a basic volcanic centre in the Kumlinge area, SW Finland. Geol. Surv. Finl. Bull. 295, 43 p.

**England, P.C., 1978.** Some thermal considerations of the Alpine metamorphism — Past, present and future. Tectonophysics 46, 21—40.

**Escher, A. & Watterson, J., 1974.** Stretching fabrics, folds and crustal shortening. Tectonophysics 22, 223—231.

**Eskola, P., 1932.** On the origin of granitic magmas. Mitt. Mineral. Petrog. 42, 455—481.

**Eskola, P. & Nieminen, E., 1938.** The quartzite area of Tiirismaa near Lahti. Bull. Comm. Géol. Finl. 123, 29—45.

**Ferguson, C.C. & Harte, B., 1975.** Textural patterns at porphyroblast margins and their use in determining the time relations of deformation and crystallization. Geol. Mag. 112, 467—480.

**Flinn, D., 1962.** On folding during three-dimensional progressive deformation. Q. J. Geol. Soc. Lond. 118, 385—433.

**Flinn, D., 1965.** On the symmetry principle and the deformation ellipsoid. Geol. Mag. 102, 36—45.

**Flood, R.H. & Vernon, R.H., 1978.** The Cooma granodiorite, Australia: an example of in situ crustal anatexis? Geology 6, 81—84.

**Fourcade, S. & Allègre, C.J., 1981**. Trace elements behavior in granite genesis: a case study — the calc-alkaline plutonic association from the Querigut complex (Pyrénées, France). Contrib. Mineral. Petrol. 76, 177—195.

**Fridrich, C.J. & Mahood, G.A., 1984.** Reverse zoning in the resurgent intrusions of the Grizzly Peak cauldron, Sawatch Range, Colorado. Geol. Soc. Am. Bull. 95, 779—787.

**Front, K., 1981.** Hämeenkyrön batoliitin litogeokemia, kivilajit ja suhde ympäröiviin liuskeisiin. Unpubl. M. Sci. thesis, Univ. Helsinki, 59 p. (in Finnish).

**Front, K. & Nurmi, P.A., 1987.** Characteristics and geological setting of synkinematic Svecokarelian granitoids in southern Finland. Precambrian Res. 35, 207—224.

**Frost, T.P. & Mahood, G.A., 1987.** Field, chemical, and physical constraints on mafic-felsic magma interaction in the Lamarck Granodiorite, Sierra Nevada, California. Geol. Soc. Am. Bull. 99, 272—291.

**Gaál, G., 1972.** Tectonic control of some Ni-Cu deposits in Finland. 24th Int. Geol. Congr., Montreal, 4, 215—224.

**Gaál, G., 1986.** 2200 million years of crustal evolution: the Baltic Shield. Bull. Geol. Soc. Finl. 58, 149—168.

**Gaál, G. & Isohanni, M., 1979.** Characteristics of igneous intrusions and various wall rocks in some Precambrian porphyry copper-molybdenum deposits in Pohjanmaa, Finland. Econ. Geol. 74, 1198—1210.

**Gaál, G. & Rauhamäki, E., 1971.** Petrological and structural analysis of the Haukivesi area between Varkaus and Savonlinna, Finland. Bull. Geol. Soc. Finl. 43, 265—337.

**Gaál, G. & Gorbatschev, R., 1987.** An outline of the Precambrian evolution of the Baltic Shield. Precambrian Res. 35, 15—52.

**Gaál, G., Front, K. & Aro, K., 1981.** Geochemical exploration of a Precambrian batholith, source of a Cu-W mineralization of tourmaline breccia type in southern Finland. *In:* A.W. Rose & H. Gundlach (Editors), Geochemical Exploration, 1980. J. Geochem. Explor. 15, 683—698.

**Ghosh, S.K., 1975.** Distortion of planar structures around rigid spherical bodies. Tectonophysics 28, 185—208.

**Gray, D.R. & Durney, D.W., 1979**. Investigations of the mechanical significance of crenulation cleavage. *In:* T.H. Bell & R.H. Vernon (Editors), Microstructural Processes during Deformation and Metamorphism. Tectonophysics 58, 35—79.

**Green, T.H., 1980.** Island arc and continent-building magmatism — a review of petrogenic models based on experimental petrology and geochemistry. *In:* M.R. Banks & D.H. Green (Editors), Orthodoxy and Creativity at the Frontiers of Earth Sciences. Tectonophysics 63, 367—385.

**Grundström, L., 1980.** The Laukunkangas nickel-copper occurrence in southeastern Finland. Bull. Geol. Soc. Finl. 52, 23—53.

**Guillet, P., Bouchez, J.L. & Wagner, J.J., 1983.** Anisotropy of magnetic susceptibility and magmatic structures in the Guérande granite massif (France). Tectonics 2, 419—429.

**Guineberteau, B., Bouchez, J.-L. & Vigneresse, J.-L., 1987.** The Mortagne granite pluton (France) emplaced by pull-apart along a shear zone: Structural and gravimetric arguments and regional implication. Geol. Soc. Am. Bull. 99, 763—770.

**Halden, N.M., 1982.** Structural, metamorphic and igneous history of migmatites in the deep levels of a wrench fault regime, Savonranta, eastern Finland. Trans. R. Soc. Edinb., Earth Sci. 73, 17—30.

**Härme, M. & Seitsaari, J. 1950.** On the structure of a tilted dome near Tampere in southwestern Finland. Bull. Comm. Géol. Finl. 150, 19—22.

**Harris, P.G., Kennedy, W.Q. & Scarfe, C.M., 1970.** Volcanism versus plutonism — the effect of chemical composition. *In*: G. Newall & N. Rast (Editors), Mechanism of Igneous Intrusion. Gallery Press, Liverpool, 187—200.

**Helovuori, O., 1979.** Geology of the Pyhäsalmi ore deposit, Finland. Econ. Geol. 74, 1084—1101.

**Hext, G.R., 1963.** The estimation of second-order tensors, with related tests and designs. Biometrika 50, 353—373.

**Himmi, R., Huhma, M. & Häkli, T.A., 1979.** Mineralogy and metal distribution in the copper-tungsten deposit at Ylöjärvi, southwest Finland. Econ. Geol. 74, 1183—1197.

**Hobbs, B.E., Means, W.D. & Williams, P.F., 1976.** An Outline of Structural Geology. Wiley, New York, 571 p.

**Hodges, K.V., Lefort, P. & Pêcher, A., 1988.** Possible thermal buffering by crustal anatexis in collisional orogens: Thermobarometric evidence from the Nepalese Himalaya. Geology 16, 707—710.

**Hollister, L.S. & Crawford, M.L., 1986.** Melt-enhanced deformation: A major tectonic process. Geology 14, 558—561.

**Holder, M.T., 1979.** An emplacement mechanism for post-tectonic granites and its implications for their geochemical features. *In:* M.P. Atherton & J.Tarney (Editors), Origin of Granite Batholiths: Geochemical Evidence. Shiva, Orpington, 116—128.

**Hölttä, P., 1986.** Observations on the metamorphic reactions and PT conditions in the Turku granulite area. *In:* K. Korsman (Editor), Development of deformation, metamorphism and metamorphic blocks in eastern and southern Finland. Geol. Surv. Finl. Bull. 339, 43—58.

**Hopgood, A.M., 1984.** Structural evolution of Svecokarelian migmatites, southern Finland: a study of Proterozoic crustal development. Trans. R. Soc. Edinb., Earth Sci. 74, 229—264.

**Hopgood, A.M., Bowes, D.R. & Addison, J., 1976.** Structural development of migmatites near Skåldö, southwest Finland. Bull. Geol. Soc. Finl. 48, 43—62.

**Hopgood, A.M., Bowes, D.R., Kouvo, O & Halliday, A.N., 1983.** U-Pb and Rb-Sr isotopic study of polyphase deformed migmatites in the Svecokarelides, southern Finland. *In:* M.P. Atherton & C.D. Gribble (Editors), Migmatites, Melting and Metamorphism. Shiva, Nantwich, 80—92.

**Hrouda, F., 1982.** Magnetic anisotropy of rocks and its application in geology and geophysics. Geophys. Surv. 5, 37—82.

**Hubbard, F. & Branigan, N., 1987.** Late Svecofennian magmatism and tectonism, Åland, southwest Finland. Precambrian Res. 35, 241—256.

**Huhma, A., Salli, I. & Matisto, A., 1952.** Geological map of Finland, 1:100 000, pre-Quaternary rocks, sheet 2122 Ikaalinen, Geol. Surv. Finl.

**Huhma, H., 1986.** Sm-Nd, U-Pb and Pb-Pb isotopic evidence for the origin of the Early Proterozoic Svecokarelian crust in Finland. Geol. Surv. Finl. Bull. 337, 48 p.

**Huhma, H., 1987.** Provenance of early Proterozoic and Archaean metasediments in Finland: a Sm-Nd isotopic study. Precambrian Res. 35, 127—143.

**Hutton, D.H.W., 1982.** A tectonic model for the emplacement of the Main Donegal Granite, NW Ireland. J. Geol. Soc. Lond. 139, 615—631.

**Hyndman, D.W., 1981.** Controls on source and depth of emplacement of granitic magma. Geology 9, 244—249.

**Hyndman, D.W. & Foster, D.A., 1988.** The role of tonalites and mafic dikes in the generation of the Idaho batholith. J. Geol. 96, 31—46.

**Irvine, T.N. & Baragar, W.R.A., 1971.** A guide to the chemical classification of the common volcanic rocks. Can. J. Earth Sci. 8, 523—548.

**Kähkönen, Y., 1987.** Geochemistry and tectonomagmatic affinities of the metavolcanic rocks of the early Proterozoic Tampere Schist Belt, southern Finland. Precambrian Res. 35, 295—311.

**Kähkönen, Y., Huhma, H. & Aro, K.** U-Pb zircon ages and Rb-Sr whole-rock isotope studies of early Proterozoic volcanic and plutonic rocks near Tampere, southern Finland (in press).

**Kilpeläinen, T., 1988.** Evolution of deformation and metamorphism as a function of time in the Rantasalmi-Sulkava area, southeastern Finland. *In:* K. Korsman (Editor), Tectono-metamorphic evolution of the Raahe-Ladoga zone. Geol. Surv. Finl. Bull. 343, 77—87.

**Koistinen, T.J., 1981.** Structural evolution of an early Proterozoic strata-bound Cu-Co-Zn deposit, Outokumpu, Finland. Trans. R. Soc. Edinb., Earth Sci. 72, 115—158.

**Korsman, K., 1977.** Progressive metamorphism of the metapelites in the Rantasalmi-Sulkava area, southeastern Finland. Geol. Surv. Finl. Bull. 290, 82 p.

**Korsman, K. & Kilpeläinen, T., 1986.** Relationship between zonal metamorphism and deformation in the Rantasalmi-Sulkava area, southeastern Finland. *In:* K. Korsman (Editor), Development of deformation, metamorphism and metamorphic blocks in eastern and southern Finland. Geol. Surv. Finl. Bull. 339, 33—42.

**Korsman, K., Niemelä, R. & Wasenius, P., 1988.** Multistage evolution of the Proterozoic crust in the Savo schist belt, eastern Finland. *In:* K. Korsman (Editor), Tectono-metamorphic evolution of the Raahe-Ladoga zone. Geol. Surv. Finl. Bull. 343, 89—96.

**Korsman, K., Hölttä, P., Hautala, T. & Wasenius, P., 1984.** Metamorphism as an indicator of evolution and structure of the crust in Eastern Finland. Geol. Surv. Finl. Bull. 328, 40 p.

**Kouvo, O. & Kulp, J.L., 1961.** Isotopic composition of Finnish galenas. Ann. N.Y. Acad. Sci. 91, 476—491.

**Kouvo, O. & Tilton, G.R., 1966.** Mineral ages from the Finnish Precambrian. J. Geol. 74, 421—442.

**Kuusola, J., 1982.** Savonlinnan eteläpuolella sijaitsevien Kaartilan ja Silvolan granitoidimassiivien petrologia, geokemia ja tektoninen asema. Unpubl. M. Sci. thesis, Univ. Helsinki, 78 p. (in Finnish).

**Laitakari, I., 1986.** Geological map of Finland, 1:100 000, pre-Quaternary rocks, sheet 2142 Orivesi, Geol. Surv. Finl.

**Leake, B.E., 1978.** Granite emplacement: the granites of Ireland and their origin. *In:* D.R. Bowes & B.E. Leake (Editors), Crustal Evolution in Northwestern Britain and Adjacent Regions. Seel House Press, Liverpool, 221—248.

**Lehijärvi, M., 1979.** Geological map of Finland, 1:100 000, pre-Quaternary rocks. sheet 3112 Heinola. Explanation to the map. Geol. Surv. Finl., 25 p. (in Finnish, with an English summary).

**Luosto, U., Lanne, E., Korhonen, H., Guterch, A., Grad, M., Materzok, R. & Perchuc, E., 1984.** Deep structure of the Earth's crust on the SVEKA profile in central Finland. Ann. Geophys. 2, 559—570.

**Luukkonen, E. & Lukkarinen, H., 1985.** Stratigraphic map of middle Finland, 1:1000 000. Geol. Surv. Finl.

**Mäkelä, K., 1980.** Geochemistry and origin of Haveri and Kiipu, Proterozoic strata-bound volcanogenic gold-copper and zinc mineralizations from southwestern Finland. Geol. Surv. Finl. Bull. 310, 79 p.

**Marre, J., 1986.** The Structural Analysis of Granitic Rocks. North Oxford Academic, Tiptree, 124 p.

**Marsh, B.D., 1982.** On the mechanics of igneous diapirism, stoping, and zone melting. Am. J. Sci. 282, 808—855.

**Masuda, T. & Ando, S., 1988.** Viscous flow around a rigid spherical body: a hydrodynamical approach. Tectonophysics 148, 337—346.

**Matisto, A., 1961.** Geological map of Finland, 1:100 000, pre-Quaternary rocks, sheet 2123 Tampere, Geol. Surv. Finl.

**Matisto, A., 1964.** Geological map of Finland, 1:100 000, pre-Quaternary rocks, sheet 2141 Kangasala, Geol. Surv. Finl.

**Matisto, A., 1967.** Geological map of Finland, 1:100 000, pre-Quaternary rocks, sheet 2121 Vammala, Geol. Surv. Finl.

**Matisto, A., 1977.** Geological map of Finland, 1:100 000, sheet 2123 Tampere. Explanation to the map of pre-

Quaternary rocks. Geol. Surv. Finl., 50 p. (in Finnish, with an English summary).

**Miyashiro, A., 1974.** Volcanic rock series in island arcs and active continental margins. Am. J. Sci. 274, 321—355.

**Nabelek, P.I., Papike, J.J. & Laul, J.C., 1986.** The Notch Peak granitic stock, Utah: origin of reverse zoning and petrogenesis. J. Petrol. 27, 1035—1069.

**Neuvonen, K.J., Korsman, K., Kouvo, O. & Paavola, J., 1981.** Paleomagnetism and age relations of the rocks in the Main Sulphide Ore Belt in central Finland. Bull. Geol. Soc. Finl. 53, 109—133.

**Nironen, M., 1985.** Eräiden svekokarjalaisten granitoidien intruusiomekanismit ja tektoninen asema sekä niihin liittyvien porfyyrityyppisten Mo- ja Cu-esiintymien rakenne. Unpubl. Ph. Lic. thesis, Univ. Helsinki, 97 p. (in Finnish).

**Nironen, M.** Tampere Schist Belt: structural style within an early Proterozoic volcanic arc system in southern Finland (in press).

**Nironen, M. & Bateman R.** Petrogenesis and syntectonic emplacement in the early Proterozoic of south-central Finland: a reversely zoned diorite-granodiorite and a granite (in press).

**Nurmi, P.A., 1983.** Trace element variations in the mid-Proterozoic Rautio batholith, Finland: petrogenetic implications. *In:* S.S. Augustithis (Editor), The Significance of Trace Elements in Solving Petrogenetic Problems & Controversies. Theophrastus Publ., Athens, 353—376.

**Nurmi, P.A. & Haapala, I., 1986.** The Proterozoic granitoids of Finland: Granite types, metallogeny and relation to crustal evolution. Bull. Geol. Soc. Finl. 58, 203—233.

**Nurmi, P.A., Front. K., Lampio, E. & Nironen, M., 1984.** Etelä-Suomen svekokarjalaiset porfyyrityyppiset molybdeeni- ja kupariesiintymät, niiden granitoidi-isäntä-kivet ja litogeokemiallinen etsintä. Svecokarelian porphyry-type molybdenum and copper occurrences in southern Finland: their granitoid host rocks and lithogeochemical exploration. Geol. Surv. Finl., Rep. Invest. 67, 88 p. (in Finnish, with an English summary).

**Nykänen, O., 1975a.** Geological map of Finland, 1:100 000, pre-Quaternary rocks, sheet 4213 Kerimäki, Geol. Surv. Finl.

**Nykänen, O., 1975b.** Geological map of Finland, 1:100 000, sheets 4213 Kerimäki and 4231 Kitee. Explanation to the maps of pre-Quaternary rocks. Geol. Surv. Finl., 43 p. (in Finnish, with an English summary).

**Nykänen, O., 1980.** Geological map of Finland, 1:100 000, pre-Quaternary rocks, sheet 4124+4142 Punkaharju, Geol. Surv. Finl.

**Nykänen, O., 1983.** Geological map of Finland, 1:100 000, sheets 4124+4142 Punkaharju and 4123+4114 Parikkala. Explanation to the maps of pre-Quaternary rocks. Geol. Surv. Finl., 81 p. (in Finnish, with an English summary).

**Oen, I.S., 1960.** The intrusion mechanism of the late-Hercynian, post-tectonic granite plutons of northern Portugal. Geol. Mijnb. 39, 257—296.

**Ojakangas, R.W., 1986.** An early Proterozoic metagreywacke-slate turbidite sequence: The Tampere schist belt, southwestern Finland. Bull. Geol. Soc. Finl. 58, 241—261.

**Pajunen, M., 1986.** Deformation analysis of cataclastic structures and faults in the Tervo area, Central Finland. *In:* K. Korsman (Editor), Development of deformation, metamorphism and metamorphic blocks in eastern and southern Finland. Geol. Surv. Finl. Bull. 339, 16—31.

**Park, A.F., 1981.** Basement gneiss domes in the Svecokarelides of eastern Finland: discussion. Earth Planet. Sci. Lett. 55, 199—203.

**Park, A.F. & Bowes, D.R., 1983.** Basement-cover relationship during polyphase deformation in the Svecokarelides of the Kaavi district, eastern Finland. Trans. R. Soc. Edinb., Earth Sci. 74, 95—118.

**Park, A.F., Bowes, D.R., Halden, N.M. & Koistinen, T.J., 1984.** Tectonic evolution at an early Proterozoic continental margin: the Svecokarelides of eastern Finland. J. Geodynamics 1, 359—386.

**Park, R.G., 1969.** Structural correlation in metamorphic belts. Tectonophysics 7, 323—338.

**Parkkinen, J., 1975.** Deformation analysis of a Precambrian mafic intrusive: Haukivesi area, Finland. Geol. Surv. Finl. Bull. 278, 61 p.

**Parras, K., 1958.** On the charnockites in the light of a highly metamorphic rock complex in southwestern Finland. Bull. Comm. géol. Finl. 181, 137 p.

**Passchier, C.W. & Simpson, C., 1986.** Porphyroclast systems as kinematic indcators. J. Struct. Geol. 8, 831—843.

**Patchett, P.J. & Arndt, N.T., 1986.** Nd isotopes and tectonics of 1.9—1.7 Ga crustal genesis. Earth Planet. Sci. Lett. 78, 329—338.

**Patchett, J. & Kouvo, O., 1986.** Origin of continental crust of 1.9—1.7 Ga age: Nd isotopes and U-Pb zircon ages in the Svecokarelian terrain of South Finland. Contrib. Mineral. Petrol. 92, 1—12.

**Phillips, W.J., Fuge, R. & Phillips, N., 1981.** Convection and crystallization in the Criffell-Dalbeattie pluton. J. Geol. Soc. Lond. 138, 351—366.

**Pitcher, W.S., 1978.** The anatomy of a batholith. J. Geol. Soc. Lond. 135, 157—182.

**Pitcher, W.S., 1979.** The nature, ascent and emplacement of granitic magmas. J. Geol. Soc. Lond. 136, 627—662.

**Pitcher, W.S., 1987.** Granites and yet more granites forty years on. Geol. Rundsch. 76, 51—79.

**Pitcher, W.S. & Berger, A.R., 1972.** The Geology of Donegal: a Study of Granite Emplacement and Unroofing. Wiley Interscience, London, 435 p.

**Prior, D.J., 1987.** Syntectonic porphyroblast growth in phyllites: textures and processes. J. Metamorph. Geol. 5, 27—39.

**Puranen, M. & Puranen, R., 1977.** Apparatus for the measurement of magnetic susceptibility and its anisotropy. Geol. Surv. Finl., Rep. Invest, 28, 46 p.

**Ramberg, H., 1967.** Gravity, Deformation and the Earth's Crust as Studied by Centrifuged Models. Academic Press, London, 214 p.

**Ramberg, H., 1970.** Model studies in relation to intrusion of plutonic bodies. *In:* G. Newall & N. Rast (Editors), Mechanism of Igneous Intrusion. Gallery Press, Liverpool, 261—286.

**Ramberg, H., 1980.** Diapirism and gravity collapse in the Scandinavian Caledonides. J. Geol. Soc. Lond. 137, 261—270.

**Ramsay, J.G., 1967.** Folding and Fracturing of Rocks. McGraw-Hill, New York, 568 p.

**Ramsay, J.G., 1981.** Emplacement mechanics of the Chindamora batholith, Zimbabwe. *In:* M.P. Coward (Editor), Diapirism and Gravity Tectonics: Report of a Tectonic Studies Group Conference, Leeds 1980. J. Struct. Geol. 3, 93.

**Ramsay, J.G. & Huber, M.I., 1983.** The Techniques of Modern Structural Geology. Volume 1: Strain Analysis.

Academic Press, London, 307 p.

**Rathore, J.S. & Kafafy, A.M., 1986.** A magnetic fabric study of the Shap region in the English Lake District. J Struct. Geol. 8, 69—77.

**Reches, Z. & Johnson, A.M., 1976.** A theory of concentric, kink and sinusoidal folding and of monoclinal flexuring of compressible, elastic multilayers. Tectonophysics 35, 295—334.

**Reymer, A. & Schubert, G., 1986.** Rapid growth of some major segments of continental crust. Geology 14, 299—302.

**Rice, A., 1981.** Convective fractionation: a mechanism to provide cryptic zoning (macrosegregation) layering, crescumulates, banded tuffs and explosive volcanism in igneous processes. J. Geophys. Res. 86, 405—417.

**Robin, P.-Y.F., 1977.** Determination of geologic strain using randomly oriented strain markers of any shape. Tectonophysics 42, T7—T16.

**Rodgers, D.A., 1980.** Analysis of pull-apart basin development produced by en echelon strike-slip faults. Spec. Publ. Int. Ass. Sedimentol. 4, 27—41.

**Sakko, M., 1971.** Varhais-Karjalaisten metadiabaasien radiometrisiä zirconi-ikiä. (Radiometric zircon ages on the Early-Karelian metadiabases). Geologi 23, 117—118.

**Salaterä, T., 1976.** Otasalo-områdets berggrund och stratigrafi i Puumala, SE Finland. Unpubl. M. Sci. thesis, Åbo Akademi, 79 p. (in Swedish).

**Saltikoff, B., 1965.** Pohjois-Säämingin (Varparannan) intrusiivimassiivi ja sen ympäristö. Unpubl. M. Sc. thesis, Univ. Helsinki, 71 p. (in Finnish).

**Sanderson, D.J. & Meneilly, A.W., 1981.** Analysis of three-dimensional strain modified uniform distributions: andalusite fabrics from a granite aureole. J. Struct. Geol. 109—116.

**Sawyer, E.W. & Barnes, S.-J., 1988.** Temporal and compositional differences between subsolidus and anatectic migmatite leucosomes from the Quetico metasedimentary belt, Canada. J. Metamorph. Geol. 6, 437—450.

**Sawyer, E.W. & Robin, P.-Y. F., 1986.** The subsolidus segregation of layer-parallel quartz-feldspar veins in greenschist to upper amphibolite facies metasediments. J. Metamorph. Geol. 4, 237—260.

**Schreurs, J., 1984.** The amphibolite-granulite facies transition in West Uusimaa, S.W. Finland. A fluid inclusion study. J. Metamorph. Geol. 2, 327—341.

**Schwerdtner, W.M., 1981.** Identification of gneiss diapirs. *In:* M.P. Coward (Editor), Diapirism and Gravity Tectonics: Report of a Tectonic Studies Group Conference, Leeds 1980. J. Struct. Geol. 3, 90—91.

**Schwerdtner, W.M., Bennett, P.J. & Janes, T.W., 1977.** Application of L-S fabric scheme to structural mapping and paleostrain analysis. Can. J. Earth Sci. 14, 1021—1032.

**Schwerdtner, W.M., Sutcliffe, R.H. & Tröeng, B., 1978.** Patterns of total strain in the crestal region of immature diapirs. Can. J. Earth Sci. 15, 1437—1447.

**Schwerdtner, W.M., Stott, G.M. & Sutcliffe, R.H., 1983.** Strain patterns of crescentic granitoid plutons in the Archean greenstone terrain of Ontario. J. Struct. Geol. 5, 419—430.

**Sederholm, J.J., 1897.** Über eine archäische Sedimentformation im Südwestlichen Finnland und ihre Bedeutung für die Erklärung der Entstehungsweise des Grundgebirges. Bull. Comm. Géol. Finl. 6, 254 p.

**Sederholm, J.J., 1915.** De bottniska skiffrarnas undre kontakter. Geol. Fören. Förh. 37, 52—118.

**Seitsaari, J., 1951.** The schist belt northeast of Tampere in Finland. Bull. Comm. Géol. Finl. 153, 120 p.

**Simonen, A., 1952.** Geological map of Finland, 1:100 000, sheet 2124 Viljakkala-Teisko. Explanation to the map of rocks. Geol. Surv. Finl., 74 p. (in Finnish, with an English summary).

**Simonen, A., 1953a.** Geological map of Finland, 1:100 000, pre-Quaternary rocks, sheet 2124 Viljakkala-Teisko. Geol. Surv. Finl.

**Simonen, A., 1953b.** Stratigraphy and sedimentation of the Svecofennidic, early Archean supracrustal rocks in southwestern Finland. Bull. Comm. Géol. Finl. 160, 64 p.

**Simonen, A., 1960.** Plutonic rocks of the Svecofennides in Finland. Bull. Comm. Géol. Finl. 189, 101 p.

**Simonen, A., 1980.** The Precambrian of Finland. Geol. Surv. Finl. Bull. 304, 58 p.

**Simonen, A. & Kouvo, O., 1951.** Archean varved schists north of Tampere in Finland. Bull. Comm. Géol. Finl. 154, 93—114.

**Simonen, A. & Neuvonen, K., 1947.** On the metamorphism of the schists in the Ylöjärvi area. Bull. Comm. Géol. Finl. 140, 247—260.

**Snowden, P.A., 1984.** Non-diapiric batholiths in the north of the Zimbabwe Shield. *In:* A. Kröner & R. Greiling (Editors), Precambrian Tectonics Illustrated. E. Schweizerbart'sche Verlaagsbuchhandlung, Stuttgart, 135—145.

**Soula, J.-C., 1982.** Characteristics and mode of emplacement of gneiss domes and plutonic domes in central-eastern Pyrenees. J. Struct. Geol. 4, 313—342.

**Sparks, R.S.J. & Marshall, L.A., 1986.** Thermal and mechanical constraints on mixing between mafic and silicic magmas. *In:* I. Kushiro (Editor), M. Sakuyama and H. Fukuyama Memorial Volume. J. Volc. Geotherm. Res. 29, 99—124.

**Sparks R.S.J., Huppert, H.E. & Turner, J.S., 1984.** The fluid dynamics of evolving magma chambers. Phil. Trans. R. Soc. Lond. A310, 511—534.

**Stow, D.A., 1986.** Deep clastic seas. *In:* H.G. Reading (Editor), Sedimentary Environments and Facies. Blackwell, Oxford, 399—444.

**Talvitie, J., 1975.** Fractures, dynamic model and Ni-Cu mineralized basic intrusives in Central Finland. Geol. Surv. Finl., Rep. Invest. 10, 3—12.

**Törnroos, R., 1982.** Sphalerite geobarometry of some metamorphosed sulphide ore deposits in Finland. Geol. Surv. Finl. Bull. 323, 42 p.

**Vaasjoki, M., 1977.** Rapakivi granites and other postorogenic rocks in Finland: their age and the lead isotopic composition of certain associated galena mineralizations. Geol Surv. Finl. Bull. 294, 64 p.

**Vaasjoki, M., 1981.** The lead isotopic composition of some Finnish galenas. Geol. Surv. Finl. Bull. 316, 30 p.

**Vaasjoki, M. & Sakko, M., 1988.** The evolution of the Raahe-Ladoga zone in Finland: isotopic constraints. *In:* K. Korsman (Editor), Tectonometamorphic evolution of the Raahe-Ladoga zone. Geol. Surv. Finl. Bull. 343, 7—32.

**Van den Driessche, J., 1986.** Structural evolution of the Thor Odin gneiss dome — discussion. Tectonophysics 121, 351—354.

**Van den Eeckhout, B., Grocott, J. & Vissers R., 1986.** On the role of diapirism in the segregation, ascent and final emplacement of granitoid magmas — discussion. Tectonophysics 127, 161—169.

**Vernon, R.H., 1983.** Restite, xenoliths and microgranitoid enclaves in granites. J. Proc. R. Soc. New South Wales 116, 77—103.

**Vernon, R.H., 1986.** K-feldspar megacrysts in granites — phenocrysts, not porphyroblasts. Earth-Sci. Rev. 23, 1—63.

**Vernon, R.H., 1987.** Growth and concentration of fibrous sillimanite related to heterogeneous deformation in K-feldspar — sillimanite metapelites. J. Metamorph. Geol. 5, 51—68.

**Watson, E.B., 1979.** Zircon saturation in felsic liquids: experimental data and applications to trace element geochemistry. Contrib. Mineral. Petrol. 70, 407—419.

**Watson, E.B. & Harrison, T.M., 1983.** Zircon saturation revisited: temperature and composition effects in a variety of crustal magma types. Earth Planet. Sci. Lett. 64, 295—304.

**Watterson, J., 1968.** Homogeneous deformation of the gneisses of Vesterland, southwest Greenland. Meddr. Grønland 175, 1—75.

**Weber, C., Barbey, P., Cuney, M. & Martin, H., 1985.** Trace element behaviour during migmatization. Evidence for a complex melt-residuum-fluid interaction in the St. Malo migmatitic dome (France). Contrib. Mineral. Petrol. 90, 52—62.

**Welin, E., 1987.** The depositional evolution of the Svecofennian supracrustal sequence in Finland and Sweden. Precambrian Res. 35, 95—113.

**Welin, E., Vaasjoki, M. & Suominen, V., 1983.** Age differences between Rb-Sr whole rock and U-Pb zircon ages of syn- and postorogenic Svecokarelian granitoids in Sottunga, SW Finland. Lithos 16, 297—305.

**White, A.J.R. & Chappell, B.W., 1977.** Ultrametamorphism and granitoid genesis. Tectonophysics 43, 7—22.

**White, A.J.R. & Chappell, B.W., 1983.** Granitoid types and their distribution in the Lachlan Fold Belt, southeastern Australia. Geol Soc. Am. Mem. 159, 21—34.

**White, A.J.R., Clemens, J.D., Holloway, J.R., Silver, L.T., Chappell, B.W. & Wall, V.J., 1986.** S-type granites and their probable absence in southwestern North America. Geology 14, 115—118.

**Wickham, S.M., 1987.** Crustal anatexis and granite petrogenesis during low-pressure regional metamorphism: the Trois Seigneurs Massif, Pyrenees, France. J. Petrol. 28, 127—169.

**Williams, P.F., 1985.** Multiply deformed terrains — problems of correlation. *In:* P.L. Hancock & C.McA. Powell (Editors), Multiple Deformation in Ductile and Brittle Rocks. J. Struct. Geol. 7, 269—280.

**Woodcock, N.H. & Fischer, M., 1986.** Strike-slip duplexes. J. Struct. Geol. 8, 725—735.

**Wyllie, P.J., 1977.** Crustal anatexis: an experimental review. *In:* D.H. Green (Editor), Experimental Petrology Related to Extreme Metamorphism. Tectonophysics 43, 41—71.

**Wyllie, P.J., 1983.** Experimental studies on biotite- and muscovite-granites and some crustal magmatic sources. *In:* M.P. Atherton & C.D. Gribble (Editors), Migmatites, Melting and Metamorphism. Shiva, Nantwich, 12—26.

**Appendix 1. Modes and modal compositions of plutonic rocks in the Tampere and Savo Schist Belts.**

| PLUTON/Phase | Sample | Map sheet | X | Y | Modal composition (*1) | Modes (*2) Plag | Q | Kfs | Bt | Hbl | Ti | Op | Chl | Mu | Others (*3) |
|---|---|---|---|---|---|---|---|---|---|---|---|---|---|---|---|
| HÄMEENKYRÖ | | | | | | | | | | | | | | | |
| Tonalite | 273-KAF-78 | 2124 04 | 6831.93 | 476.16 | grdr | 38.7 | 23.6 | 13.5 | 21.6 | | 0.9 | | 0.2 | | 1.5(a1.2) |
| | 291-KAF-78 | 2124 01 | 6837.64 | 462.62 | ton | 49.5 | 16.2 | 4.1 | 13.0 | 13.7 | 1.4 | | 2.0 | | 0.1 |
| | 292-KAF-78 | 2124 01 | 6837.52 | 463.39 | qmdr | 46.8 | 14.4 | 10.9 | 14.4 | 12.1 | 1.1 | | 0.1 | | 0.2 |
| | 372-KAF-78 | 2124 01 | 6835.06 | 464.64 | qmdr | 46.3 | 13.8 | 8.9 | 1.7 | 18.3 | 3.3 | | 7.6 | | 0.1 |
| | 399-KAF-78 | 2124 01 | 6833.46 | 463.72 | qdr | 64.0 | 15.6 | 4.2 | 7.3 | 6.4 | 1.0 | | 1.4 | | 0.1 |
| | 402-KAF-78 | 2122 10 | 6830.17 | 459.42 | grdr | 49.5 | 14.6 | 5.9 | 11.0 | 18.2 | 0.7 | | | | 0.1 |
| | 435-KAF-78 | 2123 03 | 6826.78 | 468.22 | ton | 42.7 | 23.5 | | 19.6 | 14.0 | 0.2 | | | | |
| | 52-MN-85 | 2123 06 | 6829.04 | 471.61 | ton | 49.6 | 13.6 | | 21.0 | 14.2 | 0.4 | 0.6 | | | 0.6 |
| Granodiorite | 297-KAF-78 | 2124 01 | 6837.42 | 464.67 | gr | 33.9 | 23.4 | 18.8 | 12.4 | 8.7 | 2.4 | | | | 0.4 |
| | 313-KAF-78 | 2124 01 | 6835.32 | 465.54 | grdr | 44.2 | 19.9 | 18.7 | 4.8 | 10.8 | 1.3 | | 0.1 | | 0.2 |
| | 323-KAF-78 | 2124 04 | 6838.44 | 472.08 | grdr | 27.7 | 22.1 | 14.6 | 28.3 | 0.3 | 0.4 | | 2.2 | | 4.4(a/4.3) |
| | 325-KAF-78 | 2124 04 | 6838.38 | 471.22 | gr | 34.1 | 24.4 | 22.6 | 16.0 | 0.1 | 1.1 | | 1.1 | | 0.6(a/0.5) |
| | 326-KAF-78 | 2124 04 | 6838.28 | 470.87 | grdr | 42.9 | 21.5 | 12.7 | 19.6 | | 1.1 | | 0.1 | | 2.1(a/1.7) |
| | 327-KAF-78 | 2124 04 | 6837.50 | 470.13 | gr | 31.1 | 20.9 | 23.6 | 5.2 | 16.9 | 1.3 | | 0.7 | | 0.3 |
| | 328-KAF-78 | 2124 01 | 6837.11 | 469.46 | grdr | 34.2 | 23.9 | 18.3 | 7.1 | 10.3 | 1.8 | | 4.1 | | 0.3 |
| | 329-KAF-78 | 2124 01 | 6836.66 | 469.34 | gr | 36.2 | 18.9 | 22.8 | 11.4 | 8.6 | 1.6 | | 0.1 | | 0.4 |
| | 332-KAF-78 | 2124 01 | 6835.71 | 468.37 | grdr | 31.2 | 25.6 | 17.4 | 13.9 | 10.7 | 1.2 | | | | |
| | 333-KAF-78 | 2124 01 | 6834.56 | 468.54 | grdr | 41.7 | 24.9 | 13.6 | 8.7 | 9.0 | 0.8 | | 1.3 | | |
| | 338-KAF-78 | 2124 04 | 6835.49 | 471.24 | grdr | 38.7 | 23.2 | 10.7 | 16.6 | 9.2 | 0.9 | | 0.6 | | 0.1 |
| | 340-KAF-78 | 2124 04 | 6834.70 | 470.43 | gr | 31.9 | 25.8 | 20.2 | 10.2 | 10.3 | 1.4 | | 0.1 | | 0.1 |
| | 343-KAF-78 | 2124 04 | 6832.53 | 471.14 | grdr | 38.4 | 26.3 | 18.3 | 10.6 | 5.1 | 1.1 | | | | 0.2 |
| | 381-KAF-78 | 2124 01 | 6833.56 | 461.36 | grdr | 39.4 | 24.8 | 17.5 | 8.2 | 7.6 | 0.6 | | 1.8 | | 0.1 |
| | 383-KAF-78 | 2124 01 | 6833.50 | 462.76 | grdr | 36.6 | 17.1 | 12.3 | 9.1 | 16.3 | 2.4 | | 6.1 | | 0.1 |
| | 406-KAF-78 | 2123 03 | 6827.74 | 461.43 | grdr | 39.5 | 17.6 | 7.3 | 13.7 | 19.9 | 1.0 | | 0.8 | | 0.2 |
| | 422-KAF-78 | 2123 03 | 6828.32 | 464.53 | grdr | 49.4 | 20.9 | 10.6 | 8.0 | 9.7 | 0.6 | | 0.7 | | 0.1 |
| | 425-KAF-78 | 2123 03 | 6827.59 | 463.39 | grdr | 35.8 | 23.2 | 12.1 | 13.9 | 13.7 | 1.0 | | 0.2 | | 0.1 |
| | 429-KAF-78 | 2123 03 | 6826.16 | 464.03 | grdr | 42.5 | 21.6 | 9.0 | 20.3 | 5.7 | 0.4 | | 0.5 | | |
| Granite | 301-KAF-78 | 2124 01 | 6838.52 | 465.51 | grdr | 44.5 | 21.9 | 16.2 | 7.8 | 7.8 | | 0.1 | 1.4 | | 0.3 |
| | 311-KAF-78 | 2124 01 | 6839.14 | 467.52 | gr | 38.5 | 26.4 | 23.8 | 8.5 | | | | 2.3 | | 0.5 |
| | 342-KAF-78 | 2124 04 | 6832.52 | 470.24 | gr | 33.4 | 20.3 | 23.4 | 12.8 | 8.8 | 1.1 | | 0.1 | | 0.1 |
| | 344-KAF-78 | 2124 04 | 6833.90 | 470.70 | gr | 31.6 | 25.7 | 18.9 | 11.2 | 9.8 | 1.5 | | 1.2 | | 0.1 |
| | 345-KAF-78 | 2124 04 | 6833.70 | 471.50 | gr | 27.7 | 19.8 | 31.4 | 11.5 | 8.3 | 1.1 | | | | 0.2 |
| | 368-KAF-78 | 2124 01 | 6831.31 | 466.64 | grdr | 34.2 | 35.1 | 17.7 | 6.8 | 4.6 | 1.0 | | 0.4 | | 0.2 |
| | 369-KAF-78 | 2124 01 | 6833.30 | 467.36 | gr | 38.4 | 27.1 | 20.9 | 4.6 | 6.7 | 0.7 | | | | |
| | 409-KAF-78 | 2124 01 | 6830.12 | 465.79 | gr | 34.1 | 22.6 | 23.0 | 8.9 | 8.8 | 1.6 | | 0.4 | | 0.6 |
| Feldspar porphyry | 123-KAF-78 | 2124 04 | 6831.71 | 472.91 | grdr | 48.2 | 27.0 | 19.8 | 0.2 | | 1.4 | | 3.3 | | 0.1 |
| | 189-KAF-78 | 2124 04 | 6834.17 | 472.86 | gr | 26.2 | 27.0 | 39.4 | 5.9 | | 0.1 | | | | 1.4(a/1.3) |
| Plagioclase porphyry | 116-KAF-78 | 2124 04 | 6831.65 | 473.75 | ton | 46.8 | 30.8 | | | 2.4 | 0.7 | | 14.3 | | 5.0(a/4.9) |
| VÄRMÄLÄ | | | | | | | | | | | | | | | |
| Granodiorite | 81-11005 | 2124 10 | 6836.34 | 497.86 | grdr | 41.7 | 28.7 | 18.2 | 10.9 | 0.4 | | | | | 0.1 |
| | 81-11006 | 2124 10 | 6834.45 | 497.06 | grdr | 42.8 | 33.8 | 11.5 | 11.6 | 0.2 | | | | | 0.1 |
| | 81-11010 | 2124 10 | 6832.23 | 496.17 | grdr | 45.0 | 32.7 | 10.2 | 11.9 | 0.2 | | | | | |

**App. 1, contd.**

| | | | | | | | | | | | | | | |
|---|---|---|---|---|---|---|---|---|---|---|---|---|---|---|
| | 81-11018 | 2124 10 | 6830.74 | 497.52 | grdr | 44.3 | 34.2 | 13.0 | | 2.9 | 0.6 | 3.2 | 1.5 | 0.3 |
| | 81-11029 | 2124 10 | 6833.14 | 498.62 | grdr | 40.9 | 34.3 | 15.9 | 8.0 | 0.1 | 0.3 | 0.4 | | 0.1 |
| | 81-11030 | 2124 10 | 6834.63 | 499.65 | grdr | 43.9 | 28.3 | 20.7 | 6.3 | | | 0.5 | 0.3 | 0.1 |
| | 81-11032 | 2124 10 | 6832.47 | 499.74 | grdr | 50.0 | 26.8 | 12.7 | 10.1 | | | | | 0.4(a/0.4) |
| Granite | 81-11011 | 2124 10 | 6830.37 | 493.62 | gr | 34.1 | 33.6 | 30.4 | 1.8 | | | | | 0.1 |
| | 81-11016 | 2123 12 | 6829.58 | 497.95 | gr | 34.3 | 39.1 | 24.2 | 2.4 | | | | | |
| | 81-11023 | 2124 10 | 6832.19 | 493.33 | gr | 35.2 | 26.6 | 33.4 | 4.1 | | | 0.3 | | 0.5(b/0.3) |
| | 81-11026 | 2124 10 | 6834.81 | 494.78 | grdr | 40.9 | 39.0 | 12.3 | 6.3 | | | | 2.2 | 0.3(b/0.1) |
| | 51-MN-84 | 2124 10 | 6833.61 | 493.60 | gr | 38.4 | 26.4 | 29.6 | 4.4 | | | 0.4 | | 0.8(b/0.5) |
| | 62-MN-84 | 2123 12 | 6829.36 | 495.74 | gr | 36.3 | 24.4 | 33.2 | 5.1 | 0.2 | | 0.7 | | 0.1 |
| Quartz | | | | | | | | | | | | | | |
| monzodiorite | 81-11028 | 2124 10 | 6832.44 | 497.38 | qmdr | 56.6 | 17.7 | 19.5 | 6.2 | | | | | |
| | 57-MN-84 | 2124 10 | 6833.93 | 498.25 | gr | 46.7 | 21.0 | 26.6 | 5.4 | | | 0.3 | | |
| | 92-MN-84 | 2124 10 | 6831.77 | 496.61 | grdr | 44.5 | 29.7 | 20.2 | 5.3 | | | 0.2 | | |
| | 106-MN-84 | 2124 10 | 6833.22 | 497.27 | qmdr | 55.9 | 13.4 | 24.7 | 6.0 | | | | | |
| Porphyritic granite | 2-MN-84 | 2124 10 | 6837.34 | 497.67 | gr | 35.1 | 32.6 | 24.3 | 6.0 | | | 1.0 | 0.8 | |
| | 13-MN-84 | 2124 10 | 6837.41 | 497.85 | grdr | 38.0 | 36.4 | 17.0 | 7.5 | | | 0.3 | 0.8 | |
| Diorite | 81-11015 | 2123 12 | 6829.21 | 497.72 | qdr | 51.7 | 11.9 | | 22.6 | 13.8 | | | | |
| SILVOLA | | | | | | | | | | | | | | |
| Tonalite | 80-23002 | 4122 12 | 6856.72 | 452.14 | ton | 53.1 | 29.5 | 2.8 | 2.7 | 11.6 | | | | 0.3 |
| | 80-23004 | 4122 12 | 6857.47 | 451.89 | grdr | 47.8 | 32.2 | 7.2 | 3.4 | 9.0 | 0.3 | | | 0.1 |
| | 80-23005 | 4122 12 | 6857.43 | 453.03 | ton | 48.1 | 36.0 | 1.3 | 9.3 | 3.7 | | | | 1.6(a/1.5) |
| | 80-23006 | 4122 12 | 6858.20 | 453.50 | ton | 59.6 | 26.2 | 4.2 | 5.3 | 3.8 | 0.7 | | | 0.2 |
| | 80-23008 | 4122 12 | 6857.80 | 452.68 | grdr | 47.0 | 36.9 | 7.5 | 3.4 | 3.8 | 1.1 | | | 0.3 |
| | 80-23009 | 4122 12 | 6859.77 | 455.26 | ton | 51.7 | 33.5 | 4.6 | 4.5 | 5.6 | | | | 0.1 |
| | 80-23010 | 4122 12 | 6859.26 | 454.17 | ton | 51.4 | 35.4 | 1.9 | 0.8 | 7.4 | 2.8 | | | 0.2 |
| | 80-23012 | 4122 12 | 6859.69 | 452.98 | ton | 58.7 | 25.1 | 0.6 | 8.6 | 6.2 | | | | 0.8 |
| | 80-23013 | 4122 12 | 6859.80 | 451.67 | ton | 63.6 | 17.9 | 4.9 | 1.9 | 11.7 | | | | |
| | 17-2-MN-85 | 4211 10 | 6861.14 | 456.24 | ton | 66.6 | 18.6 | 2.5 | 4.9 | 7.4 | | | | |
| | 19-2-MN-85 | 4211 10 | 6863.12 | 456.40 | ton | 59.1 | 24.6 | 5.3 | 3.9 | 5.1 | 0.2 | | | 1.8 |
| | 46-2-MN-85 | 4211 10 | 6863.81 | 457.00 | ton | 59.2 | 25.0 | 0.7 | 4.0 | 10.6 | 0.2 | | | 0.3 |
| | 52-2-MN-85 | 4211 10 | 6866.82 | 456.50 | ton | 60.5 | 21.7 | 2.2 | 8.7 | 5.5 | | | 0.1 | 1.0 |
| | 84-2-MN-85 | 4211 10 | 6861.00 | 450.68 | ton | 65.7 | 20.8 | 0.3 | 3.9 | 9.2 | | | | 0.1 |
| | 98-2-MN-85 | 4211 10 | 6861.83 | 452.09 | ton | 55.2 | 27.9 | 2.1 | 5.3 | 7.3 | 0.6 | 0.6 | | 1.0 |
| Trondhjemite | 80-23007 | 4122 12 | 6858.56 | 453.73 | tr | 54.2 | 37.9 | 2.9 | 2.9 | 1.4 | 0.4 | | 0.1 | 0.1 |
| | 80-23011 | 4122 12 | 6859.31 | 453.38 | ton | 62.4 | 22.2 | 0.6 | 8.9 | 5.6 | 0.1 | | | 0.2 |
| | 80-23015 | 4122 12 | 6859.68 | 454.02 | tr | 59.6 | 30.3 | 5.7 | 4.2 | 0.2 | | | | |
| | 12-2-MN-85 | 4211 10 | 6861.41 | 454.41 | tr | 48.5 | 42.1 | 5.5 | 3.5 | 0.2 | | | 0.2 | |
| | 15-2-MN-85 | 4211 10 | 6862.21 | 454.98 | tr | 53.3 | 33.7 | 5.3 | 2.4 | 4.1 | 1.2 | | | |
| | 30-2-MN-85 | 4211 10 | 6862.90 | 454.20 | tr | 57.4 | 31.9 | 1.8 | 2.9 | 5.2 | 0.8 | | | |
| | 44-2-MN-85 | 4211 10 | 6865.84 | 454.10 | tr | 53.4 | 35.9 | 5.2 | 3.4 | 1.5 | 0.1 | | | 0.5 |
| | 45-2-MN-85 | 4211 10 | 6864.44 | 455.26 | tr | 59.5 | 32.0 | 1.1 | 6.2 | | | 0.6 | 0.6 | |
| | 47-2-MN-85 | 4211 10 | 6864.73 | 456.54 | tr | 56.1 | 35.0 | 1.6 | 4.0 | 2.6 | 0.3 | | | 0.4 |
| | 61-2-MN-85 | 4211 10 | 6865.59 | 455.23 | tr | 56.6 | 31.9 | 4.1 | 4.2 | 2.6 | 0.5 | | | 0.1 |
| | 66-2-MN-85 | 4211 10 | 6862.12 | 453.18 | tr | 64.5 | 26.1 | 1.5 | 3.1 | 3.7 | 1.1 | | | |
| | 71-2-MN-85 | 4211 10 | 6860.37 | 453.49 | ton | 59.1 | 27.5 | 3.2 | 3.5 | 6.3 | 0.4 | | | |
| | 80-2-MN-85 | 4211 10 | 6863.02 | 451.26 | tr | 57.6 | 32.7 | 3.8 | 5.0 | 0.7 | | | | 0.2 |
| | 94-2-MN-85 | 4211 07 | 6862.18 | 449.65 | tr | 51.8 | 37.8 | 2.1 | 6.2 | 2.1 | | | | |
| Granodiorite | 80-23001 | 4122 12 | 6859.05 | 450.81 | grdr | 51.2 | 32.9 | 7.3 | 3.2 | 4.7 | 0.7 | | | |
| | 80-23003 | 4122 12 | 6858.04 | 451.49 | grdr | 46.3 | 36.6 | 5.7 | 5.4 | 6.0 | | | | |

**App. 1, contd.**

| | | | | | | | | | | | | | | | |
|---|---|---|---|---|---|---|---|---|---|---|---|---|---|---|---|
| | 99-2-MN-85 | 4211 10 | 6860.17 | 451.17 | grdr | 56.7 | 24.1 | 12.1 | 5.3 | 1.3 | | 0.5 | | | |
| KAARTILA | | | | | | | | | | | | | | | |
| | 80-24002 | 4122 09 | 6856.83 | 447.72 | ton | 43.2 | 44.4 | 0.9 | 7.2 | 4.2 | | | | | 0.1 |
| | 80-24003 | 4122 09 | 6856.81 | 446.67 | grdr | 40.1 | 39.9 | 18.6 | 1.1 | | | 0.3 | | | |
| | 80-24004 | 4122 09 | 6856.12 | 446.78 | ton | 57.1 | 30.8 | 1.1 | 8.7 | 1.2 | | 0.1 | | | 1.0 |
| | 80-24005 | 4122 09 | 6858.24 | 446.14 | grdr | 37.7 | 38.2 | 19.1 | 1.3 | 2.9 | | 0.7 | | | 0.1 |
| | 80-24006 | 4122 09 | 6857.28 | 445.97 | grdr | 43.6 | 40.1 | 11.5 | 2.6 | 1.7 | | 0.5 | | | |
| | 80-24007 | 4122 09 | 6856.54 | 447.21 | gr | 26.5 | 37.1 | 26.3 | 8.0 | 1.7 | | 0.1 | | | 0.3(c/0.3) |
| | 80-24008 | 4122 09 | 6855.50 | 445.84 | grdr | 40.4 | 40.1 | 9.8 | 8.7 | 0.5 | | | | | 0.5(c/0.5) |
| | 80-24009 | 4122 09 | 6856.10 | 446.19 | gr | 22.0 | 40.5 | 32.3 | 1.3 | 1.5 | | 2.4 | | | |
| | 80-24010 | 4122 09 | 6857.58 | 444.85 | gr | 28.1 | 38.1 | 26.4 | | 3.6 | 3.2 | | | | 0.6 |
| | 80-24011 | 4122 09 | 6855.40 | 445.66 | gr | 29.3 | 34.2 | 32.7 | 1.6 | 1.6 | | 0.6 | | | |
| | 80-24013 | 4122 09 | 6857.14 | 446.38 | tr | 46.6 | 42.4 | 1.6 | 6.8 | 2.2 | | 0.3 | | | |
| | 80-24014 | 4122 09 | 6857.87 | 447.16 | grdr | 40.3 | 38.5 | 8.9 | 3.5 | 8.8 | | | | | |
| | 80-24015 | 4122 09 | 6857.45 | 446.77 | grdr | 39.5 | 42.4 | 11.4 | 3.7 | 2.3 | | 0.7 | | | |
| VARPARANTA | | | | | | | | | | | | | | | |
| Trondhjemite | 69-K-62 | 4211 05 | 6876.72 | 438.00 | tr | 61.6 | 25.8 | 1.9 | 7.1 | | | | 0.6 | 2.4 | 0.6 |
| | 114-K-62 | 4211 05 | 6879.70 | 433.48 | grdr | 56.4 | 26.2 | 10.9 | 4.7 | | | | 0.9 | | 1.0 |
| | 270-K-62 | 4211 06 | 6881.74 | 433.70 | tr | 59.8 | 28.9 | 2.9 | 6.1 | 0.7 | | | | 1.2 | 0.4 |
| | 81-07001 | 4211 06 | 6880.36 | 433.45 | tr | 54.4 | 33.5 | 5.9 | 5.6 | | | | | 0.3 | |
| | 81-07003 | 4122 06 | 6881.81 | 433.34 | ton | 57.2 | 29.3 | 2.5 | 11.3 | 3.3 | | | | | |
| Fem-rich | | | | | | | | | | | | | | | |
| trondhjemite | 81-07027 | 4211 05 | 6876.80 | 438.45 | tr | 57.7 | 28.9 | 4.0 | 8.4 | 0.3 | | | | 0.3 | |
| | 81-07053 | 4211 05 | 6876.96 | 438.36 | tr | 61.2 | 23.6 | 6.5 | 8.0 | | | | | 0.4 | |
| Granodiorite dike | 221B-MN-85 | 4211 05 | 6876.13 | 436.70 | grdr | 50.5 | 29.2 | 12.1 | 7.8 | | | 0.1 | | 0.3 | |
| Porpyritic tonalite | 221A-MN-85 | 4211 05 | 6876.13 | 436.70 | ton | 52.8 | 31.6 | 0.1 | 13.2 | | | 0.1 | | 2.2 | |
| Homog. tonalite | 81-07008 | 4211 05 | 6877.52 | 437.68 | tr | 54.7 | 33.5 | 2.1 | 6.7 | | | | 0.7 | 0.8 | |
| | 81-07017 | 4211 05 | 6878.58 | 437.10 | tr | 64.8 | 22.8 | | | 3.9 | | | 0.2 | | |
| | 81-07030 | 4211 05 | 6876.89 | 438.34 | ton | 57.6 | 25.0 | 2.7 | 2.0 | 1.5 | | | 6.3 | 3.0 | |
| | 81-07031 | 4211 05 | 6877.81 | 438.36 | ton | 55.8 | 33.7 | 0.3 | 10.0 | | | | | | |
| | 81-07038 | 4211 06 | 6880.24 | 432.80 | ton | 56.5 | 32.3 | 0.5 | 6.7 | 3.3 | | | | 0.2 | |
| | 81-07059 | 4211 06 | 6880.03 | 437.76 | ton | 54.8 | 30.4 | 0.5 | 12.7 | | | | | 0.5 | |
| Heterog. tonalite | 55-K-62 | 4211 05 | 6877.66 | 436.34 | ton | 59.6 | 23.4 | | 10.6 | 4.5 | | | 0.2 | 0.6 | 1.2 |
| | 13-D-63 | 4211 05 | 6877.70 | 436.34 | ton | 62.9 | 19.0 | | 3.0 | 6.9 | | 0.2 | 0.2 | 7.6 | 0.1 |
| | 81-07013 | 4211 05 | 6877.96 | 436.78 | ton | 56.0 | 31.0 | | 8.8 | 3.3 | | | 0.2 | 0.2 | |
| | 81-07020 | 4211 05 | 6877.43 | 436.20 | ton | 54.0 | 29.0 | 0.5 | 9.7 | 6.1 | | | | | |
| | 81-07050 | 4211 05 | 6879.68 | 437.71 | ton | 59.9 | 23.7 | 0.4 | 10.7 | 3.2 | | | | 0.1 | |
| Quartz diorite | 55-K-62 | 4211 05 | 6877.66 | 436.34 | qdr | 46.7 | 7.4 | | 15.4 | 23.2 | | 3.5 | 1.7 | | 2.4 |
| | 13-D-63 | 4211 05 | 6877.70 | 436.34 | qdr | 65.0 | 4.7 | | 11.6 | 14.1 | | 2.0 | | | 2.6 |
| Diorite | 91-K-62 | 4211 05 | 6878.06 | 433.34 | qdr | 30.0 | 6.8 | | 0.2 | 54.0 | 3.6 | 0.8 | 0.4 | 3.1 | 1.4 |
| | 130-K-62 | 4211 05 | 6879.55 | 434.53 | dr | 45.9 | | | 1.3 | 35.1 | 0.2 | 4.7 | 1.3 | 7.8 | 3.6 |
| CONGLOMERATE CLASTS | | | | | | | | | | | | | | | |
| Tervalahti | A26 | 2124 10 | 6831.3 | 490.0 | qmdr | 57.8 | 14.9 | 19.1 | 2.5 | | | 1.8 | 3.1 | | 0.8 |
| | A393 | 2124 10 | 6831.7 | 491.1 | grdr | 60.8 | 25.7 | 8.2 | 2.5 | | | 1.0 | 1.0 | | 0.5 |
| | A768 | 2124 10 | 6831.3 | 490.5 | grdr | 49.4 | 21.0 | 18.8 | 8.1 | | | 0.9 | 1.2 | | 0.6 |
| Lavia | A144 | 2122 02 | 6842.56 | 422.64 | ton | 54.1 | 21.7 | | 15.9 | 8.3 | | | | | |

*1 gr = granite, grdr = granodiorite, ton = tonalite, tr = trondhjemite, qmdr = quartz monzodiorite, qdr = quartz diorite, dr = diorite
*2 Plag = plagioclase, Q = quartz, Kfs = K-feldspar, Bt = biotite, Hbl = hornblende, Ti = titanite, Op = opaque mineral, Chl = chlorite, Mu = muscovite
*3 a/ carbonate; b/ fluorite; c/ garnet

**Appendix 2. U-Pb isotopic data from the Tampere and Savo Schist Belts. The analyses were made in the Unit for Isotope Geology, Geological Survey of Finland. See Vaasjoki (1977) and Huhma (1986) for details of the method.**

| Sample | Fraction [*1] | Concentration (ppm) | | Measured $^{206}Pb/^{204}Pb$ | Isotopic composition of lead ($^{206}Pb$=100) | | | Atomic ratios and radiometric ages (Ma) | | |
|---|---|---|---|---|---|---|---|---|---|---|
| | | $^{238}U$ | $^{206}Pb$ radiog. | | 204 | 207 | 208 | $^{206}Pb/^{238}U$ | $^{207}Pb/^{235}U$ | $^{207}Pb/^{206}Pb$ |
| HÄMEENKYRÖ, granodiorite | | | | | | | | | | |
| A428 Äkönmaa [*2] | E d>4.6; abr | 259.1 | 75.50 | 20600 | 0.003247 | 11.567 | 8.621 | 0.3368 | 5.350 | 0.11523 |
| | | | | | | | | 1871 | 1876 | 1883±9 |
| | F 4.2<d<4.6; abr: Ø>70 | 379.3 | 109.03 | 8362 | 0.01063 | 11.666 | 8.312 | 0.3322 | 5.278 | 0.11523 |
| | | | | | | | | 1849 | 1865 | 1883±8 |
| YLÖJÄRVI, tourmaline breccia | | | | | | | | | | |
| A3 [*3] | uraninite | 48.63(%) | 13.89(%) | 142.37 | 0.7012 | 20.859 | 26.793 | 0.3301 | 5.181 | 0.11385 |
| | | | | | | | | 1838 | 1849 | 1861±11 |
| VÄRMÄLÄ, granodiorite | | | | | | | | | | |
| 54-MN-84 | d>3.6; abr | 1394 | 293.68 | 3277 | 0.02853 | 11.569 | 7.249 | 0.2434 | 3.753 | 0.11182 |
| | | | | | | | | 1404 | 1582 | 1829±6 |
| 55-MN-84 | A d>3.8; abr | 1398 | 283.35 | 1820 | 0.05201 | 11.842 | 7.823 | 0.2343 | 3.598 | 0.11136 |
| | | | | | | | | 1357 | 1549 | 1821±5 |
| | B 3.6<d<3.8; abr | 1965 | 306.58 | 1348 | 0.06920 | 11.739 | 8.169 | 0.1804 | 2.685 | 0.10796 |
| | | | | | | | | 1068 | 1324 | 1765±5 |
| | C d>3.6; abr short crystals | 1563 | 271.97 | 1324 | 0.06808 | 11.896 | 8.455 | 0.2011 | 3.042 | 0.10971 |
| | | | | | | | | 1181 | 1418 | 1794±7 |
| 105-MN-84 | 3.6<d<4.2; abr | 1326 | 321.15 | 2264 | 0.04219 | 11.894 | 7.698 | 0.2799 | 4.369 | 0.11322 |
| | | | | | | | | 1590 | 1706 | 1851±3 |
| NOKIA, granodiorite | | | | | | | | | | |
| A2 Siuro | A d>4.2; Ø>160 | 494.0 | 129.12 | 2118 | 0.04446 | 12.192 | 8.814 | 0.3021 | 4.828 | 0.11591 |
| | | | | | | | | 1701 | 1789 | 1894±3 |
| | B 4.0<d<4.2 | 920.4 | 200.48 | 1836 | 0.05257 | 11.988 | 9.775 | 0.2517 | 3.913 | 0.11275 |
| | | | | | | | | 1447 | 1616 | 1844±4 |
| | C 3.8<d<4.0 | 959.4 | 197.93 | 1392 | 0.06487 | 12.037 | 10.773 | 0.2384 | 3.668 | 0.11157 |
| | | | | | | | | 1378 | 1564 | 1825±6 |
| | D[*4] total; borax fusion | 520.0 | 135.4 | | 0.0339 | 12.02 | 8.05 | 0.3009 | 4.796 | 0.1156 |
| | | | | | | | | 1696 | 1784 | 1890 |
| | E d>4.6 | 390.0 | 106.21 | 1704 | 0.05590 | 12.260 | 9.063 | 0.3147 | 4.992 | 0.11505 |
| | | | | | | | | 1763 | 1817 | 1880±6 |
| | F d>4.6; HF | 303.1 | 85.27 | 24262 | 0.003241 | 11.645 | 7.169 | 0.3252 | 5.201 | 0.11601 |
| | | | | | | | | 1814 | 1852 | 1895±3 |
| | G d>4.6; 70< Ø <160 clear, long crystals | 400.4 | 113.17 | 2734 | 0.03455 | 12.005 | 8.048 | 0.3267 | 5.197 | 0.11538 |
| | | | | | | | | 1822 | 1852 | 1885±5 |

**App. 2, contd.**

| | | | | | | | | | | |
|---|---|---|---|---|---|---|---|---|---|---|
| | H d>4.6; abr; 70< Ø <160 turbid, short crystals | 394.2 | 114.74 | 4406 | 0.01661 | 11.984 | 7.538 | 0.3364<br>1869 | 5.454<br>1893 | 0.11760<br>1920±5 |
| | I d>4.6; abr »microgems» | 286.0 | 82.63 | 5778 | 0.01442 | 11.805 | 9.309 | 0.3339<br>1857 | 5.345<br>1876 | 0.11610<br>1897±4 |
| | J 4.2<d<4.6; abr turbid, short crystals | 516.5 | 138.3 | 1744 | 0.04130 | 12.572 | 9.567 | 0.3094<br>1737 | 5.127<br>1840 | 0.12017<br>1958±8 |
| | K 4.2<d<4.6; abr »microgems» | 527.4 | 145.12 | 5123 | 0.01629 | 11.711 | 7.256 | 0.3180<br>1780 | 5.039<br>1825 | 0.11491<br>1878±4 |
| | L 4.2<d<4.6 long crystals | 613.3 | 158.61 | 2889 | 0.03294 | 11.872 | 7.471 | 0.2989<br>1685 | 4.709<br>1768 | 0.11427<br>1868±3 |
| | M d>3.8 long crystals | 917.2 | 222.56 | 1994 | 0.04620 | 11.907 | 8.487 | 0.2805<br>1593 | 4.362<br>1705 | 0.11281<br>1845±4 |
| | N 3.8<d<4.0; abr turbid, short crystals | 1330 | 280.84 | 1230 | 0.07965 | 12.244 | 14.331 | 0.2440<br>1407 | 3.755<br>1583 | 0.11163<br>1826±7 |
| | O 4.2<d<4.6; Ø <130 long crystals | 595.0 | 155.22 | 2083 | 0.04649 | 12.039 | 8.443 | 0.3015<br>1698 | 4.743<br>1774 | 0.11410<br>1865±6 |
| TERVALAHTI, conglomerate clasts | | | | | | | | | | |
| A90 Iso-Kartano | A[*4] total; borax fusion | 962.2 | 234.54 | 1985 | 0.03727 | 11.921 | 18.176 | 0.2817<br>1599 | 4.434<br>1718 | 0.11417<br>1866±8 |
| | B d>3.6; abr 2 h | 886.7 | 246.01 | 12986 | 0.006446 | 11.613 | 17.670 | 0.3207<br>1792 | 5.096<br>1835 | 0.11526<br>1884±4 |
| | C d>3.6; abr 4 h | 894.3 | 251.99 | 16568 | 0.004953 | 11.596 | 17.594 | 0.3257<br>1817 | 5.177<br>1848 | 0.11529<br>1884±3 |
| A26 Vähä-Linna | A 3.6<d<4.0; abr Ø >50 | 1585 | 428.08 | 12995 | 0.007030 | 11.506 | 14.864 | 0.3121<br>1751 | 4.910<br>1804 | 0.11411<br>1866±4 |
| | B 3.6<d<4.0; abr Ø <50 | 1604 | 437.20 | 9323 | 0.009119 | 11.547 | 15.170 | 0.3151<br>1765 | 4.962<br>1812 | 0.11424<br>1868±4 |
| | C d>3.8 | 1690 | 436.66 | 8530 | 0.01081 | 11.509 | 14.976 | 0.2986<br>1684 | 4.677<br>1763 | 0.11362<br>1858±5 |
| | D 3.6<d<3.8; abr Ø >70 | 1825 | 413.64 | 4503 | 0.02135 | 11.432 | 14.595 | 0.2619<br>1499 | 4.024<br>1639 | 0.11142<br>1822±4 |
| A393 Hormistonlahti | d>3.6 | 770.7 | 195.75 | 3624 | 0.02474 | 11.704 | 15.201 | 0.2936<br>1659 | 4.602<br>1749 | 0.11369<br>1859±4 |
| A768 Kärki | d>3.6; abr | 1457 | 388.78 | 9308 | 0.008730 | 11.543 | 16.760 | 0.3084<br>1732 | 4.857<br>1794 | 0.11425<br>1868±3 |
| LAVIA, conglomerate clast | | | | | | | | | | |
| A144 Välimäki | A total | 191.4 | 48.87 | 1947 | 0.000451 | 11.385 | 8.683 | 0.2952<br>1667 | 4.631<br>1754 | 0.1138<br>1860±23 |
| | B d>4.2; HF | 131.0 | 36.61 | 9520 | 0.007905 | 11.622 | 9.955 | 0.3230<br>1804 | 5.128<br>1840 | 0.11515<br>1882±4 |

**App. 2, contd.**

| | | | | | | | | | | |
|---|---|---|---|---|---|---|---|---|---|---|
| | C 4.3<d<4.6; HF | 126.3 | 35.55 | 2406 | 0.03627 | 11.995 | 10.973 | 0.3254<br>1815 | 5.161<br>1846 | 0.11505<br>1880±9 |
| | D 4.3<d<4.6<br>abr 3 h | 151.4 | 42.21 | 5642 | 0.01510 | 11.704 | 9.909 | 0.3223<br>1801 | 5.111<br>1837 | 0.11500<br>1880±4 |
| | E 4.3<d<4.6<br>abr 6 h | 156.0 | 43.94 | 8437 | 0.009421 | 11.643 | 10.012 | 0.3257<br>1817 | 5.170<br>1847 | 0.11515<br>1882±4 |
| | F 4.3<d<4.6; Ø >70 | 178.6 | 45.47 | 1999 | 0.04533 | 12.039 | 10.856 | 0.2942<br>1662 | 4.635<br>1755 | 0.11425<br>1868±5 |
| | G 4.3<d<4.6; Ø <70 | 253.4 | 62.38 | 2503 | 0.03463 | 11.842 | 9.539 | 0.2845<br>1613 | 4.461<br>1723 | 0.11373<br>1860±5 |
| SILVOLA, tonalite<br>A302 | A d>4.6; Ø >160 | 268.2 | 65.74 | 7744 | 0.01065 | 11.547 | 8.023 | 0.2833<br>1607 | 4.454<br>1722 | 0.11403<br>1864±5 |
| | B d>4.6; Ø <160 | 281.8 | 65.46 | 11650 | 0.007165 | 11.471 | 6.992 | 0.2685<br>1533 | 4.211<br>1676 | 0.11374<br>1860±4 |
| | C 4.2<d<4.6 | 358.6 | 76.51 | 12136 | 0.007214 | 11.337 | 6.403 | 0.2466<br>1420 | 3.821<br>1597 | 0.11239<br>1838±4 |
| | D 4.0<d<4.2 | 507.9 | 84.95 | 5974 | 0.01551 | 11.217 | 5.871 | 0.1933<br>1139 | 2.933<br>1390 | 0.11006<br>1800±4 |
| | E d>4.6; HF | 166.3 | 46.85 | 18798 | 0.003548 | 11.555 | 7.153 | 0.3257<br>1817 | 5.166<br>1847 | 0.11507<br>1881±4 |
| | F 3.6<d<4.0 | 502.7 | 85.90 | 2834 | 0.03390 | 11.477 | 6.591 | 0.1975<br>1161 | 3.000<br>1407 | 0.11016<br>1802±5 |
| 66-2-MN-85 | A d>3.6; abr | 273.1 | 75.41 | 6058 | 0.009895 | 11.580 | 9.021 | 0.3192<br>1785 | 5.037<br>1825 | 0.11446<br>1871±5 |
| | B titanite<br>3.4<d<3.5; abr | 190.8 | 52.43 | 730.4 | 0.13544 | 13.007 | 15.474 | 0.3176<br>1778 | 4.891<br>1800 | 0.11168<br>1827±7 |

*1 All fractions are zircon unless otherwise indicated. d = density (g $cm^{-3}$); Ø = size (μm); HF = preleached in HF; abr = grains abraded
*2 For other fractions, see Patchett and Kouvo (1986)
*3 Recalculated from Himmi et al. (1979)
*4 Recalculated from Kouvo and Tilton (1966)
$\lambda^{238}U = 1.55125 \times 10^{-10}/a$
$\lambda^{235}U = 9.8485 \times 10^{-10}/a$

**Appendix 3. Location of samples for U-Pb isotopic analyses.**

| Location | Sample | Map sheet | X | Y |
|---|---|---|---|---|
| Hämeenkyrö | A248 Äkönmaa | 2124 01 | 6834.96 | 469.16 |
| Ylöjärvi | A3 Paroistenjärvi | 2124 04 | 6833.5 | 473.6 |
| Värmälä | 54-MN-84 Vattula | 2124 10 | 6834.26 | 497.83 |
| | 55-MN-84 Vattula | 2124 10 | 6834.10 | 497.13 |
| | 105-MN-84 Vattula | 2124 10 | 6833.66 | 497.13 |
| Nokia | A2 Siuro | 2123 02 | 6819 | 465 |
| Tervalahti | A90 Iso-Kartano | 2124 10 | 6834.21 | 493.55 |
| | A26 Vähä-Linna | 2124 10 | 6831.3 | 490.0 |
| | A393 Hormistonlahti | 2124 10 | 6831.7 | 491.1 |
| | A768 Kärki | 2124 10 | 6831.3 | 490.5 |
| Lavia | A144 Välimäki | 2122 02 | 6842.56 | 422.64 |
| Silvola | A302 Simpala | 4122 12 | 6858.56 | 453.73 |
| | 66-2-MN-85 Silvola | 4211 10 | 6862.12 | 453.18 |